White Paper
Application of PBPK Models to Pyrethroid Risk Assessment

Demonstration with Deltamethrin and *cis*-Permethrin

For submission to the US Environmental Protection Agency

prepared for:
The Council for the Advancement of Pyrethroid Human Risk Assessment

Scientific representative
Dr. Thomas Osimitz

July 24th, 2017

Miyoung Yoon
Director of Biokinetics and Biosimulations
919-558-1340
myoon@scitovation.com
6 Davis Drive, PO Box 110566
Research Triangle Park, NC 27709

Table of Contents

List of abbreviations

I: Background

A. Physiologically based pharmacokinetic (PBPK) models for risk assessment

B. Development of PBPK models for pyrethroids

C. Applications of PBPK models to pyrethroid risk assessment

a. Age-related uncertainty factor or FQPA safety factor for human pharmacokinetics

b. Inter-species extrapolation uncertainty factor for human pharmacokinetics

c. Intra-species extrapolation uncertainty factor for human pharmacokinetics

d. Other applications

II: Age-specific PBPK Models for Deltamethrin and *cis*-Permethrin, and trans-Permethrin in Rats

A. Introduction

B. Modeling approach

a. Structure of the model

b. Model Parameters

i. Life-stage parameters

1. Physiological parameters

2. Ontogeny of metabolism

ii. Restricted clearance

iii. *in vitro* to *in vivo* extrapolation (IVIVE)

1. *In vitro* data

2. Scaling process

3. Intrinsic clearance calculation

iv. Chemical specific parameters

1. Oral absorption-related parameters

2. Tissue partitioning

3. Tissue permeability

c. Evaluation of the approach

i. *In vivo* data

ii. *In vivo* PK simulations

iii. Use of generic structure and read across approaches

C. Sensitivity analysis

D. Model outputs

a. Clearance

b. Plasma and brain Cmax at different ages

c. Comparison of dose-response

E. Estimation of the internal dose at Point of departure (POD)

F. Discussion

G. References

H. List of the appended files for the rat model

III: Age-specific PBPK Models for Deltamethrin and *cis*-Permethrin in Humans

A. Introduction

B. Modeling approach

a. Structure of the Model

b. Model parameters

i. Life-stage parameters

1. Physiological parameters

2. Enzyme ontogeny

ii. *In vitro to in vivo* extrapolation (IVIVE)

1. *In vitro* data

2. Scaling process

3. Age-specific intrinsic clearance calculation

4. Restricted clearance and age-specific hepatic clearance calculation

iii. Chemical specific parameters

1. Tissue partitioning

2. Tissue permeability

c. Modeling Exposure

i. Oral exposure

ii. Inhalation

iii. Dermal

C. Simulation of exposure scenarios and reverse dosimetry

a. Exposure scenarios

b. Point of departure (POD)

c. Reverse dosimetry

d. DDEF calculation

D. Sensitivity analysis

E. Model outputs

a. Comparison of hepatic clearance in children and adults

b. Age-dependent plasma and brain concentrations under various exposure scenarios

c. EPA provided exposure scenarios: reverse dosimetry

d. MC analysis

F. Uncertainty analysis

G. Discussion

H. References

I. List of the appended files for the human model

J. Link to the PLETHEM interface

IV. Appendices

Appendix 1. Age-dependent *in vitro* intrinsic clearance for DLM.

Appendix 2. Age-dependent *in vitro* intrinsic clearance for CPM.

Appendix 3. Age-dependent *in vitro* intrinsic clearance for TPM.

Appendix 4. Scaling of *in vitro* DLM, CPM and TPM metabolic constants for *in vitro* to *in vivo* extrapolation.

Appendix 5. Comparison of age-specific hepatic blood flow and total hepatic intrinsic clearance for DLM, CPM and TPM.

Appendix 6. Tissue-to-plasma partition coefficients for DLM, CPM and TPM in rats.

Appendix 7. Comparison of tissue-to-plasma PCs based on *in vivo* studies to those derived from QSAR

Appendix 8. DLM, CPM, and TPM concentrations in brain in PND15 and PND90 rats when compound specific brain to plasma partition coefficients in PND90 rats are used for DLM, CPM and TPM, respectively.

Appendix 9. DLM concentrations in brain and plasma in PND90 rats.

Appendix 10. DLM concentrations in brain and plasma in PND15 rats.

Appendix 11. Pulmonary parameters for human males and females.

Appendix 12. DLM source-specific external dose PODs derived from the animal POD for decreased motor activity.

Appendix 13. CPM source-specific external dose PODs derived from the animal POD for decreased motor activity.

Appendix 14. CPM source-specific external dose PODs derived from the animal POD for decreased motor activity.

List of abbreviations

BMD	Bench mark dose
BW	Body weight
CAPHRA	Council for the Advancement of Pyrethroid Human Risk Assessment
CES	Carboxylesterase
Clh	Hepatic clearance
Clint	Intrinsic clearance
Cmax	Maximum concentration
CPM	*Cis*-permethrin
CPPGL	Cytosol Protein Per Gram Liver
CSAF	Chemical specific adjustment factor
CYP	Cytochrome P450
DDEF	Data-driven extrapolation factor
DLM	Deltamethrin
EPA	Environmental Protection Agency
FQPA	Age-related safety factor (as defined in the Food Quality Protection Act, 1996)
FU	Fraction unbound
FuPLS	Plasma protein binding
GI	Gastrointestinal tract
ISEF	Inter-System Extrapolation Factor
IVIVE	*In vitro* to *in vivo* extrapolation
K_x	Rate constant
Km	Michaelis-Menten constant
KMF	Free-concentration adjustment factor
LD50	Lethal dose 50 percent
LW	Liver weight
MC	Monte Carlo
MPPGL	Microsomal Protein Per Gram Liver
NRC	National Research Council
NHANES	National Health and Nutrition Examination Survey
PB	Air partition coefficient
PBPK	Physiologically based pharmacokinetic

PBRN	Brain partition coefficient
PC	Partition coefficient
PK	Pharmacokinetic
PND	Post-natal day
POD	Point of departure
QAlv	Alveolar ventilation rate
QGI	Portal blood flow from GI to liver
QH	Hepatic arterial blood flow
QL	Total hepatic blood flow (sum of hepatic arterial and portal)
RfD	Reference dose
SA	Sensitivity Analysis
SC	Sensitivity Coefficient
SS	Steady state
TPM	*Trans*-permethrin
UF	Uncertainty factor
US EPA	United States Environmental Protection Agency
VL	Factor liver weight
VLDL	Very low density lipoprotein
Vmax	Maximum rate of metabolism
VP	Plasma volume

Note: The data used in these evaluations came from the referenced reports. With the exception of the data packages from CXR Biosciences (or its new name Concept Life Sciences), they represent final, audited reports. It is possible that, upon confirmation and audit, some of the CXR/CLS data may be revised. However, in our judgment, these changes would not significantly affect the outcome of our evaluations or the conclusions derived therefrom.

ScitoVation contributors

1. **Rat life stage PBPK models** – Gina Song, Marjory Moreau, Alina Efremenko, Salil Pendse, Harvey Clewell, and Miyoung Yoon

2. **Human life stage PBPK models** – Marjory Moreau, Gina Song, Pankajini Mallick, Alina Efremenko, Salil Pendse, Harvey Clewell, and Miyoung Yoon

I. Background

A. Physiologically based pharmacokinetic (PBPK) models for risk assessment

Biological responses to compounds are related to the free concentrations of active compounds at a target site, rather than directly to the amount of compound administered. Therefore, the internal exposure at the target tissue is the appropriate dose metric for use in safety assessment. PBPK modeling offers a scientifically-sound framework to integrate mechanistic data for physiology and biochemical processes and serves as a tool to predict internal exposure at the target tissue for a wide range of exposure conditions in animals or humans. PBPK models differ from classical compartmental models in that they include biologically realistic descriptions of tissues and processes involved in exposure, distribution, biotransformation and clearance processes (Clewell and Andersen, 1994). Since physiology and metabolism are described using physiologically meaningful parameters, a different species can be modeled by simply replacing the appropriate parameters with those for the species of interest. Similarly, the behavior for a different route of administration or exposure scenario can be determined by adding the equations that describe the nature of the input function. The mechanistic basis of PBPK models enhances their predictive power, allowing for various applications of this tool in a risk assessment context. These applications include inter- and intra-species extrapolation, route-to-route extrapolation, and high-to-low dose extrapolation (Clewell and Andersen, 1985), as well as the recent application area of quantitative *in vitro* to *in vivo* extrapolation (IVIVE), supporting the new safety assessment paradigm based on *in vitro* and computational methods (Yoon *et al.,* 2012; 2016). The advantages of applying PBPK modeling in risk assessment have led to widespread acceptance by regulators (NRC, 1987; Clewell and Clewell, 2008; Loizou *et al*, 2008). Beyond their applications for quantitative risk assessment, PBPK models can be used to interpret human biomonitoring data (Clewell and Clewell, 2008) and epidemiological data (Wu *et al.,* 2015; Verner *et al.*, 2015; Song *et al.*, 2016).

The approach of predicting *in vivo* metabolic clearance based on *in vitro* data using biologically-based scaling processes has gained strong support in recent years (*e.g.,* Yoon *et al.,* 2012, Houston *et al.,* 2008). By using population-appropriate exposure information, physiological and biochemical parameter values, PBPK models are well-equipped to predict population-specific internal exposure at the target tissue. Because key parameters for PBPK models, *e.g.,* metabolism parameters, are provided from *in vitro* assays based on human-derived or human-relevant systems, this modern parameterization

approach based on *in vitro* methods provides a high degree of confidence in using the model predictions for human health risk assessment.

B. Development of PBPK models for pyrethroids

A study performed by the United States Environmental Protection Agency (USEPA) found that lethality occurred in 11- and 21-day old rats (LD50 ,lethal dose 50 percent, of 5.1 and 11 mg/kg, respectively) at significantly lower doses than in adult rats (LD50 of 81 mg/kg), suggesting higher susceptibility in early life (Sheets *et al.* 1994). However, these investigators also found equivalent brain concentrations at the LD50 doses; they concluded that the lower LD50s in young animals were due to age-related differences in pharmacokinetics (PK) rather than to greater susceptibility to the effects of deltamethrin. A subsequent investigation provided additional support for this conclusion (Figure I-1), and demonstrated that the age-dependence of deltamethrin PK and the resulting differential effects could be predicted using a PBPK model with age-specific *in vitro* metabolism data (Anand *et al.*, 2006b; Tornero-Velez *et al.* 2010).

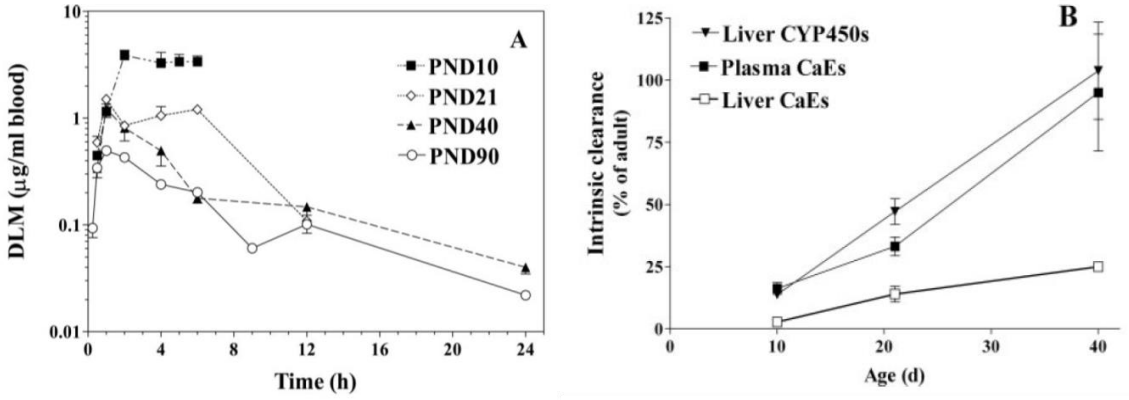

Figure I-1. Age dependence of deltamethrin internal exposure and metabolic detoxification capacity in the liver and plasma of rats.
A) Shows age-dependent changes in the blood concentration of deltamethrin (DLM) in postnatal day (PND) 10, 21, 40 and 90 rats after a single oral gavage dose at 10 mg/kg. B) Shows the age-related changes in the intrinsic clearance of DLM in PND10, 21 and 90 rats via carboxylesterases (CES) and cytochrome P450 (CYP) enzymes (Reproduced from Anand *et al.*, 2006b with permission from The American Society for Pharmacology and Experimental Therapeutics).

The Council for the Advancement of Pyrethroid Human Risk Assessment (CAPHRA) has been developing PBPK models for pyrethroids based on the modern parameterization approach of

IVIVE, with a focus on supporting risk assessment for potentially-sensitive life stages. PBPK models require rather extensive data for their development, including physiological, physicochemical, and biochemical parameters. The physiological, mechanistic basis of the models is both their strength (the mechanistic basis provides exceptional utility) and their weakness (PBPK models can be expensive and time-consuming to construct). Obtaining chemical-specific parameters, metabolism parameters in particular have been the biggest challenge in expanding the use of PBPK models to a wide range of chemicals, as well as in gaining acceptance by regulatory agencies. The recent advances in *in vitro* and *in silico* technologies for predicting chemical absorption, distribution, metabolism, and excretion and their variability in humans, along with the availability of the 'generic' PBPK modeling software like SimCyp simulation tool (Certara, Sheffield, UK), has significantly contributed to a rise in the application of PBPK modeling in recent years, particularly in drug development (Rostami-Hodjegan, 2007). The *in vitro* and *in silico*-based parameterization strategies can be applied to build a generic PBPK modeling tool for chemicals. The validity of the IVIVE-based parameterization approach has been demonstrated for a number of environmental chemicals (Table I-1) adapted from the review in Yoon *et al.* (2012). In this modern parameterization approach, key parameters for PBPK models, *e.g.*, metabolism parameters are provided from *in vitro* assays. Use of human-derived or human-relevant materials/systems in this approach increases confidence in using the model predictions for human health risk assessment.

In the current study, two representative pyrethroids were used as case compounds; deltamethrin and *cis*-permethrin. Built upon these lead compound models, the goal is to develop a generic modeling platform for all pyrethroids using a read-across strategy (Figure I-2). To support the read-across approach, CAPHRA has sponsored research to collect both *in vitro* metabolism and *in vivo* PK data for five other pyrethroids, in addition to deltamethrin and *cis*- and *trans*-permethrin. Again, the key data for read-across are provided by human-relevant *in vitro* metabolism experiments. CAPHRA's major focus for the PBPK model is to address age-related PK differences for pyrethroids in humans and to provide a scientific basis for an age-related safety factor for PK. Although the model can also be applied to address a broader set of risk assessment questions, that is beyond the scope of this submission.

Table I-1. Summary of published cases of *in vitro* to *in vivo* extrapolation of kinetics for environmental chemicals (Adapted from Yoon *et al.* 2012).

Environmental compound(s)	Primary metabolic enzymes/pathways	In vitro system	Species	References
Furan	CYP2E1	Hepatocytes	Human, rat and mouse	Kedderis *et al.* 1993; Kedderis *et al.* 1996
1,2-Dichlorobenzene	Oxidation (CYPs)	Microsomes	Human rat	Hissink *et al.* 1997
m-xylene	CYP2E1	Microsomes	Human rat	Loizou *et al.* 1999
Trichloroethylene	CYPs, ADH, ALDH	Hepatocytes / microsomes	Human	Lipscomb *et al.* 1998
Tetrachlorobenzyltoluenes		Microsomes	rat	Kramer *et al.* 2000
Ethylene bromide	GST isoforms, CYP2E1, 2A6, and 2B6	Purified enzymes	Human rat	Ploemen *et al.* 1997
Molinate	Oxidation (CYPs), GSH conjugaison	Microsomes / Cytosol / liver slices	Human rat	Campbell, 2009
Estragole	Oxidation (CYPs) / Glucuronidation / Sulfation / Dehydrogenation	Microsomes / S9 fraction / Expressed enzymes	Human rat	Punt *et al.* 2009; Punt *et al.* 2010
Bisphenol A	Glucuronidation/Sulfation	Primary cultured hepatocytes	Human, rat and mouse	Pritchett *et al.* 2002
Chlorpyrifos/Diazinon	CYPs	Microsomes	rat	Timchalk and Poet, 2008
	Esterases	plasma		
Deltamethrin	CYPs	Microsomes	rat	Mirfazaelian *et al.* 2006
	CES	plasma		Tornero-Velez *et al.* 2010

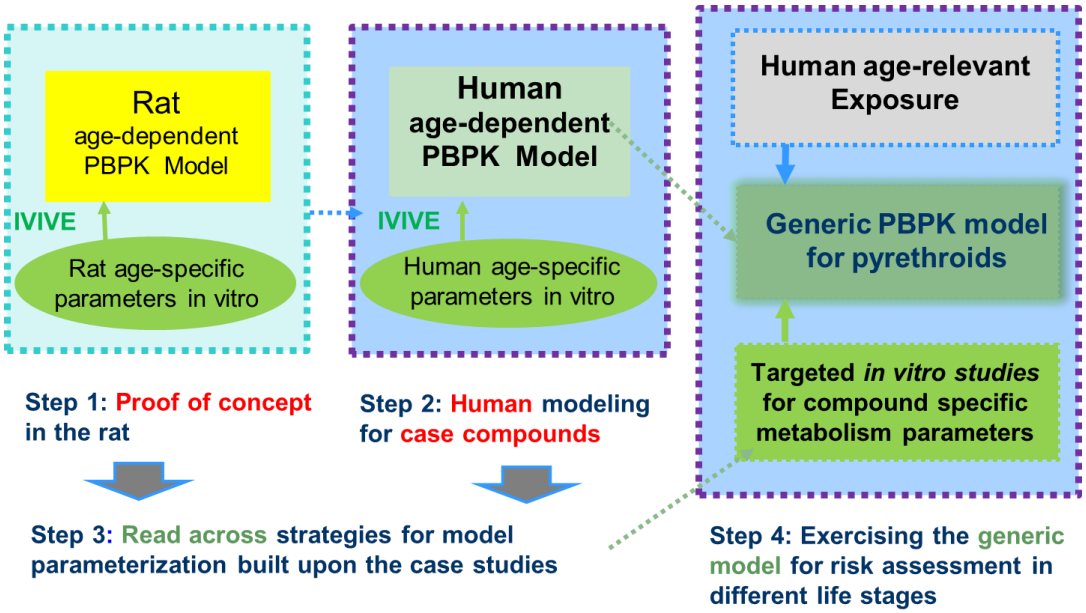

Figure I-2. Building a Generic PBPK Model for Pyrethroid Risk Assessment

C. Applications of PBPK models to pyrethroid risk assessment

a. Age-related uncertainty factor or FQPA safety factor for human pharmacokinetics

The purpose of early age dosimetry is to calculate a chemical specific adjustment factor (CSAF) or a data-derived extrapolation factor (DDEF) to address age-related PK differences for pyrethroids in humans. A PBPK model based DDEF (CSAF and DDEF are used interchangeably in this white paper) may replace the FQPA safety factor (US EPA 2015). A DDEF is calculated using the age-specific internal dose metrics simulated by the model; in the case of pyrethroids, the maximum concentration (Cmax) in the brain or in plasma is used as the internal exposure at the target tissue (Moser *et al.* 2016; Scollon *et al.* 2011). For example, DDEF values can be calculated based on the average or distribution of Cmax in the population. We have derived DDEFs using the Eq. I-1 using the population distribution data in juvenile and adult populations:

$$\textbf{Juvenile Cmax}_{\text{50\% percentile}} / \textbf{Adult Cmax}_{\text{50\% percentile}} \qquad \textbf{(Eq. I-1)}$$

b. Inter-species extrapolation uncertainty factor for human pharmacokinetics

We have developed PBPK models for both the rat and human. When the point of departure (POD) from rat studies is used for risk assessment, reverse dosimetry is performed to estimate the

human external exposure (*i.e.*, human POD); at which the brain internal exposure (*e.g.*, Cmax in brain) equals the internal exposure in the rat. As this process uses a PBPK model for human POD estimation, the inter-species uncertainty factor (UF) can be eliminated.

c. Intra-species extrapolation uncertainty factor for human pharmacokinetics

Inter-individual variability in humans is largely attributable to population variability in metabolism resulting from the large variation in metabolizing enzyme expression. In rats, pyrethroids are metabolized in the liver and in plasma. In humans, results found in the literature (Crow *et al.* 2007; Godin *et al.* 2007) have shown there is no significant metabolism of pyrethroids in plasma. The human *in vitro* data developed in support of the pyrethroid PBPK model provides an estimate of the variability in the metabolic capacity in the human population. The appropriateness of the intra-species UF for PK can be evaluated using population-specific PBPK models. For this purpose, the DDEF is calculated as $Cmax_{95\%\ percentile}/Cmax_{50\%\ percentile}$ in the given population.

d. Other applications

Current models simulate oral and inhalation routes of administration. The dermal exposure route will be added in the final model. PBPK models can be used to perform route-to-route extrapolation. Thus, the rat oral POD, can be used to derive a human POD for other routes of exposure such as inhalation and dermal.

II. Age-specific PBPK Models for Deltamethrin, *cis*-Permethrin, and *trans*-Permethrin in Rats

A. Introduction

Rat physiologically based pharmacokinetic (PBPK) models for three case compounds, deltamethrin (DLM), *cis*-permethrin (CPM), and *trans*-permethrin (TPM), have been developed using an *in vitro* to *in vivo* extrapolation (IVIVE)-based parameterization strategy to support pyrethroid risk assessment for potentially-sensitive life stages. The IVIVE approach has been evaluated and validated using the rat models for these compounds. *In vitro* metabolism data (Vmax and Km values) for DLM, CPM, and TPM were collected using microsomes, cytosol, and plasma prepared from juvenile and adult rats (see the appended CXR1574 Report I Deltamethrin, CXR1574 Report II *Cis*-permethrin, and CXR1574 Report III *Trans*-permethrin). *In vitro* maximum rate of metabolism (Vmax) and Michaelis-Menten constant (Km) values for metabolism of DLM, CPM, or TPM obtained in liver microsomes and cytosol, and plasma obtained from juvenile and adult rats were scaled using biologically relevant scaling factors for use in the PBPK model. The main goal of the rat PBPK modeling of pyrethroids is to develop PBPK models for pyrethroids in rats of different ages using *in vitro* metabolism data and evaluate the validity of the *in vitro* to *in vivo* extrapolation (IVIVE) for parameterization using *in vivo* pharmacokinetic (PK) data collected in juvenile and adult rats. The model has the capability to simulate oral exposure in two different vehicle types to allow the use of published studies for model evaluation. Model outputs include *in vivo* hepatic clearance as well as DLM, CPM, and TPM concentrations in plasma and brain (target tissue) under various dosing scenarios. The purpose of the rat modeling was to evaluate the validity of the IVIVE approach in parameterizing PBPK models for various ages. Our results indicate that a single model structure can be used for other pyrethroids, along with compound-specific and age-specific metabolism parameters.

B. Modeling Approach

a. Structure of the model

The previously-published growing rat PBPK model for DLM (Tornero-Velez *et al.*, 2010) was refined to incorporate the results of CAPHRA-sponsored *in vitro* and *in vivo* studies (Figure II-1). The model simulates pyrethroid exposure by oral and intravenous dosing, and incorporates age-dependent rat physiology, as well as maturation profiles of pyrethroid metabolism mediated by carboxylesterase

(CES) and Cytochrome P450 (CYP) enzymes in plasma and liver. Liver, gastrointestinal (GI) tract, and rapidly-perfused tissues are described as perfusion-limited, whereas brain, fat and slowly-perfused tissues are described as diffusion-limited. Several modifications were made including 1) the addition of a vehicle compartment to describe vehicle-related absorption differences observed in the early time kinetics of blood and other tissue concentration profiles after oral gavage, 2) the inclusion of restricted clearance based on *in vivo* pyrethroid clearance being lower than anticipated from the intrinsic metabolic clearance measured *in vitro*.

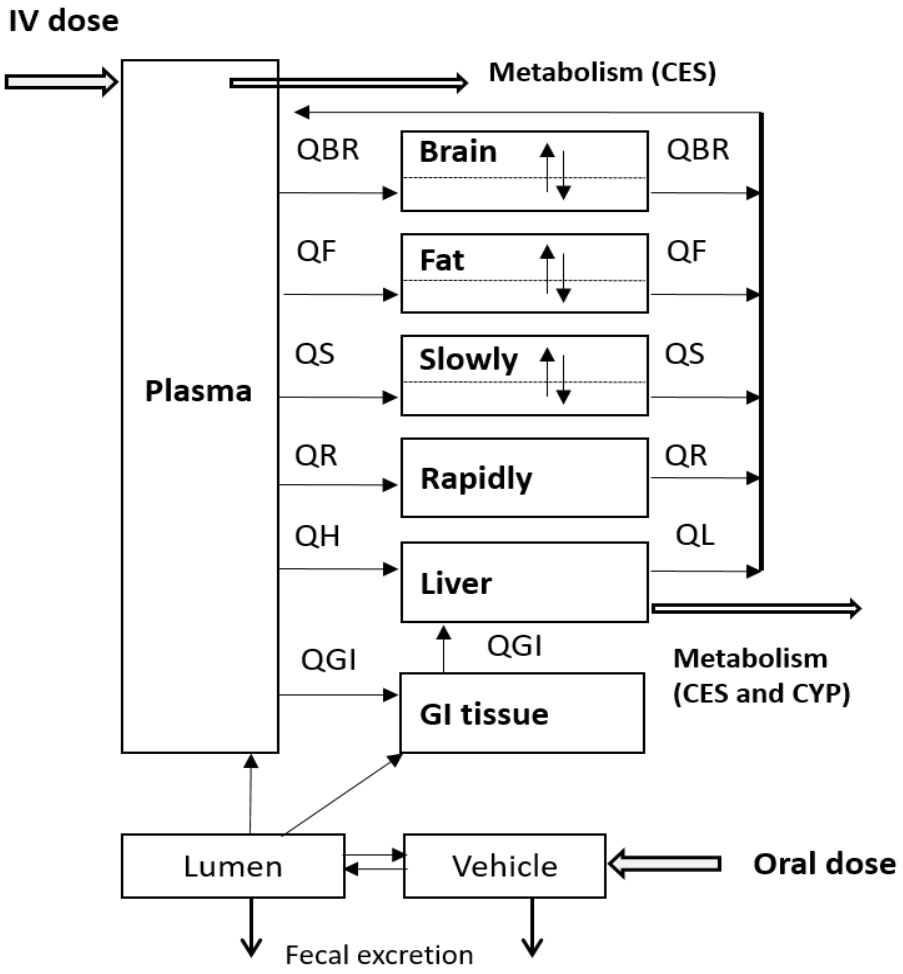

Figure II-1. Structure of the rat PBPK model for pyrethroids.
QGI, QH, QR, QS, QF, and QBR represent plasma flow to each tissue compartment. QL is the sum of portal blood flow (QGI) and hepatic arterial flow (QH). Metabolism occurs in the liver via CYP and CES enzymes and in the plasma via CESs. The vehicle compartment is only presented in the rat model to describe the experimental dosing and associated delay in oral absorption. In the current model structure, we assume 100% by-pass of the first hepatic metabolism with 0% absorption to the GI tissue as part of the restricted clearance description.

b. Model parameters

i. Life-stage parameters

1. Physiological parameters

The descriptions of age-dependent physiology in rats were refined from the previously-published rat PBPK models for DLM (Tornero-Velez *et al.*, 2010). All physiological parameters used in the current model are summarized in Table II-1. Age-dependent changes in total cardiac output, tissue volume and tissue plasma flow are from the literature (Brown *et al.*, 1997; Mirfazaelian and Fisher, 2007; Rodriguez *et al.*, 2007; Stulcová, 1977; Yoon *et al.*, 2009). Fractional plasma flow to the brain and liver was based on the interpolation of the available data in rats. (Stulcová, 1977; Yoon *et al.,* 2009).

2. Ontogeny of metabolism

The ontogeny of DLM, CPM, and TPM metabolism in rat liver microsome, cytosol, and plasma was demonstrated based on age-dependent *in vitro* intrinsic clearance (Clint) values for DLM, CPM, and TPM. The Clint values were calculated using age-specific Vmax and Km as Vmax/Km. The Vmax and Km values were appropriately scaled up to *in vivo* and were used in the model to describe dose-dependent saturation of metabolism in juvenile rats. The ontogeny of metabolism is shown as Clint normalized to the protein content in each subcellular fraction at various ages from PND15 to PND90 rats. Age-dependent *in vitro* Vmax, Km, and the calculated Clint values for DLM, CPM, or TPM are summarized in Appendices 1-3.

ii. Restricted clearance

Initial evaluation of the IVIVE in rats showed that *in vivo* metabolic clearance of DLM, CPM, and TPM was lower than anticipated from *in vitro* estimated metabolic clearance. In other words, clearance of these pyrethroids appears to be restricted *in vivo*. This is described in the model using an empirical adjustment factor, KMF. This parameter, the name standing for 'a factor that adjusts an apparent Km from *in vitro* to an *in vivo* free concentration based Km', reduces the free concentration available for metabolism in the liver and plasma *in vivo* so that the model outputs are consistent with the *in vivo* kinetic data in rats. In addition, tissue uptake of DLM, CPM, and TPM is described assuming

the equilibration of the free pyrethroid between plasma and tissue. The brain uptake of DLM has been shown to be limited to free DLM in plasma that is not bound to plasma proteins (Amaraneni *et al.,* 2016).

The general applicability of restricted clearance and KMF derived for DLM is demonstrated by the successful application of the same approach to CPM and TPM. A single KMF value is applicable to DLM, CPM and TPM regardless of the age of the rats, supporting our assumption that there is neither age-dependency nor compound-dependency in clearance restriction.

Table II-1. Physiological parameters used for pyrethroid rat PBPK model

Parameters	Values		References
	PND15	PND90	
Body weight (BODYWT, kg)	0.0343	0.3517	Mirfazaelian and Fisher, 2007
Cardiac output (CARDOUTPC, L/hr)	0.7372	3.1197	Rodriguez et al., 2007, Yoon et al., 2009
Hematocrit (HCT)	0.45	0.45	Davies and Morris, 1993
Tissue Volume (fraction of BW)			
Blood (VOLBLOODC)	0.074	0.074	Brown et al., 1997
Brain (VOLBRAINC)	0.0359	0.005587	Mirfazaelian and Fisher, 2007
Fat (VOLADPC)	0.0709	0.0513	Mirfazaelian and Fisher, 2007
GI (VOLGIC)	0.0426	0.0437	Mirfazaelian and Fisher, 2007
Liver (VOLLIVERC)	0.0308	0.0387	Mirfazaelian and Fisher, 2007
Rapidly perfused tissue (VOLRPC)	0.0294	0.0155	Mirfazaelian and Fisher, 2007
Slowly perfused tissue (VOLSPC)	0.5864	0.4122	Calculated as difference
Tissue plasma flow (fraction of cardiac output)			
Brain (FRBRNC)	0.0877	0.02	Stulcová_, 1977, Yoon et al., 2009
Fat (FRADIPC)	0.009441	0.07	Mirfazaelian and Fisher, 2007, Tornero Velez et al., 2010
GI (FRLIVC*0.95)	0.21185	0.17385	Stulcová_, 1977, Yoon et al., 2009
Liver (total, FRLIVC)	0.223	0.183	Stulcová_, 1977, Yoon et al., 2009
Liver (arterial, FRLIVC*0.05)	0.0115	0.00915	Stulcová_, 1977, Yoon et al., 2009
Slowly perfused tissues (FRSPC)	0.15	0.15	Mirfazaelian and Fisher, 2007, Tornero Velez et al., 2010
Rapidly perfused tissues (FRRPC)	0.5298	0.577	Calculated as difference

iii. *In vitro* to *in vivo* extrapolation (IVIVE)

The rationale for extrapolating *in vitro* metabolism to *in vivo* is that the capacity of metabolism (*e.g.*, Vmax) can be related by considering the total amount of enzyme present in each system. The affinity of metabolism (*e.g.*, Km) can be related by free substrate concentration for enzyme reaction. Therefore, *in vitro*-measured metabolic constants can be 'scaled-up' to respective *in vivo* metabolism parameters used in the PBPK models by relating enzyme content *in vitro* (*e.g.*, Vmax per mg protein *in vitro*) to that *in vivo* (*e.g.*, Vmax per g liver *in vivo)*. There are several different *in vitro* systems available for metabolism studies and the IVIVE process required for each system varies. IVIVE to estimate *in vivo* hepatic metabolic clearance is an accepted concept and has become common practice in drug PBPK models for pediatrics (Johnson *et al.*, 2006).

1. *In vitro* data

The metabolism of DLM, CPM and TPM has been examined by loss of substrate in liver microsomes (CYP and CES enzymes), liver cytosol (CES enzyme) and plasma preparations (CES enzyme) from male Sprague-Dawley rats aged 15, 21, and 90 days. The *in vitro* data summary for DLM, CPM and TPM may be found in the CXR reports (see CXR1574 Report I Deltamethrin , CXR1574 Report II *Cis*-permethrin, and CXR1574 Report III *Trans*-permethrin). Both the capacity (Vmax) and the affinity (Km) of pyrethroids metabolism in juvenile and adult microsomes, cytosol, and plasma were determined.

2. Scaling process

The scaling factors for IVIVE of *in vitro* Clint values obtained in microsomes, cytosol, and plasma from juvenile and adult rats for metabolism of DLM, CPM or TPM are microsomal protein per gram liver (MPPGL), cytosolic protein per gram liver (CPPGL), liver weight (LW), and plasma volume as described by Yoon *et al.* (2012). These values are in the spreadsheet titled 'MPPGL_CPPGL' in the "Rats_PYR_clearance_calculation.xlsx". The age-dependent MPPGL and CPPGL values are based on the microsomal and cytosolic protein content per gram liver in PND90 rats (Houston and Galetin, 2008) and their age-dependent changing patterns, as reported in Yoon *et al.*, 2006. Note that scaling factor liver weight (LW) and plasma volume (VP) are incorporated as age-dependent parameters in the model.

3. Intrinsic clearance calculation

The *in vitro* Clint data measured with microsomes, cytosol, and plasma from juvenile and adult rats were scaled up to corresponding *in vivo* enzyme Clint for DLM, CPM and TPM in juvenile (in this case study, PND15) and adult (in this case study, PND90) rats using appropriate scaling factors as detailed above through IVIVE (Yoon *et al.*, 2012), while Km was directly used in the model without scaling.

Clint_*vivo*_m_CYP = Clint_*vitro*_m_CYP × MPPGL × LW **(Eq.II-1)**

Clint_*vivo*_m_CES = Clint_*vitro*_m_CES × MPPGL × LW **(Eq. II-2)**

Clint_*vivo*_c_CES = Clint_*vitro*_c_CES × CPPGL × LW **(Eq. II-3)**

Clint_*vivo*_p_CES = Clint_*vitro*_p_CES × VP **(Eq. II-4)**

The *in vivo* metabolic capacity (Vmax) for DLM, CPM, and TPM in PND15 and PND90 rats was determined from Clint and Km according to the equation (II-5).

Vmax_*vivo*_enzyme = Clint_*vivo*_enzyme × Km_*vitro*_enzyme **(Eq. II-5)**

where 'enzyme' refers to CYP- or CES-mediated metabolism pathway for DLM, CPM, or TPM, 'm' to microsomes, 'c' to cytosol, and 'p' to plasma.

The IVIVE calculation above is described in the "Rats_PYR_clearance_calculation.xlsx" under the spreadsheet titled 'DLM', 'CPM', and "TPM', and summarized in Appendix 4. The final parameters for *in vivo* metabolic capacity (Vmax) and Km of DLM, CPM, and TPM used in the rat PBPK model are summarized in Table II-3 to Table II-5.

Total hepatic intrinsic clearance (Clint_*vivo*_estimated), if not restricted, for DLM, CPM, and TPM in PND15 and PND90 rats was estimated as the sum of Clint_*in vivo* _m_CYP, Clint_*in vivo* _m_CES, and Clint_*in vivo* _c_CES. This total hepatic Clint is calculated solely based on the *in vitro* measured values. As noted above, the empirical free-concentration adjustment factor (KMF), was applied to adjust the *in vitro*-derived hepatic and plasma Clint to obtain the Clint_*vivo* as below. By dividing the Clint_*vivo*_estimated by the KMF, we are converting the *in vitro* determined Km to a corresponding Km effective *in vivo* that accounts for *in vivo* free concentration. Therefore, the effective Km *in vivo* would be greater than the *in vitro* determined Km by a factor of KMF.

Clint_*vivo* = Clint_*vivo*_estimated/KMF **(Eq. II-6)**

Hepatic clearance (Clh) was calculated with equation (II-7) to compare the hepatic clearance in juvenile and adult rats.

$$\mathbf{Clh = Clint_\textit{vivo} \times QL/(QL/FuPLS+Clint_\textit{vivo})} \qquad \textbf{(Eq. II-7)}$$

Where QL is the liver blood flow and FuPLS is the unbound fraction in the plasma. Comparing age-specific hepatic blood flow (QL) and total hepatic Clint under the restricted clearance condition suggests that hepatic clearance is flow-limited in PND90 rats, whereas both hepatic intrinsic clearance and liver blood flow influence hepatic clearance in PND15 pups (Appendix 5).

iv. Chemical specific parameters

1. Oral absorption-related parameters

Parameters describing absorption of pyrethroids from the gut lumen to the systemic circulation are summarized in Table II-2 for DLM, CPM and TPM. Oral absorption-related parameters in Table II-2, including KA, KVL, KLV, KFEC, and KMF, were estimated to be consistent with the *in vivo* DLM PK data in PND90 rats. This single set of absorption rate constant (KA), rate constants for pyrethroid transfer from vehicle compartment to lumen compartment (KVL) and from lumen compartment to vehicle compartment (KLV), and fecal excretion rate (KFEC) was able to describe all DLM, CPM, and TPM kinetics in rats. A more detailed summary of the *in vivo* PK study may be found in the final reports by the University of Georgia (UGA-TK-1 FINAL 3-10-15, UGA-TK-3 FINAL 3-10-15, UGA TK-4 FINAL 2-1-2016, UGA TK-6 FINAL 3-3-2016, UGA-TK-7 FINAL 3-28-2016, and UGA-TK-9 FINAL 3-28-2016).

In addition to the PK data from the University of Georgia, model performance was evaluated and validated using the published PK studies of high-dose DLM in rats by Kim *et al.* (2010). One of the major differences between the new and previously-published *in vivo* PK studies for DLM in maturing rats is the use of different vehicles and their administered volumes. Glycerol formal was used as oral gavage vehicle at a volume of 1 ml/kg body weight (BW) in the published study, whereas corn oil at a volume of 5 ml/kg BW was used for new studies conducted by the University of Georgia. There was vehicle- and/or volume-dependent absorption and distribution kinetics of DLM in the body observed. Use of a larger volume of corn oil appears to extend the absorption phase and to lower maximum concentration (Cmax) compared to a smaller volume of glycerol formal vehicle. Thus, another set of the rate constants for DLM transfer from vehicle to the lumen compartment (KVL)

and from lumen to the vehicle compartment (KLV) was estimated to describe the data collected with DLM dosing in glycerol formal in 1 ml/kg BW (Kim *et al.,* 2010) (Table II-2). The vehicle compartment and associated absorption delay would be highly likely only relevant in animal experiments, where a large volume of lipid-based vehicle is administered, *e.g.,* 5 ml corn oil per kg BW.

Table II-2. Parameters used for DLM, CPM, and TPM rat PBPK model

Parameters	Values		Source
	PND15	PND90	
Partition coefficients			
Liver/plasma (PLIV)	1.71	1.71	CAPHRA current[a] Lam *et al.*, 1982
Fat/plasma (PADIP)	68.7	68.7	CAPHRA current
GI/plasma (PGI)	Same as Liver/plasma	Same as Liver/plasma	CAPHRA current
Brain/plasma (PBRN)	0.44	0.44	CAPHRA current Average of PND90 DLM and CPM values
Slowly perfused/plasma (PSP)	3.94	3.94	CAPHRA current
Rapidly perfused/plasma (PRP)	Same as Liver/plasma	Same as Liver/plasma	CAPHRA current
Oral absorption related parameters			
Uptake rate constant (h^{-1}) (KA)	0.31	0.31	Fitted
Rate constant for pyrethroid transfer from corn oil compartment to gut lumen compartment (h^{-1}) (KVL)	0.20 (1.2)[b]	0.20 (1.2)[b]	Fitted
Rate constant for pyrethroid transfer from gut lumen compartment to corn oil compartment (h^{-1}) (KLV)	0.000026 (0.0)[b]	0.000026 (0.0)[b]	Fitted
Fecal excretion rate (h^{-1}) (KFEC)	0.025	0.025	Fitted
Empirical adjustment factor for free concentration *in vivo* (KMF)	10	10	Fitted
Protein binding			
Total unbound fraction (FuPLS)	0.2	0.2	CAPHRA current
Tissue permeability area-cross product (L/hr/tissue weight^0.75)			
Fat (PAFC)	1.5	1.5	Fitted
Brain (PABRC)	0.095	0.095	Fitted
Slowly perfused (PASC)	0.05	0.05	Fitted

[a]: CAPHRA current represents the most up to date data made available to model development as of July 18, 2017.

[b]: values in parenthesis are to simulate the vehicle used in Kim *et al.,* 2010.

Table II-3. Compound-specific metabolic rate constants used for DLM rat PBPK model

Metabolic rate constants	Values		Source
	PND15	PND90	
Liver cytochrome P450 (CYP)			
$V_{max_m_CYP}$ (μmol/h/kg tissue)	1,295.24	3,279.85	CAPHRA current
$Km_{_m_CYP}$ (μmol/l)	1.27	0.76	CAPHRA current, Apparent Km
Liver carboxylesterase (CaE)			
$V_{max_m_CES}$ (μmol/h/kg tissue)	0	294.59	CAPHRA current
$Km_{_m_CES}$ (μmol/l)	1.42	0.76	CAPHRA current, Apparent Km
$V_{max_c_CES}$ (μmol/h/kg tissue)	381.56	373.40	CAPHRA current
$Km_{_c_CES}$ (μmol/l)	2.86	0.93	CAPHRA current, Apparent Km
Plasma carboxylesterase (CaEP)			
$V_{max_p_CES}$ (μmol/h/kg tissue)	213.01	1,986.9	CAPHRA current
$Km_{_p_CES}$ (μmol/l)	1.22	1.79	CAPHRA current, Apparent Km

Table II-4. Compound-specific metabolic rate constants used for CPM rat PBPK model

Metabolic rate constants	Values		Source
	PND15	PND90	
Liver cytochrome P450 (CYP)			
$V_{max_m_CYP}$ (μmol/h/kg tissue)	1,283.18	6,515.7	CAPHRA current
$Km_{_m_CYP}$ (μmol/l)	0.81	0.77	CAPHRA current, Apparent Km
Liver carboxylesterase (CaE)			
$V_{max_m_CES}$ (μmol/h/kg tissue)	194.44	1,386.49	CAPHRA current
$Km_{_m_CES}$ (μmol/l)	3.88	8.19	CAPHRA current, Apparent Km
$V_{max_c_CES}$ (μmol/h/kg tissue)	245.78	246.91	CAPHRA current
$Km_{_c_CES}$ (μmol/l)	1.57	0.78	CAPHRA current, Apparent Km
Plasma carboxylesterase (CaEP)			
$V_{max_p_CES}$ (μmol/h/kg tissue)	94.27	802.3	CAPHRA current
$Km_{_p_CES}$ (μmol/l)	2.03	1.37	CAPHRA current, Apparent Km

Table II-5 Compound-specific metabolic rate constants used for TPM rat PBPK model

Metabolic rate constants	Values		Source
	PND15	PND90	
Liver cytochrome P450 (CYP)			
$V_{max_m_CYP}$ (µmol/h/kg tissue)	5,451.4	26,049.6	CAPHRA current
$Km_{_m_CYP}$ (µmol/l)	2.64	7.2	CAPHRA current, Apparent Km
Liver carboxylesterase (CaE)			
$V_{max_m_CES}$ (µmol/h/kg tissue)	7003.2	28,823.0	CAPHRA current
$Km_{_m_CES}$ (µmol/l)	3.23	2.78	CAPHRA current, Apparent Km
$V_{max_c_CES}$ (µmol/h/kg tissue)	8,421.8	6,902.5	CAPHRA current
$Km_{_c_CES}$ (µmol/l)	1.55	0.42	CAPHRA current, Apparent Km
Plasma carboxylesterase (CaEP)			
$V_{max_p_CES}$ (µmol/h/kg tissue)	241.2	2,667.6	CAPHRA current
$Km_{_p_CES}$ (µmol/l)	0.6	0.6	CAPHRA current, Apparent Km

2. Tissue partitioning

Tissue:plasma partition coefficients (PCs) are defined as the ratio of the concentration of a test chemical in two phases (*i.e.*, tissue and plasma), once equilibrium is reached. PCs are important determinants of the disposition of chemicals in different tissues. DLM, CPM, or TPM fat-to-plasma and slowly-perfused tissue-to-plasma partition coefficients were determined *in vivo* studies in PND90 and PND15 rats. Experimental details for these studies along with the measured PCs for DLM, CPM and TPM in PND15 and PND90 rat tissues are summarized in Appendix 6. We compared *in vivo* measured tissue-to-plasma PCs including brain for DLM, CPM, and TPM (Appendix 6). Overall, there was no significant difference in each tissue-to-plasma PC among these compounds and different ages. Thus, DLM fat-to plasma and slowly-perfused tissue-to-plasma PCs determined in PND90 rats were also used for both CPM and TPM and for juvenile (PND15) rats. For the brain-to-plasma PC, the average of *in vivo* measured brain PCs for DLM and CPM in PND90 rats was used for simulations of DLM, CPM, and TPM kinetics in both juvenile and adult rats. There was no statistical difference among experimentally measured brain PCs for these three pyrethroids, the mean values for each compound show slightly lower brain-to-plasma PC for DLM than CPM in both ages. TPM PC appears

in the same range, but the variability of brain PC for TPM is greater than average value, based on which we did not include it to estimate an average brain PC. Simulation results supported the use of a single value of the brain-to-plasma PC for all three compounds. When the *in vivo* measured compound-specific values for brain-to-plasma PC were used, the simulated brain concentration profiles of DLM, CPM, or TPM in juvenile and adult rats were similar to those simulated with a single value of brain-to-plasma PC for DLM, CPM, or TPM (Appendix 7). The *in vivo* measured tissue-to-plasma PCs were compared to those predicted by QSAR (Appendix 8) using the method from Poulin and Haddad (2012). The comparison showed the current challenge in predicting a brain PC based on tissue composition-based QSAR methods.

The apparent liver-to-plasma partition *in vivo* is affected by hepatic metabolism, *i.e.,* the observed distribution ratio between plasma and liver would be lower than the true partition coefficient, as the chemical is constantly consumed by metabolism. True liver-to-plasma PC is estimated by the method of constant infusion using a formula below (Lam *et al.,* 1982) to account for this effect.

True liver to plasma PC = Css_Liver /(Css_Plasma×(1-Clh/Qh)) (Lam *et al.,* 1982)

Css_Liver is the concentration of DLM at steady-state (SS) in the liver and Css_Plasma is the concentration of DLM at SS in the plasma determined at 72 hours following constant infusion of DLM (0.36 mg/h) as described in the appended report (UGA-PC-1 FINAL 1-20-2016). Clh is the estimated hepatic clearance and QH is the liver plasma flow. The true liver-to-plasma PC estimated in adult rat for DLM was used for CPM and TPM, as we assume a single set of PCs can describe tissue partitioning for all pyrethroids.

3. Tissue permeability

Tissue permeability-area cross products for diffusion were scaled to tissue weight$^{0.75}$ instead of using a fixed value for all ages. Permeability-area products for brain, fat and slowly-perfused organ compartment were estimated to let the model output be consistent with the observed time-courses of DLM, CPM or TPM concentrations in the brain, fat and slowly-perfused compartments in PND15 and PND90 rats following a single oral dose of DLM, CPM or TPM, respectively (UGA-TK-1 FINAL 3-10-15, UGA-TK-3 FINAL 3-10-15, UGA-TK-4 FINAL 2-01-2016, UGA-TK-6 FINAL3-3-2016, UGA-TK-7 FINAL 3-28-2016, and UGA-TK-9 FINAL 3-28-2016). The estimated values for tissue permeability-area products are summarized in Table II-2.

c. Evaluation of the approach

i. *In vivo* data

A detailed summary of the *in vivo* PK study of DLM, CPM and TPM may be found in the final reports by the University of Georgia (UGA-TK-1 FINAL 3-10-15, UGA-TK-3 FINAL 3-10-15, UGA TK-4 FINAL 2-1-2016, UGA TK-6 FINAL 3-3-2016, UGA-TK-7 FINAL 3-28-2016, and UGA-TK-9 FINAL 3-28-2016). One thing to note is that most concentrations observed at 48 hours post oral exposure were either undetectable or, if any, below detection limit of quantitation (LOQ). In that case, half of LOQ was used if it is no less than limit of detection (LOD), or half of LOD was used if it is less than LOD. LOD is assumed to be 1/3 of LOQ. Thus, there was uncertainty related to the PK data at the later time points, which is common in any PK studies. More details are described in the cited reports from the University of Georgia as described above.

ii. *In vivo* PK simulations

The performance of the model was first evaluated using the newly collected *in vivo* PK studies for DLM in maturing rats following a single oral dose at 0.1 mg/kg, 0.25 mg/kg or 0.5 mg/kg in 5 ml/kg corn oil via gavage. The IVIVE-PBPK model for growing rats recapitulated the DLM plasma and brain internal exposure well in juvenile and adult rats (Figure II-2 and -3).

To demonstrate the robustness and reliability of the model in simulating *in vivo* kinetics regardless of vehicle types, published DLM PK data was simulated after an oral dose at 0.4, 2, or 10 mg/kg in glycerol formal at 1 ml/kg BW (Kim *et al.*, 2010). Except for the vehicle-specific absorption parameters, other model parameters were kept the same (details are provided for each of the appropriate model parameters as annotation in the model code appended in this submission package). The model was able to recapitulate the DLM concentrations in plasma and brain in PND90 rats and PND10 rats reasonably well (Figure II-4 and -5). Note that we used PND15 *in vitro* data to estimate PND10 *in vivo* metabolism parameters, as there was no in vitro data available for PND10.

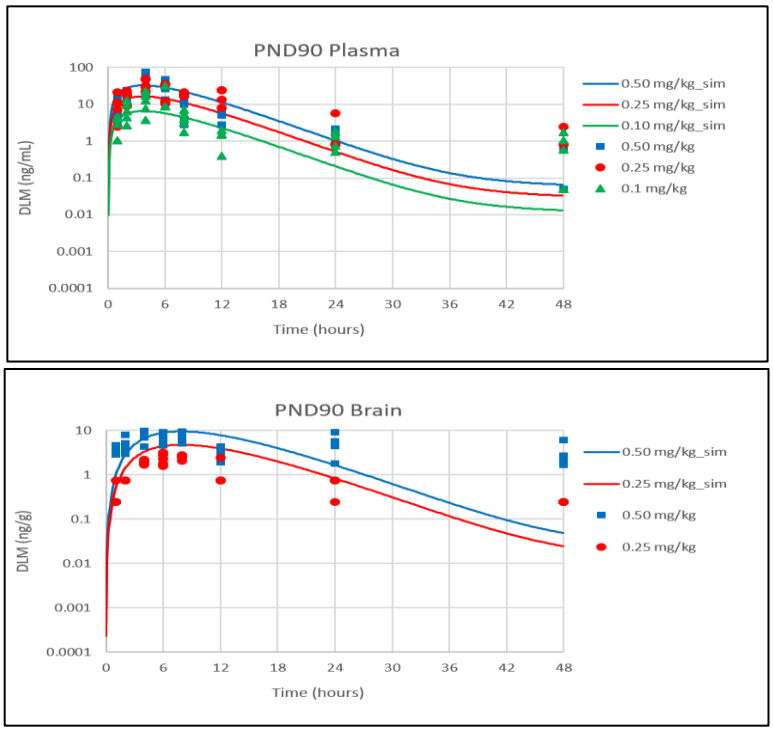

Figure II-2. DLM concentrations in brain and plasma in PND90 rats - simulation using new *in vivo* PK data from the University of Georgia.

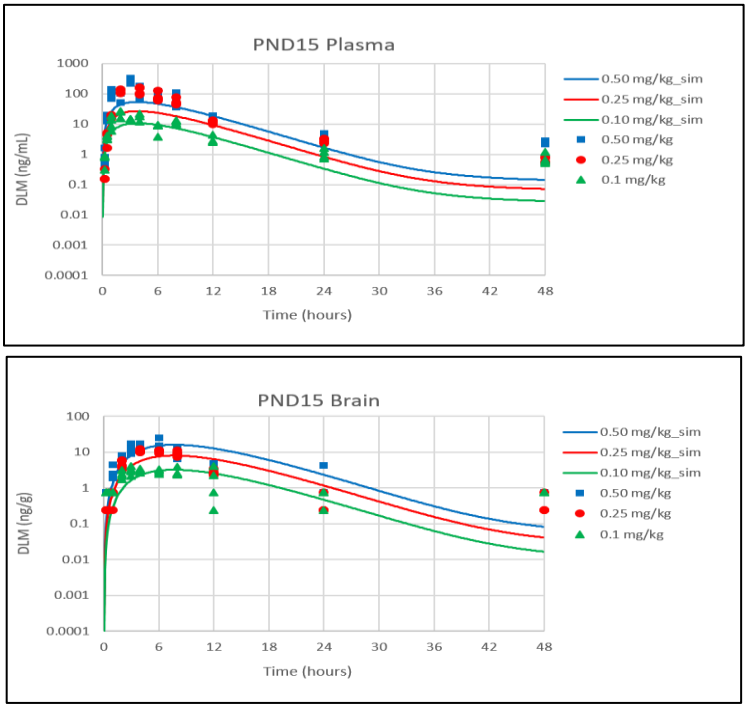

Figure II-3. DLM concentrations in brain and plasma in PND15 rats - simulation using the new *in vivo* PK data from the University of Georgia.

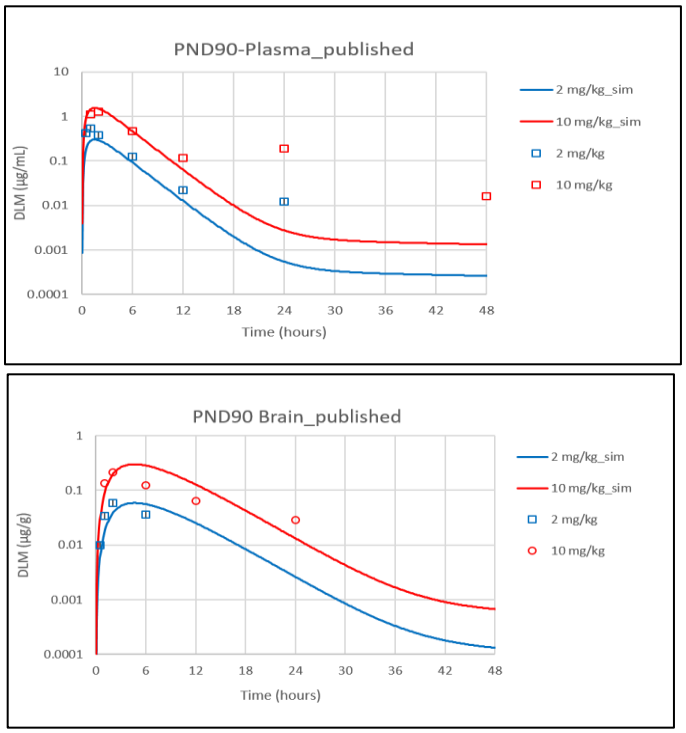

Figure II-4. DLM concentrations in brain and plasma in PND90 rats - simulation using published PK data (Kim *et al.,* 2010).

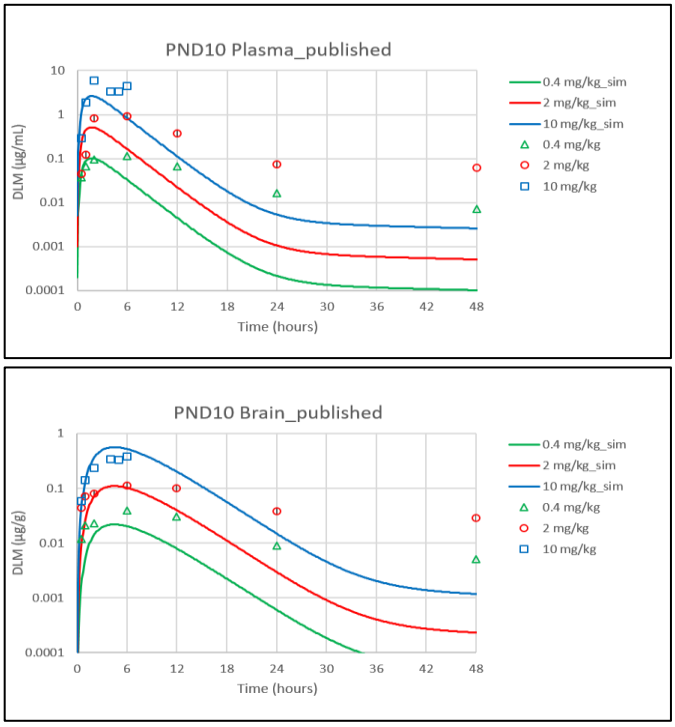

Figure II-5. DLM concentrations in brain and plasma in PND10 rats - simulation using published PK data (Kim *et al.,* 2010).

iii. Use of generic model structure and read across approaches

In addition to DLM, CPM and TPM were selected as the second case compounds for rat modeling to serve as a proof-of-concept to demonstrate the validity of IVIVE-based read-across modeling for pyrethroids of different types (Type II vs. I) and different degree of lipophilicity (reported log P ranging from 5.43-6.20 vs. 6.50 in PubChem Compound Database CID = 40585 and 40236). Given that permethrin is known to be metabolized by different metabolizing enzymes compared to DLM (Scollon *et al.,* 2009), the capability of the model to simulate the plasma and brain internal exposure for CPM and TPM using the same model structure as DLM except the metabolism parameters provides confidence in IVIVE-based read across for model development for pyrethroids as a group. The performance of the model was evaluated using the new *in vivo* PK data for CPM collected in maturing rats following an oral dose at 15 mg/kg, 30 mg/kg, or 45 mg/kg in PND15 rats or at 60 mg/kg, 90 mg/kg or 120 mg/kg in PND90 rats. For TPM, the performance of the model was evaluated using the new *in vivo* PK data for TPM collected in maturing rats following an oral dose at 300 mg/kg, 450 mg/kg, or 600 mg/kg in PND15 rats or at 120 mg/kg, 150 mg/kg or 300 mg/kg in PND90 rats. The IVIVE-PBPK model reasonably well recapitulated the CPM and TPM concentrations in plasma and brain in juvenile and adult rats (Figure II-6 through II-9). The successful use of the same KMF value as in the DLM model supports the incorporation of restricted clearance description in the model independent of the pyrethroid identity.

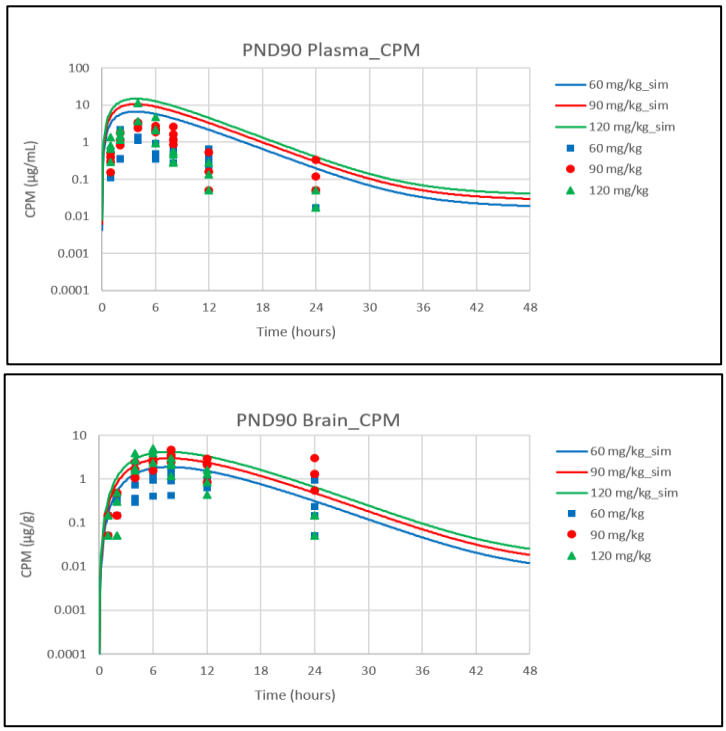

Figure II-6. CPM concentrations in brain and plasma in PND90 rats - simulation using the new *in vivo* PK data from the University of Georgia.

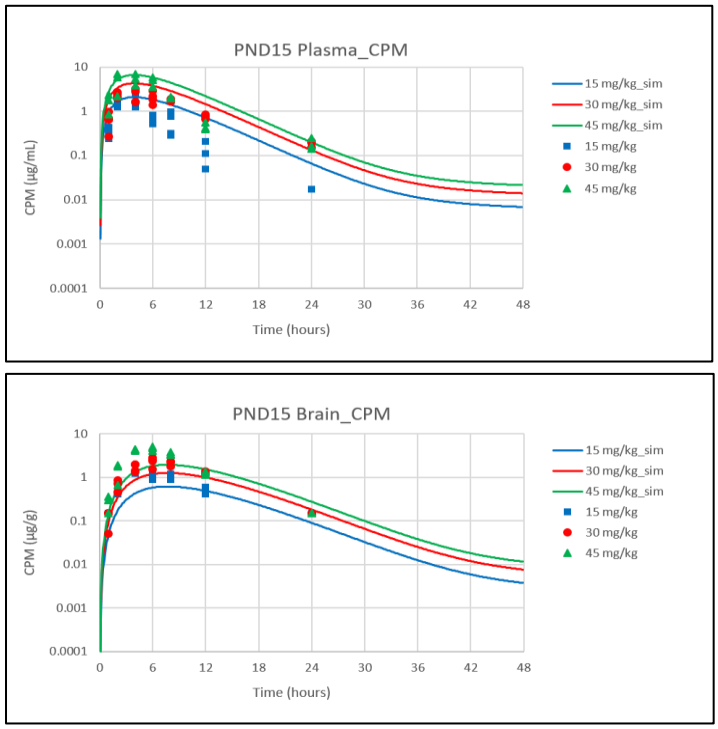

Figure II-7. CPM concentrations in brain and plasma in PND15 rats - simulation using the new *in vivo* PK data from the University of Georgia.

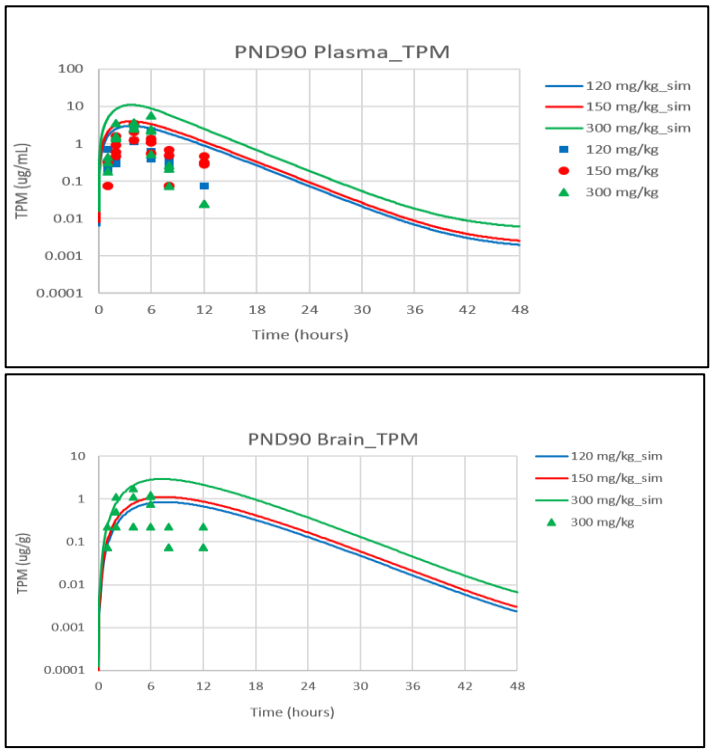

Figure II-8. TPM concentrations in brain and plasma in PND90 rats - simulation using the new *in vivo* PK data from the University of Georgia. TPM concentrations in brain following 120 mg/kg and 150 mg/kg were not detected.

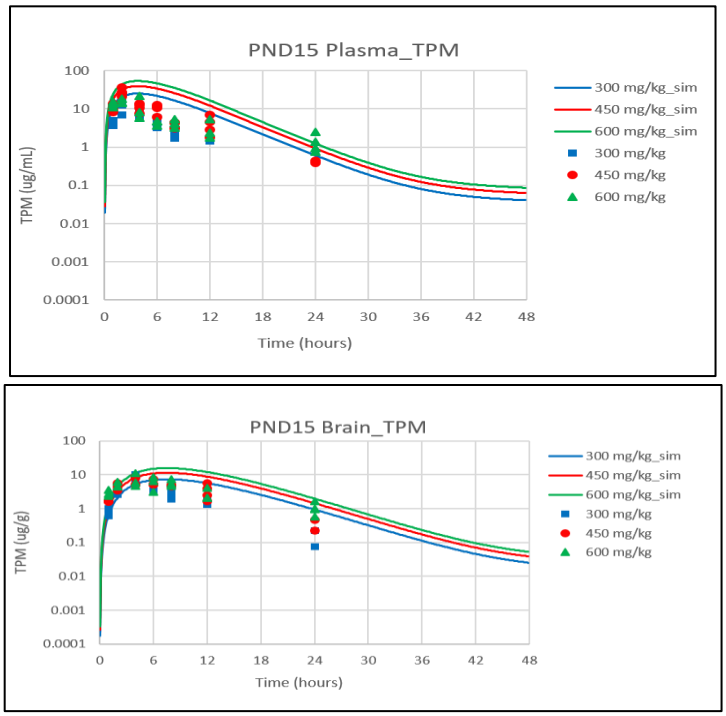

Figure II-9. TPM concentrations in brain and plasma in PND15 rats - simulation using the new *in vivo* PK data from the University of Georgia.

The performance of the model for describing other routes of exposure was also evaluated with currently available from literature. Gammon *et al.* (2014) demonstrated that the internal exposure to pyrethroid bifenthrin as measured by plasma and brain Cmax and AUC following a single inhalation of an aerosol was not significantly different from that after equivalent oral dosing (Gammon *et al.*, 2014). These findings indicate that PK of pyrethroids as represented by bifenthrin in their study would be expected to be similar after inhalation and oral dosing. Thus, it is reasonable to assume rapid onset of metabolic clearance restriction following inhalation or IV exposure like that observed after oral exposure. To test this assumption in simulating *in vivo* kinetics following inhalation exposure, from which compounds are delivered directly to the systemic circulation before they reach other tissue compartments, *in vivo* PK data from a single IV dose at 0.5 mg/kg in 0.5 ml/kg glycerol formal in adult rats conducted by the University of Georgia and a published single IV dose study at 1.75 mg/kg in 0.5 ml/kg in glycerol formal (Gray and Rickard, 1982) were simulated. No other model parameters were changed except adding IV infusion to the plasma compartment. The model reasonably well captured the DLM concentrations in plasma, brain and liver in adult rats following a single IV dose especially at early time points when rapid onset of clearance restriction was included (Figure II-10 and -11). It should be noted that there is a potential vehicle effect with IV exposure leading to possible extended retention of the compound in plasma compared to other routes of exposure such as oral ingestion as the compound was dosed with lipophilic vehicle to the plasma. Similar vehicle effects have been reported for lipophilic drug IV dosing studies (Hippalgaonkar *et al.*, 2010; Sakaeda and Hirano, 1995). This potential vehicle effect would not be relevant for oral exposure as the compound is not absorbed together with the vehicle. As evidence by consistent model simulation with measured drug concentration at early time points in plasma, brain and liver following IV administration of DLM, the need for the incorporation of rapid onset of restricted clearance is supported for modeling multi-routes of pyrethroids exposure in addition to oral exposure.

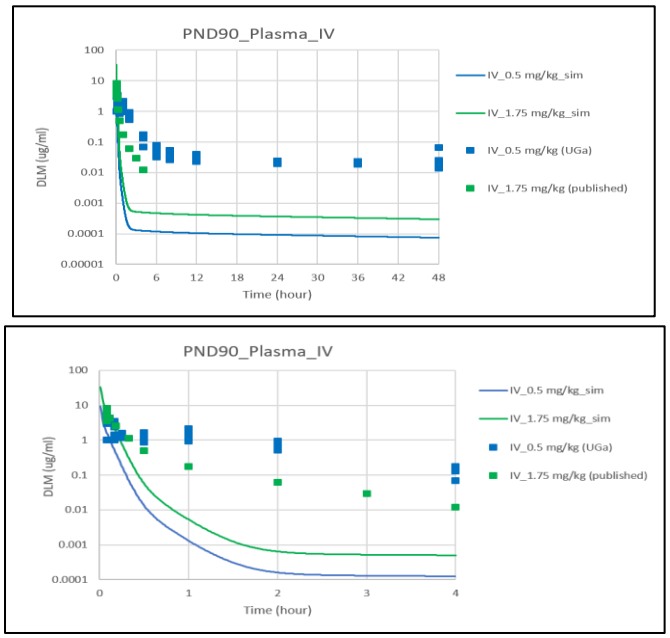

Figure II-10. DLM concentrations in plasma in PND90 rats following a single IV dose - simulation using the new *in vivo* PK data from the University of Georgia (top) and published data (Gray and Rickard, 1982) (bottom).

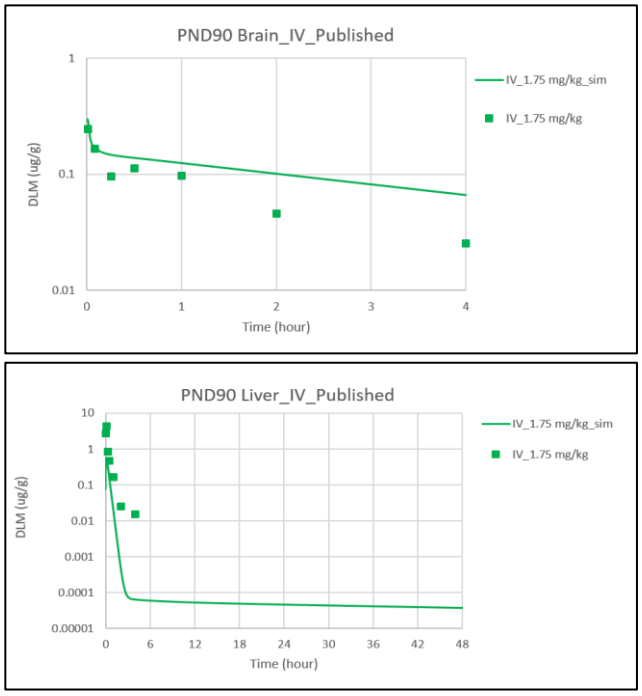

Figure II-11. DLM concentrations in brain and liver in PND90 rats following a single IV dose - simulation using the published data (Gray and Rickard, 1982).

C. Sensitivity analysis

To evaluate the relative impact of each of the model parameters on DLM, CPM and TPM brain Cmax, a sensitivity analysis was performed. The sensitivity coefficient (SC) was calculated as below (Yoon *et al.,* 2009):

SC = Fractional change in model output/ Fractional change in parameter (Eq. II-8)

Each parameter was individually increased only by 1% of their original value with the other parameters held constant. The larger the absolute value of the sensitivity coefficient, the more important the parameter. A sensitivity coefficient of 1 represents 1:1 relationship between the change in the parameter and the internal dose metric of choice. A negative SC indicates the given parameter influences the dose metric in an inverse direction. The SCs are grouped in three categories, high (absolute values greater than or equal to 0.5), medium (absolute values greater than or equal to 0.2 but less than 0.5), or low (absolute values greater than or equal to 0.1 but less than 0.2), according to the IPCS guideline (World Health Organization, 2010)

Sensitivity of model parameters was examined in the rat model for the brain maximum concentration (Cmax) at 8 hours after high and low oral doses of DLM, CPM, and TPM in a volume of 5 ml/kg corn oil. For DLM, 0.1 and 0.5 mg/kg were used in PND15 and PND90 rats; for CPM, 15 and 45 mg/kg in PND15 rats and 60 and 120 mg/kg in PND90 rats were examined; for TPM, 120 and 300 mg/kg in PND15 rats and 300 and 600 mg/kg in PND90 rats were evaluated. Results from the sensitivity analysis are in the EXCEL entitled "Sensitivity_analysis_DLM_CPM_TPM_Rat.xlsx". The most sensitive parameters are the brain to plasma PC (PBRN) as well as unbound fraction in plasma (FuPLS) and KMF as they affect metabolism in plasma and liver. The analysis showed that physiological parameters including body weight, cardiac output, hematocrit, blood volume, and liver blood flow are medium sensitivity parameters. Parameters for absorption and plasma metabolism are also medium sensitivity parameters. Note that hepatic metabolism parameters showed medium sensitivity in juvenile rats, but low to no sensitivity in adult rats. This doesn't mean that metabolism is not influential in brain Cmax in adult rats, but indicates that in adult rats, metabolism is so efficient, *i.e.,* Clint_*vivo* well exceeds liver plasma flow (Appendix 5), that a 1% increase wouldn't make a difference as it is largely limited by liver blood flow, which is one of the sensitive parameters. In juvenile rats, metabolism is governed by both liver blood flow and intrinsic metabolic activity and thus, a small change in intrinsic metabolism parameters can now result in a noticeable impact. Note that plasma flow is proportional to blood flow.

D. Model outputs

a. Clearance

The hepatic clearances (Clh) for DLM, CPM, and TPM was calculated using the Eq. II-7 (Table II-6) as described in 'Rats_PYR_clearance_calculation.xlsx'. The Clh is determined by four factors, *in vivo* hepatic Clint, hepatic blood flow, unbound fraction in plasma, and the KMF. Ontogeny of metabolic activity was evident for all three pyrethroids with Clh increasing with age (Table II-6). Note that the apparent Km values were used in this study. If any refinement would need to be made, the apparent Km values can be adjusted based on the extent of binding experimentally determined in the *in vitro* incubation mixture (*i.e.,* free fractions in the microsomes, cytosol, or plasma incubation systems) and the congruence with *in vivo* kinetic data. As the Km and KMF are inversely associated in our model, these updates are not expected to change the model outcomes substantially regardless of the age of animals or the pyrethroid identity.

Table II-6. *In vitro*-based total hepatic Clint and model predicted hepatic clearance in rats

Parameter	DLM		CPM		TPM		unit
	PND15	PND90	PND15	PND90	PND15	PND90	
Total hepatic Clint (Clint_*vivo*)	0.16	6.99	0.24	12.25	1.30	41.67	L/h
Hepatic clearance (Clh)	0.027	0.407	0.039	0.465	0.113	0.537	L/h

b. Plasma and brain Cmax at different ages

The model for DLM, CPM and TPM were run to simulate the PK studies conducted by the University of Georgia (single oral dose for DLM, CPM, and TPM in PND15 and PND90 rats). Concentration-time profiles of DLM, CPM and TPM in the plasma and brain, target tissue, of rats at different ages following different doses as used in these studies were simulated and brain Cmax for each dosing scenario was generated (Figure II-12). The results for DLM suggest that brain Cmax was about 2-fold higher in PND15 than in PND 90 rats at doses of 0.25 mg/kg and 0.5 mg/kg (Figure II-12, Top). Plasma and brain Cmax in juvenile and adult rats under the different dosing conditions used in *in vivo* PK studies were presented for CPM and TPM as well (Figure II-12, Middle and Bottom)

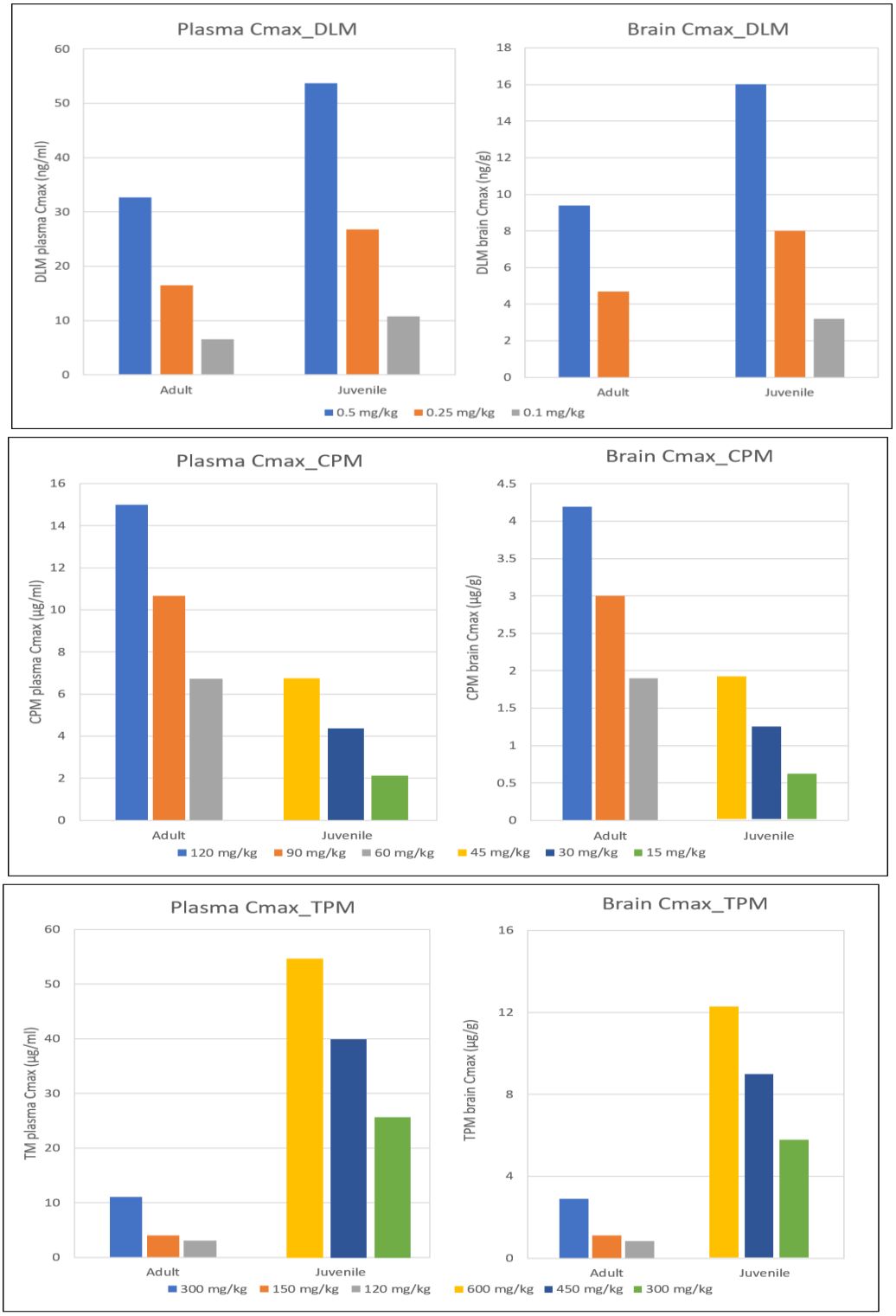

Figure II-12. Model predicted plasma and brain Cmax for DLM, CPM and TPM in PND15 and PND90 rats.

c. Comparison of dose-response

The model for DLM were run with the various dosing scenarios (single oral dose of 0.001- 10 mg/kg) in PND15 and PND90 rats to demonstrate the capability of each model to simulate age-difference in impacts of metabolic saturation on pyrethroid internal exposure levels at the target tissue. Note that the dose-range used in this analysis is simply for a demonstration purpose, as the higher end of the dose range used here would already be at a lethal level for juvenile animals. Cmax values were used for comparison of dose-response at different ages as they are considered to be correlated with the neurotoxic effects of pyrethroids (Moser *et al.* 2016; Scollon *et al.* 2011). Cmax values at different ages following oral doses are described in Figure II-13. The difference between juvenile and adult increases become larger as the metabolism is approaching saturation in juvenile rats.

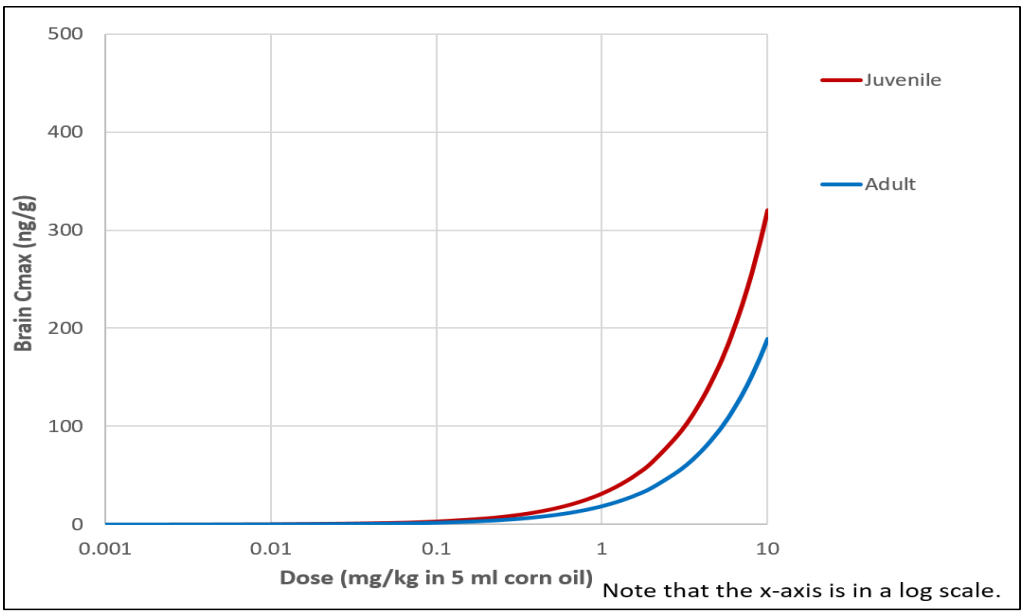

Figure II-13. Simulation of dose-dependent brain Cmax profiles of pyrethroids in PND15 and PND90 rats.

E. Estimation of the internal dose at Point of departure (POD)

The POD was selected from the Benchmark Dose (BMD) Analysis of the Wolansky *et al.* 2006 data (DER #D422817, US EPA), where individual dose-response curves for *in vivo* motor function in adult rats were characterized and relative potencies for eleven commonly used pyrethroids were calculated. All the pyrethroids tested in their study, including DLM, CPM and TPM, induced a dose-dependent decrease in motor activity. The Lowest Benchmark Dose at 1 standard deviation ($BMDL_{1SD}$) was used as POD, which was equal to 1.49 and 44.4 mg/kg BW for DLM and permethrins

including CPM and TPM, respectively. The rat PBPK model was used to estimate the brain tissue internal dose (brain Cmax) in the adult rat at the respective external POD in rats for DLM, CPM, and TPM. It is noted that corn oil at a volume of 1 ml/kg BW was used as oral gavage vehicle in the Wolansky *et al.* (2006) study, whereas corn oil at a volume of 5 ml/kg BW was used for new *in vivo* studies conducted by the University of Georgia. Impacts of the vehicle volume used for oral gavage on DLM kinetics were reported by Chen *et al.* (2015). They showed that pharmacokinetic parameters of 1 mg/kg DLM in different vehicles including 5 ml/kg corn oil, 1 ml/kg corn oil, and 1 ml/kg glycerol formal appear to be affected by vehicle type (corn oil vs. glycerol formal), but not by vehicle volume (Chen *et al.*, 2015). Thus, we used the gut absorption parameters estimated using the new *in vivo* PK data following various oral doses of DLM using corn oil at a volume of 5 ml/kg BW. The simulation results are summarized in Table II-7. Reverse dosimetry was conducted using the human life stage PBPK model to determine the equivalent external exposure level that yields the target tissue internal exposure to the estimated rat internal exposure above at a given age and for a given exposure route in humans (Section III). Note that we used one single internal exposure estimated in the adult rat brain at the $BMDL_{1SD}$ for each pyrethroid to conduct reverse dosimetry for both early and adult ages in humans.

Table II-7. Estimated adult brain tissue internal dose at the reported BMDL as POD in adult rats from EPA DER based on the BMD analysis of the Wolansky *et al.* (2006) data.

Exposure	DLM	CPM	TPM	Notes
External POD in rats (mg/kg)*	1.49	44.4	44.4	EPA DER (D422817) of Wolansky *et al.*, 2006
Brain Cmax (ng/g)	28.28	1,371.80	279.87	PND90 simulated

* The external PODs for cis- and trans-permethrin were obtained from the rat study where the rats were dosed with a 40:60 mixture of cis-:trans-permethrin.

F. Discussion

The case-studies in rats were intended to serve as proof-of-concept to demonstrate the validity of IVIVE approach for the development of life stage PBPK models for pyrethroids. The IVIVE-PBPK model performed reasonably well for describing plasma and brain internal exposure of DLM, CPM, and TPM in juvenile rats as well as in adult rats at different doses. These findings support the application of a similar approach of using *in vitro*-derived kinetic, especially age-specific metabolism, information to parameterize the age-specific PBPK models for different species, *e.g.,* humans.

From the perspective of applying PBPK models to support risk assessments for pyrethroids, one of the most important findings from our rat modeling case studies is the demonstration of the validity of the use of a single generic model structure for pyrethroids as a group, as well as a common set of parameters apart from compound-specific metabolism. This conclusion is also supported by other evidences, including the similarity of the half-lives of several pyrethroids in humans and rats (Ratelle *et al.,* 2015; Starr *et al.,* 2014). Therefore, a read-across approach can be used to predict internal exposure to other pyrethroids using the generic model developed and evaluated with the case study compounds together with targeted *in vitro* metabolism studies.

The current model is able to recapitulate both the published and newly collected *in vivo* PK data, indicating that with appropriate parameterization, the model is robust in simulating different exposure conditions. In addition to oral exposure, the model was able to reproduce the DLM concentrations in plasma, brain and liver in adult rats following a single IV dose. Despite the caveat of IV data due to potential vehicle effects (*i.e.,* extended retention of the compound in plasma due to vehicle partitioning), comparison of published DLM concentration-time course data in plasma and tissues to our simulation results shows that our model can reasonably recapitulate pyrethroid kinetics after a non-oral exposure. Moreover, this agreement between model simulation and *in vivo* PK data provides greater confidence in the model assumptions regarding the restricted clearance of pyrethroids *in vivo* and the description of free pyrethroid concentration in the *in vitro* and *in vivo* systems. Collectively, these findings support the use of the rat model structure as a generic structure to simulate pyrethroid kinetics with different routes of exposure in humans.

From the *in vitro* studies conducted to date by the CAPHRA research team, we discovered that the free concentration *in vitro* appears to be largely affected by system-specific factors, such as slowly-reversible binding. In fact, previously-reported Km values in the literature for DLM metabolism in rat

microsomes are much higher compared to those collected in a more refined condition to reduce the effects of non-specific binding to the extent possible (Anand *et al.*, 2006a and Anand *et al.*, 2006b; LFR report 5503/6). When corrected for non-specific binding, however, they become comparable to the results from LFR. Previously collected preliminary data by LFR (Appendix 8 of LFR report 5503/6) demonstrated that the apparent Km depends on protein concentrations used for the incubation and that the apparent Clint appeared to reach a plateau at approximately 0.02 mg/ml microsomal or cytosolic protein/ml incubation mixture, indicating that the apparent Km values collected using 0.1 mg/ml microsomal or cytosolic protein/ml would likely be higher than 'true' Km values. We tested the impact of lowering Km by using 3-fold lower Km values than the apparent ones we currently used (Appendix 9 and 10) and the overall age-related differences in target tissue concentrations remain the same. As the Km and KMF are inversely associated in our model, updating the apparent Km to true Km values will not change the model outcomes regardless of the age of animals or the pyrethroid identity. Therefore, the current version of the model is considered adequate to demonstrate the concept and evaluate model performance regarding the validity of using *in vitro* data for pyrethroids in general.

In conclusion, this case study in rats demonstrated the proof-of-concept for using IVIVE in PBPK model development for pyrethroids and using a metabolism-based read-across approach in building a PBPK model for this group of compounds to predict internal exposure in different populations of various ages. Therefore, the rat model structure together with the IVIVE-based model parameterization strategies were used for human life stage models for DLM and CPM as described in the subsequent sections of this white paper.

G. References

Anand, S.S., Bruckner, J.V., Haines, W.T., Muralidhara, S., Fisher, J.W., and Padilla, S. 2006a. Characterization of deltamethrin metabolism by rat plasma and liver microsomes. *Toxicol Appl Pharmacol.* 212(2):156-166.

Anand, S.S., Kim, K.B., Padilla, S., Muralidhara, S., Kim, H.J., Fisher, J.W., and Bruckner, J.V. 2006b. Ontogeny of hepatic and plasma metabolism of deltamethrin *in vitro*: role in age-dependent acute neurotoxicity. *Drug Metab Dispos.* 34(3):389-397.

Amaraneni, M., Sharma, A., Pang, J., Muralidhara, S., Cummings, B.S., White, C.A., Bruckner, J.V., and Zastre J. 2016. Plasma protein binding limits the blood brain barrier permeation of the pyrethroid insecticide, deltamethrin. *Toxicol Lett.* 250-251:21-28.

Brown, R.P., Delp, M.D., Lindstedt, S.L., Rhomberg, L.R., and Beliles, R.P. 1997. Physiological parameter values for physiologically based pharmacokinetic models. *Toxicol Ind Health.* 13(4):407-484.

Campbell, A. 2009. Development of PBPK model of molinate and molinate sulfoxide in rats and humans. *Regul Toxicol Pharmacol.* 53(3):195-204.

Chen, C. 2015. Toxicokinetics of deltamethrin in rats: vehicle, dosage, and age dependency (Unpublished master thesis). The University of Georgia, Athens, Georgia.

Clewell, H.J., and Andersen, M.E. 1985. Risk assessment extrapolations and physiological modeling. *Toxicol. Ind. Health* 1(4):111 131.

Clewell H.J., and Andersen ME. 1994. Physiologically-based pharmacokinetic modeling and bioactivation of xenobiotics. *Toxicol Ind Health* 10(1-2):1-24.

Clewell, R.A., and Clewell, H.J. 2008. Development and Specification of Physiologically Based Pharmacokinetic Models for Use in Risk Assessment. *Regul. Toxicol. Pharmacol.* 50(1):129-143.

Crow, J.A., Borazjani, A., Potter, P.M., Ross, M.K. 2007. Hydrolysis of pyrethroids by human and rat tissues: examination of intestinal, liver and serum carboxylesterases. *Toxicol Appl Pharmacol.* 221(1):1-12.

Davies, B., and Morris, T. 1993. Physiological parameters in laboratory animals and humans. *Pharm Res* 10(7):1093-1095.

Gammon, D., Liu, Z., Chandrasekaran, A., and ElNaggar, S. 2014. The pharmacokinetic properties of bifenthrin in the rat following multiple routes of exposure. *Pest Manang Sci*. 71(6):835-841.

Godin, S.J., Crow, J.A., Scollon, E.J., Hughes, M.F., DeVito, M.J., and Ross, M.K. 2007. Identification of rat and human cytochrome p450 isoforms and a rat serum esterase that metabolize the pyrethroid insecticides deltamethrin and esfenvalerate. *Drug Metab Dispos*. 35(9):1664-71.

Gray, A.G., and Rickard, J. 1982. The toxicokinetics of deltamethrin in rats after intravenous administration of a toxic dose. *Pest Biochem Physiol*. 18(2):205-215.

Hippalgaonkar, K., Majumdar, S., and Kansara, V. 2010. Injectable lipid emulsions -Advancements, opportunities and challenges. *AAPS PharmSciTech*. 11(4):1526-1540.

Hissink, A.M., Van Ommen, B., Krüse, J., and Van Bladeren, P.J. 1997. A physiologically based pharmacokinetic (PB-PK) model for 1,2-dichlorobenzene linked to two possible parameters of toxicity. *Toxicol Appl Pharmacol*. 145(2):301-310.

Houston, J.B. and Galetin, A. 2008. Methods for predicting *in vivo* pharmacokinetics using data from *in vitro* assays. *Curr Drug Metab*. 9(9):940-951.

Johnson, T. N., Rostami-Hodgegan, A., and Tucker, G.T. 2006. Prediction of the clearance of eleven drugs and associated variability in neonates, infants, and children. *Clin. Pharmacokinet*. 45(9):931-956.

Kedderis, G.L., Carfagna, M.A., Held, S.D., Batra, R., Murphy, J.E., and Gargas, M.L. 1993. Kinetic analysis of furan biotransformation by F-344 rats in vivo and in vitro. *Toxicol Appl Pharmacol*. 123(2):274-282.

Kedderis, G.L., and Held, S.D. 1996. Prediction of furan pharmacokinetics from hepatocyte studies: comparison of bioactivation and hepatic dosimetry in rats, mice, and humans. *Toxicol Appl Pharmacol*. 140(1):124-130.

Kim, K.-B., Anand, S.S., Kim, H.J., White, C.A., Fisher, J.W., Tornero-Velez, R., and Bruckner, J.V. 2010. Age-, Dose-and Time-Dependency of Plasma and Tissue Distribution of Deltamethrin in Immature Rats. *Toxicol Sci.* 115(2):354-368.

Kramer, H.J., van den Berg, M., Delang, R.J., Brandsma, L., and Dejongh, J. Biotransformation rates of Ugilec 141 (tetrachlorobenzyltoluenes) in rat and trout microsomes. 2000. *Chemosphere*. 40(9-11):1283-8.

Lam, G., Chen, M.L., and Chiou, W.L. 1982. Determination of tissue to blood partition coefficients in physiologically- based pharmacokinetic studies. *J Pharm Sci* 714(4):454-456.

Lipscomb, J.C., Fisher, J.W., Confer, P.D., and Byczkowski, J.Z. 1998. In vitro to in vivo extrapolation for trichloroethylene metabolism in humans. *Toxicol Appl Pharmacol.* 152(2): 376-387.

Loizou, G.D., Jones, K., Akrill, P., Dyne, D., and Cocker, J. 1999. Estimation of the dermal absorption of m-xylene vapor in humans using breath sampling and physiologically based pharmacokinetic analysis. *Toxicol Sci.* 48(2):170-179.

Loizou, G., Spendiff, M., Barton, H.A., Bessems, J., Bois, F.Y., d'Yvoire, M.B., Buist, H., Clewell, H.J., 3rd, Meek, B., Gundert-Remy, U., Goerlitz, G., and Schmitt, W. 2008. Development of good modelling practice for physiologically based pharmacokinetic models for use in risk assessment: The first steps. *Regul. Toxicol. Pharmacol.* 50(3):400-411.

Mirfazaelian, A., Kim, K.-B., Anand, S.S., Kim, H.J., Tornero-Velez, R., Bruckner, J.V., and Fisher, J.W. 2006. Development of a physiologically based pharmacokinetic model for deltamethrin in the adult male Sprague-Dawley rat. *Toxicol Sci.* 93(2)432-442.

Mirfazaelian, A., and Fisher, J.W. 2007. Organ growth functions in maturing male Sprague-Dawley rats based on a collective database. *J Toxicol Environ Health A.* 70(12):1052-63.

Moser, V.C., Liu, Z., Schlosser, C., Spanogle, T.L., Chandrasekaran, A., and McDaniel, K.L. 2016. Locomotor activity and tissue levels following acute administration of lambda- and gamma-cyhalothrin in rats. *Toxicol Appl Pharmacol.* 313: 97-103.

National Center for Biotechnology Information. PubChem Compound Database; CID=40585, https://pubchem.ncbi.nlm.nih.gov/compound/40585 (accessed Apr. 29, 2017)

National Center for Biotechnology Information. PubChem Compound Database; CID=40326, https://pubchem.ncbi.nlm.nih.gov/compound/40326 (accessed Apr. 29, 2017)

National Research Council (NRC). 1987. Pharmacokinetics in risk assessment. Drinking water and health. Volume 8. National Academy Press, Washington D.C.

Ploemen, J.P., Wormhoudt, L.W., Haenen, G.R., Oudshoorn, M.J., Commandeur, J.N., Vermeulen, N.P., de Waziers, I., Beaune, P.H., Watabe, T., and van Bladeren, P.J. 1997. The use of human in vitro metabolic parameters to explore the risk assessment of hazardous compounds: the case of ethylene dibromide. *Toxicol Appl Pharmacol.* 143(1):56-69.

Poulin, P. and Haddad, S. 2012. Advancing prediction of tissue distribution and volume of distribution of highly lipophilic compounds from a simplified tissue composition-based model as a mechanistic animal alternative method. *J Pharm Sci.* 101:2250-2261.

Pritchett, J.J., Kuester, R.K., and Sipes, I.G. 2002. Metabolism of bisphenol a in primary cultured hepatocytes from mice, rats, and humans. *Drug Metab Dispos.* 30(11):1180-1185.

Punt, A., Jeurissen, S.M., Boersma, M.G., Delatour, T., Scholz, G., Schilter, B., van Bladeren, P.J., and Rietjens, I.M. 2010. Evaluation of human interindividual variation in bioactivation of estragole using physiologically based biokinetic modeling. *Toxicol Sci.* 113(2):337-348.

Punt, A., Paini, A., Boersma, M.G., Freidig, A.P., Delatour, T., Scholz, G., Schilter, B., van Bladeren, P.J., and Rietjens, I.M. 2009. Use of physiologically based biokinetic (PBBK) modeling to study estragole bioactivation and detoxification in humans as compared with male rats. *Toxicol Sci.* 110(2):255-269.

Ratelle, M., Cote, J., and Bouchard, M. 2015. Time profiles and toxicokinetic parameters of key biomarkers of exposure to cypermethrin in orally exposed volunteers compared with previously available kinetic data following permethrin exposure. *J Appl Toxicol.* 35(12):1586-1593.

Rodriguez, C.E., Mahle, D.A., Gearhart, J.M., Mattie, D.R., Lipscomb, J.C., Cook, R.S., and Barton, H.A. 2007. Predicting age-appropriate pharmacokinetics of six volatile organic compounds in the rat utilizing physiologically based pharmacokinetic modeling. *Toxicol Sci.* 98(1):43-56.

Rostami-Hodjegan, A. and Tucker, G.T. 2007. Simulation and prediction of in vivo drug metabolism in human populations from in vitro data. Nat. Rev. *Drug Discovery*. 6(2):140-148.

Sakaeda, T. and Hirano, K. 1995. O/W lipid emulsions for parenteral drug delivery. II. Effect of composition on pharmacokinetics of incorporated drug. *J Drug Target*. 3(3):221-230.

Scollon, E.J., Starr, J.M., Godin, S.J., DeVito, M.J., and Hughes, M.F. 2009. In vitro metabolism of pyrethroid pesticides by rat and human hepatic microsomes and cytochrome P450 isoforms. *Drug Metab Dispos*. 37(1):221-228.

Scollon, E.J., Starr, J.M., Crofton, K.M., Wolansky, M.J., DeVito, M.J., and Hughes, M.F. 2011. Correlation of tissue concentrations of the pyrethroid bifenthrin with neurotoxicity in the rat. *Toxicology*. 290(1):1-6.

Sheets, L.P., Doherty, J.D., Law, M.W., Reiter, L.W. and Crofton, K.M. 1994 Age-dependent differences in the susceptibility of rats to deltamethrin. *Toxicol. Appl. Pharmacol*. 126(1):186-190.

Song, G., Peeples, C.R., Yoon, M., Wu, H., Verner, M.A., Andersen, M.E., Clewell, H.J. 3rd, and Longnecker, MP. 2016. Pharmacokinetic bias analysis of the epidemiological associations between serum polybrominated diphenyl ether (BDE-47) and timing of menarche. *Environ Res*. 150:541-548.

Starr, J.M., Graham, S.E., Ross, D.G., Tonero-Velez, R., Scollon, E.J., DeVito, M.J., Crofton, K.M., Wolansky, M.J., and Hughes, M.F. 2014. Environmentally relevant mixing ratios in cumulative assessments: a study of the kinetics of pyrethroids and their ester cleavage metabolites in blood and brain; and the effect of a pyrethroid mixture on the motor activity of rats. *Toxicology*. 320:15-24.

Stulcová, B. 1977. Postnatal development of cardiac output distribution measured by radioactive microspheres in rats, *Biol Neonate*. 32(3-4):119-124.

Timchalk, C., and Poet, T.S. 2008. Development of a physiologically based pharmacokinetic and pharmacodynamic model to determine dosimetry and cholinesterase inhibition for a binary mixture of chlorpyrifos and diazinon in the rat. *Neurotoxicology*. 29(3):428-443.

Tornero-Velez, R., Mirfazaelian, A., Kim, K.-B., Anand, S.S., Kim, H.J., Haines, W.T., Bruckner, J.V., and Fisher, J.W. 2010. Evaluation of deltamethrin kinetics and dosimetry in the maturing rat using a PBPK model. *Toxicol Appl Pharmacol.* 244(2):208-217.

US EPA 2015. Guidance for Applying Quantitative Data to Develop Data-Derived Extrapolation Factors for Interspecies and Intraspecies Extrapolation. https://www.epa.gov/sites/production/files/2015-01/documents/ddef-final.pdf

Verner, M.A., Loccisano, A.E., Morken, N.H., Yoon, M., Wu, H., McDougall, R., Maisonet, M., Marcus, M., Kishi, R., Miyashita, C., Chen, M.H., Hsieh, W.S., Andersen, M.E., Clewell, HJ 3rd., and Longnecker, M.P. 2015. Associations of Perfluoroalkyl Substances (PFAS) with Lower Birth Weight: An Evaluation of Potential Confounding by Glomerular Filtration Rate Using a Physiologically Based Pharmacokinetic Model (PBPK). *Environ Health Perspect.* 123(12):1317-1324.

Wolansky, M.J., Gennings, C., and Crofton, K.M. 2006. Relative potencies for acute effects of pyrethroids on motor function in rats. *Toxicol Sci.* 89(1):271-7.

World Health Organization (WHO) Characterization and Application of Physiologically Based Pharmacokinetic Models in Risk Assessment. 2010. Geneva, Switzerland: World Health Organization, International Programme on Chemical Safety.

Wu, H., Yoon, M., Verner, M.A., Xue, J., Luo, M., Andersen, M.E., Longnecker, M.P., and Clewell, H.J. 3rd. 2015. Can the observed association between serum perfluoroalkyl substances and delayed menarche be explained on the basis of puberty-related changes in physiology and pharmacokinetics? *Environ Int.*82:61-68.

Yoon, M., Madden, M.C., and Barton, H.A. 2006. Developmental expression of aldehyde dehydrogenase in rat: a comparison of liver and lung development, *Toxicol Sci*, 89(2):386-398.

Yoon, M., Nong, A., Clewell, H.J., Taylor, M.D., Dorman, D.C., and Andersen, M.E. 2009. Lactational transfer of manganese in rats: predicting manganese tissue concentration in the dam and pups from inhalation exposure with a pharmacokinetic model, *Toxicol Sci*, 112(1):23-43.

Yoon, M., Campbell, J.L., Andersen, M.E., and Clewell, H.J. 2012. Quantitative *in vitro* to *in vivo* extrapolation of cell-based toxicity assay results. *Crit Rev Toxicol.* 42(8):633-652.

https://www.ncbi.nlm.nih.gov/pubmed/22667820

Yoon, M., and Clewell, HJ 3rd. 2016. Addressing Early Life Sensitivity Using Physiologically Based Pharmacokinetic Modeling and in vitro to in vivo Extrapolation. *Toxicol Res.* 32(1):15-20. (PDF appended – open access for non-profit use)

https://www.ncbi.nlm.nih.gov/pmc/articles/PMC4780231/

H. List of the appended files for the rat model

1. Model folder "R submission_Rat"

a. This is the current version of the pyrethroid growing rat model in R as of July 18th, 2017. Model file (model. R) is saved in the folder named 'Model' and parameter files for DLM, CPM, and TPM simulations in PND15 and PND90 rats following oral or IV exposures are saved in the folders named 'DLM', 'CPM', or 'TPM' respectively. R files are included in the folder named 'Scenarios' to simulate plasma and tissue concentration profiles of DLM, CPM, or TPM at a given exposure scenario in rats at specific age.

b. Installing R, R studio and packages needed to run models

Installing R

1. In a web-browser, navigate to https://cran.r-project.org/
2. Select "Download R for Windows" under "Download and Install R"
3. Select "Install R for the first time"
4. Select "Download R 3.(version) for Windows "
5. Save and run the installer file

Installing Rstudio

1. In a web-browser navigate to https://www.rstudio.com/
2. On the homepage select Download Rstudio
3. Download the open source license version of Rstudio (first from left)
4. Select windows installer (Under Installers -> RStudio 1.(ver) – Windows Vista /7/8/10
5. Save and Run the executable file

Installing Packages:

1. Run Rstudio
2. Select Packages tab from the bottom right panel in RStudio
3. Select Install in the packages tab
4. Under packages enter deSolve and select install

This will setup the environment needed to run the models

c. Copy the whole model folder (RSubmission_Rat) and open a specific file in the folder named 'Scenarios' in RStudio. Change and set the working directory to where you downloaded the scripts (All the \ need to be replaced by a /). In all scenario files, appropriate paramFile from DLM, CPM, and TPM folders corresponding to the selected exposure scenario is currently defined. To run the scenario file selected, click on Source. There are 25 scenario files for simulations of DLM, CPM, and TPM *in vivo* PK data in rats at specific age as described as below:

Scenario file in R	Note
DLM_Oral_Scenario1_90d	It is to simulate new *in vivo* DLM PK in PND90 rats after oral dose at 0.5 mg/kg
DLM_Oral_Scenario2_90d	It is to simulate new *in vivo* DLM PK in PND90 rats after oral dose at 0.25 mg/kg
DLM_Oral_Scenario3_90d	It is to simulate new *in vivo* DLM PK in PND90 rats after oral dose at 0.1 mg/kg
DLM_Oral_Scenario4_15d	It is to simulate new *in vivo* DLM PK in PND15 rats after oral dose at 0.5 mg/kg
DLM_Oral_Scenario5_15d	It is to simulate new *in vivo* DLM PK in PND15 rats after oral dose at 0.25 mg/kg
DLM_Oral_Scenario6_15d	It is to simulate new *in vivo* DLM PK in PND15 rats after oral dose at 0.1 mg/kg
DLM_Oral_Scenario_PUB1_90d	It is to simulate published DLM PK in PND90 rats after oral dose at 2 mg/kg
DLM_Oral_Scenario_PUB2_90d	It is to simulate published DLM PK in PND90 rats after oral dose at 10 mg/kg
DLM_Oral_Scenario_PUB3_10d	It is to simulate published DLM PK in PND10 rats after oral dose at 0.4 mg/kg
DLM_Oral_Scenario_PUB4_10d	It is to simulate published DLM PK in PND10 rats after oral dose at 2 mg/kg
DLM_Oral_Scenario_PUB5_10d	It is to simulate published DLM PK in PND10 rats after oral dose at 10 mg/kg

DLM_IV_Scenario1_90d	It is to simulate new *in vivo* DLM PK in PND90 rats after IV dose at 0.5 mg/kg
DLM_IV_Scenario2_90d	It is to simulate published DLM PK in PND90 rats after IV dose at 1.75 mg/kg
CPM_Oral_Scenario1_90d	It is to simulate new *in vivo* CPM PK in PND90 rats after oral dose at 60 mg/kg
CPM_Oral_Scenario2_90d	It is to simulate new *in vivo* CPM PK in PND90 rats after oral dose at 90 mg/kg
CPM_Oral_Scenario3_90d	It is to simulate new *in vivo* CPM PK in PND90 rats after oral dose at 120 mg/kg
CPM_Oral_Scenario4_15d	It is to simulate new *in vivo* CPM PK in PND15 rats after oral dose at 15 mg/kg
CPM_Oral_Scenario5_15d	It is to simulate new *in vivo* CPM PK in PND15 rats after oral dose at 30 mg/kg
CPM_Oral_Scenario6_15d	It is to simulate new *in vivo* CPM PK in PND15 rats after oral dose at 45 mg/kg
TPM_Oral_Scenario1_90d	It is to simulate new *in vivo* TPM PK in PND90 rats after oral dose at 120 mg/kg
TPM_Oral_Scenario2_90d	It is to simulate new *in vivo* TPM PK in PND90 rats after oral dose at 150 mg/kg
TPM_Oral_Scenario3_90d	It is to simulate new *in vivo* TPM PK in PND90 rats after oral dose at 300 mg/kg
TPM_Oral_Scenario4_15d	It is to simulate new *in vivo* TPM PK in PND15 rats after oral dose at 300 mg/kg
TPM_Oral_Scenario5_15d	It is to simulate new *in vivo* TPM PK in PND15 rats after oral dose at 450 mg/kg
TPM_Oral_Scenario6_15d	It is to simulate new *in vivo* TPM PK in PND15 rats after oral dose at 600 mg/kg

d. Model outputs include simulation results named 'SimResults.csv' which will be saved in the same folder named 'RSubmission_Rat'. In addition, brain max concentration and plasma

max concentration as well as CLINT_VIVO_ESTIMATED and *in vivo* hepatic clearance (Clh) will be provided.

2. IVIVE calculations 'Rats_PYR_Clearance_calculation.xlsx'

   This EXCEL file contains the ontogeny data, scaling factors and IVIVE clearance calculations for DLM, CPM, and TPM in PND15 and PND90 rats.

3. Sensitivity analysis table "Sensitivity_analysis_DLM_CPM_TPM_Rat"

   This EXCEL file contains the sensitivity coefficient for the parameters used in the PBPK model for DLM, CPM and TPM in rats.

III. Age-specific PBPK Models for Deltamethrin and *cis*-Permethrin in Humans

A. Introduction

Pyrethroids are among the most commonly used insecticides. They act on the neural system principally by interfering with sodium-gated ion channels (Soderlund, 2012). Metabolism plays an important role in detoxification and elimination of pyrethroids in both rats and humans, but species differences exist in the enzymes involved in pyrethroids metabolism (Crow *et al.*, 2007; Godin *et al.*, 2006; Hideo *et al.*, 2012). In rats, pyrethroids are metabolized by several cytochrome P450 (CYP) enzymes and carboxylesterases (CESs) in the liver and by CESs in the plasma. As carboxylesterases are not present in human plasma, no significant hydrolysis of pyrethroids in plasma is expected in humans (Crow *et al.,* 2007). Furthermore, the ontogeny of CYP and CES enzymes that play a major role in pyrethroids metabolism shows substantial species differences between rats and humans (Hines, 2007; Saghir *et al.,* 2012; Yang *et al.,* 2009). Metabolic competency clearly develops much earlier in humans than in rats. In humans, CES enzymes are expressed at adult levels by 3 months of age (Hines *et al.,* 2012; Pope *et al.,* 2005). Some of the CYP enzymes involved in deltamethrin (DLM) and *cis*-permethrin (CPM) metabolism show a rapid increase in their protein expression during the first 5 months of life to levels that are approximately 80% of the adult values (Koukouritaki *et al.,* 2004).

Due to the increased lethality observed in neonatal rats (Sheets *et al.,* 1994), concerns for potentially higher sensitivities to the effect of pyrethroid exposure in infants and children have been raised. However, given the experimental evidence on age-related and species differences in pyrethroid metabolism pathways and their ontogeny described above, it is likely that the differential ontogeny of these enzymes is a key driver for the age-related sensitivity observed in rats after the high dose of DLM. As the pyrethroid metabolizing enzymes are immature in juvenile animals, concentrations of DLM at the target tissue in juvenile rats would have been higher than in adults as the metabolic capacity is getting close to saturation in juvenile animals at the high dose (Anand *et al.,* 2006; Kim *et al.,* 2010). This example clearly shows the limitations of using neonatal animal toxicity studies to infer human early life sensitivity. In addition, other age-dependent physiological changes can affect the clearance of these pyrethroids (blood flow to the liver, renal clearance, protein binding, etc.), which also cannot be adequately accounted for using neonatal animal-based high dose toxicity studies.

To address the question of the potential age-related sensitivity to pyrethroids, human life stage PBPK models for pyrethroids have been developed. PBPK models integrate the three major determinants of pyrethroid internal exposure at different life stages; namely, age-appropriate exposure, age-related changes in physiology, and age-related changes in biochemical processes such as metabolism. The IVIVE approach evaluated in rat modeling (as described in Section II) was similarly applied to the human model development. *In vitro* human metabolism data, for which intrinsic clearance (Clint) values were measured for each enzyme contributing to DLM and CPM metabolism, were collected in human expressed enzymes (see the CXR reports 1575 Deltamethrin Expressed Enzyme Data package and 1575 *Cis*-permethrin Expressed Enzyme Data package). Together with the published enzyme ontogeny data for the enzymes showing metabolic activity to DLM and CPM were used to scale up the *in vitro* Clint values for their *in vivo* counterparts used in the life stage PBPK model for humans. As evaluated in rat modeling, a generic model structure, together with compound-specific metabolism parameters, was used for building life stage human PBPK models for DLM and CPM.

DLM and CPM are the two first case compounds for life stage PBPK modeling of pyrethroids to investigate whether the age-related differences in internal exposure to pyrethroids observed in animal studies are present in humans. In addition to the main goal of the early life sensitivity evaluation based on PK differences, the life stage PBPK model was also used to support risk assessment of pyrethroids as a group. Because of the powerful extrapolation capability of the PBPK models, target tissue exposures to pyrethroids under realistic human exposure scenarios can be simulated and the point of departure values can be derived based on the human relevant information.

B. Modeling approach

a. Structure of the model

The human life stage PBPK model for pyrethroids submitted here has the capability to simulate oral, inhalation and dermal exposures and was used to simulate DLM or CPM kinetics in humans of various ages from birth to adulthood and of both genders. It predicts the internal exposure to DLM or CPM, *e.g.,* concentrations in plasma and brain (the target tissue), at different ages under different exposure scenarios. The rat modeling of DLM and CPM supports the validity of using a metabolism-based read-across approach to build a generic PBPK model for pyrethroids as a group. Apart from metabolism parameters, a single set of chemical specific parameters can describe the kinetics of both pyrethroids reasonably well.

The structure of the human life stage PBPK model for pyrethroids is shown in Figure III-1. The current model can simulate DLM and CPM kinetics through oral ingestion and inhalation in single or multiple daily exposure scenarios. Once it is absorbed, the compound is partitioned to the tissue or metabolized in the liver. To describe the rapid onset of restricted clearance, regardless of exposure routes, ingested pyrethroids enter directly into the plasma compartment, by-passing hepatic first pass metabolism. The portal absorption from gastrointestinal (GI) lumen to GI tissue is currently described as zero accordingly. Key assumptions on the model structure and parameters are based on those evaluated in the rat model (Section II). As described in the rat model section, an empirical adjustment was used to describe the observed restricted clearance of pyrethroids *in vivo*. While work continues on developing a complete understanding of this process, there is much evidence to support the need for the inclusion of the restricted clearance description in the model. The rapid and effective reduction of *in vivo* clearance of pyrethroid to a level that is lower than the anticipated based on its intrinsic capacity determined *in vitro* appears not to be dependent on the identity of pyrethroids, age of animals, or route of exposure, as shown by the applicability of one single empirical adjustment factor (KMF) as discussed in the Section II. It is important to note that the current description of restricted clearance does not imply that clearance of pyrethroids is slow. Although clearance is reduced, pyrethroids are rapidly and completely cleared from the body as indicated by results from human volunteer studies using several pyrethroids (Ratelle *et al.,* 2015a; Ratelle *et al.,* 2015b). The use of the restricted clearance was further supported by the good congruence of the model predicted CPM metabolic clearance as a measure of elimination with the observed metabolites cumulative excretion in the urine of human volunteers.

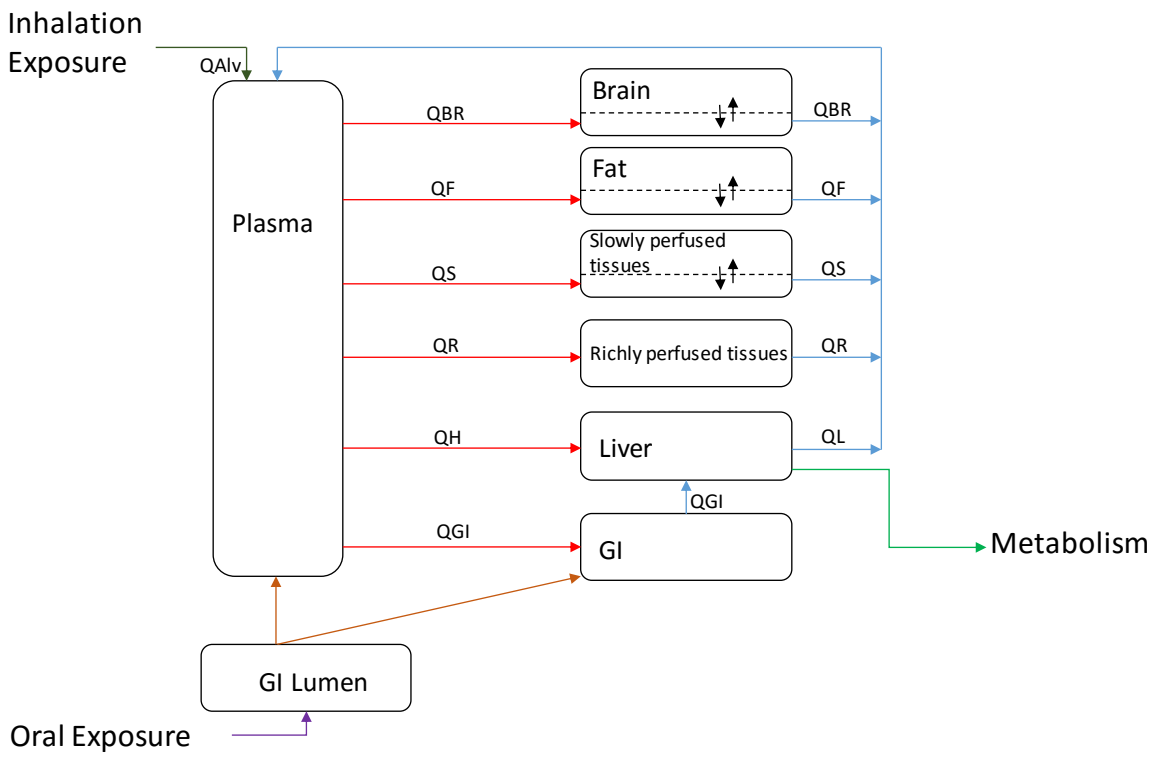

Figure III-1. Structure of the life stage pyrethroid PBPK model.
QGI, QH, QR, QS, QF, QBR refer to blood flow to each tissue compartment. QL is the sum of QGI and QH. QAlv refers to the alveolar ventilation rate. Brain, fat and slowly-perfused tissue compartments are described as diffusion-limited tissues, whereas all other tissue compartments are described as flow limited.

b. Model parameters

i. Life-stage parameters

1. Physiological parameters

Age-specific physiological parameters, including body weight (BW), cardiac output, tissue weights (volumes), and tissue blood flows, were adapted from published life-stage models (Wu *et al.*, 2015; Song *et al.*, 2016; Ruark *et al.*, 2017). As the published life-stage models reported age-specific physiological parameters of females, they were also modified to represent males, based on the most recent population data for physiological parameters from National Health and Nutrition Examination Survey (NHANES, 2005-2006). Growth curves for males and females used for modeling in this white

paper are summarized in the MS EXCEL spreadsheet titled "Life stage parameters_ female.xlsx" and "Life stage parameters_ male.xlsx" and in the supplementary materials. For use in the model simulation, age-specific values for each physiological parameter were computed from these growth curves and were listed for males and females from birth to adulthood in the same spreadsheets.

2. Enzyme ontogeny

In vitro studies performed by the CAPHRA research team indicated that CYP1A2, CYP3A4, CYP2C9, CYP2C19 CYP2B6, CES1m, CES1c, CES2m and CES2c showed activities to DLM or CPM metabolism (CXR reports 1575 Deltamethrin Expressed Enzyme Data package and 1575 *Cis*-permethrin Expressed Enzyme Data package). Here, 'm' represents the CES enzyme in microsomes and 'c' represents that in cytosol. Their ontogeny curves are listed in the Excel worksheets, titled 'CYP1A2', 'CYP3A4', 'CYP2C9', 'CYP2C19', 'CYP2B6', 'CES1m', 'CES1c', 'CES2m' and 'CES2c' within the master life stage metabolism parameter file: "PYR_clearance_calculation.xlsx". CYP3A5 has not been incorporated into the analysis, due to its negligible contribution of less than 1%.

The enzyme ontogeny curves for these enzymes contributing to DLM or CPM metabolism in humans were derived using non-linear regression analyses of the age-specific protein expression data from birth to young adulthood reported in the literature (Hines *et al.,* 2008; Hines *et al.,* 2016, and Song *et al.,* 2016). Lognormal, hyperbola, allosteric-sigmoidal, dose-response and Gompertz growth curves were used, among which the best fit curve was chosen to describe the maturation profiles of each enzyme expression as a fraction of the adult expression. The resulting ontogeny curves for each enzyme are included in their respective worksheets in "PYR_clearance_calculation.xlsx". These ontogeny curves were then utilized for IVIVE, as shown in the 'CL ontogeny' worksheet.

ii. *In vitro* to *in vivo* extrapolation (IVIVE)

The rationale for extrapolating *in vitro* metabolism parameters to *in vivo* is that the capacity of metabolism (*e.g.,* Vmax) can be related between *in vitro* and *in vivo* by considering the total amount of enzyme present in each system. The affinity of metabolism (*e.g.,* Km) can be related by considering free concentration of the compound available for enzyme reaction in each system. Therefore, *in vitro*-measured metabolic constants can be 'scaled-up' to respective *in vivo* metabolism parameters used in the PBPK models by relating enzyme content *in vitro* (*e.g.,* Vmax per mg protein *in vitro*) to that *in vivo* (*e.g.,* Vmax per g liver *in vivo)*. There are several different *in vitro* systems available for metabolism

studies and the IVIVE process required for each system varies. Metabolism IVIVE is an accepted concept and has become common practice in drug PBPK models for pediatrics (Johnson *et al.* 2006).

1. *In vitro* data

Biological scaling (*i.e.*, IVIVE) was used to calculate age-specific intrinsic metabolic clearance (Clint) of the given pyrethroid, based on *in vitro* expressed enzyme Clint data. Together with age-specific enzyme expression data from the ontogeny curves and age-dependent physiological parameters, age-specific hepatic clearance can be estimated within the PBPK model, based on *in vitro* data, without the need for early age metabolism or PK data. Within this framework of IVIVE-based life stage PBPK modeling, both changes in physiological factors (*e.g.,* liver weight, BW, biological scaling factors such as microsomal protein content in the liver) and biochemical factors (*e.g.,* maturation of metabolic enzyme systems) are taken into account when predicting internal exposure in different ages of humans. The expressed enzyme-based IVIVE approach was employed to tackle the challenge of obtaining pediatric liver tissue samples, as well as uncertainties in the *in vitro* metabolic constants. This bottom-up IVIVE approach using expressed enzymes in conjunction with the well-documented database on the ontogeny of human xenobiotic metabolizing enzymes provides a reasonable solution to describe human variability in PK, based on the population variability in metabolism enzyme expression levels (Rostami-Hodjegan and Tucker, 2007; Yoon *et al.,* 2016).

To estimate age-specific total intrinsic metabolic clearance, knowledge of the contribution of each specific metabolic clearance pathway in adults/juveniles and quantitative information regarding the age-related changes in each metabolic clearance pathway *i.e.,* enzyme ontogeny is required. DLM and CPM Clint values were determined in human expressed enzymes *in vitro*, including both CYP and CES enzymes, after screening for any metabolic activity towards DLM or CPM (see the CXR reports 1575 Deltamethrin Expressed Enzyme Data package and 1575 *Cis*-permethrin Expressed Enzyme Data package). The enzymes showing activity toward DLM and CPM metabolism were used for IVIVE.

2. Scaling process

The scaling factors used to conduct IVIVE of human-expressed enzyme Clint results for DLM and CPM are Inter-System Extrapolation Factor (ISEF) and Microsomal Protein Per Gram Liver (MPPGL), Cytosolic Protein Per Gram Liver (CPPGL), and Liver weight (LW), as reviewed by Yoon

et al. (2012) (Table III-1). Typically, the recombinant enzymes are expressed in non-mammalian microsomes. Therefore, it is important to consider the differences in the environment in which the biotransformation enzymes are located in the *in vitro* system, compared to the *in vivo* liver that could result in differences in both substrate availability and enzyme performance. The ISEF integrates the difference in the expression level, as well as the intrinsic activities of the accessory proteins between recombinant systems and human liver microsomes (Chen *et al.* 2011; Proctor *et al.* 2004).

Table III-1. Scaling processes for IVIVE using various *in vitro* metabolism systems (modified from Yoon *et al.,* 2012)

System	Typical units for enzyme content in the system	Scaling factor to whole body
Expressed enzymes	pmol/min/pmol enzyme	(ISEF × CYPabundance or RAF) × MPPGL × LW
Microsomes	nmol/min/mg protein	MPPGL × LW
Cytosol	nmol/min/mg protein	CPPGL × LW
Hepatocytes	nmol/min/10^6 hepatocytes	HPGL × LW
Liver	nmol/min/g liver	LW
Whole body	nmol/min/whole liver	n/a

Notes: LW, liver weight; MPPGL, microsomal protein per gram liver (mg microsomal protein/g liver); CPPGL, cytosolic protein per gram liver (mg cytosolic protein/g liver); HPGL, hepatocellularity per gram liver (number of hepatocytes/g liver).

These values are in the "PYR_clearance_calculation.xlsx" Excel worksheets titled 'CL ontogeny' and 'MPPGL', respectively. ISEF values, listed in the 'CL ontogeny' worksheet, are from Wetmore *et al.*, study (2014) and the age-dependent MPPGL values are from Barter *et al.,* study (2008). Cytosolic Protein Per Gram Liver (CPPGL) was used to perform IVIVE of cytosolic CES1 and 2, whereas MPPGL was used for CYPs and microsomal CESs. Contrary to MPPGL, there is little data available for age-dependent changes in CPPGL in the literature. For the adult, 80.7 mg cytosolic protein/g liver is used (Houston *et al.*, 2008). Assuming that the ratio of MPPGL/CPPGL would be constant across ages, age-specific CPPGL values were calculated and listed in the "PYR_clearance_calculation.xlsx" document under the worksheet titled 'CPPGL'. Note that these scaling factors including MPPGL, CPPGL and LW are incorporated as age-dependent parameters in the model.

3. Age-specific intrinsic clearance calculation

First, total hepatic Clint (L/h) values for DLM and CPM in adults were estimated using the *in vitro* Clint data measured with human adult microsomes and cytosol (see CXR1574 Draft report I Deltamethrin version 4 and CXR1574 Draft report II *cis*-permethrin version 4) through IVIVE as described in Yoon *et al.*, 2012.

Total Clint_*vivo*_adult = Clint_*vitro*_m × MPPGL × LW + Clint_*vitro*_c × CPPGL × LW (Eq. III-1)

Here 'm' and 'c' represent microsomes and cytosol, respectively. The *in vitro* Clint values for the enzymes (CXR reports) showing metabolic activity toward DLM or CPM were scaled up to corresponding *in vivo* enzyme Clint values in adults, using the appropriate scaling factors as described in Eqs. III-2, 3a. and 3b below.

Clint_CYP_*vivo*_adult = Clint_CYP_*vitro* × ISEF_CYP × MPPGL × LW × CYP_abundance (Eq. III-2)

Clint_CES_*vivo*_adult = Clint_CES_*vitro* × ISEF_CES × MPPGL × LW × CES_abundance (Eq. III-3a)

Clint_CES_*vivo*_adult = Clint_CES_*vitro* × ISEF_CES × CPPGL × LW × CES_abundance (Eq. III-3b)

Microsomal CESs were scaled with MPPGL (Eq. III-3a), while cytosolic CESs were scaled with CPPGL (Eq. III-3b). Information of the abundance of each CYP enzyme in adult liver for this calculation was taken from the published meta-analysis of several population studies (Achour *et al.*, 2014). For CES enzymes, the data from Boberg *et al.* (2016) were used. In Boberg *et al.* (2016), the abundance of each CES was given, except for cytosolic CES2 (CES2c). CES2c abundance was calculated based on the relative abundance of this enzyme, compared to the microsomal CES2 (CES2m) using the expression level ratio of CES2m/CES2c from Hines *et al.* (2016). Note that the ISEF values for both subcellular fraction CES enzymes are set to 1 currently, which will be updated once the data become available. However, no major change in the results is expected, as the inter-system differences are largely due to the accessory proteins required for CYP-mediated oxidation reactions, which would not be expected to be a major factor for CES-mediated hydrolysis.

Then the relative contribution of each enzyme to total hepatic Clint for the given pyrethroid in adult liver was calculated using Eq. III-4.

% Contribution = (Clint_enzyme_*vivo*_adult/Total hepatic Clint_*vivo*_adult) *100 (Eq. III-4)

Clint values for each enzyme in the adult liver *in vivo* (Clint_enzyme_*vivo* in Eq. III-4) were calculated using Eq. III-5 below and also illustrated in Figures III-2 to III-5.

Clint_enzyme_*vivo* _adult = Clint_enzyme_*vitro*× ISEF_enzyme × MPPGL or CPPGL × LW × Enzyme abundance_adult (Eq. III-5)

Enzyme ontogeny, expressed as fractions of adult expression over time, was used to scale adult Clint values for each enzyme described above to those for different ages (Figures III-2 to III-5) as described in Eq. III-6.

Clint_enzyme_*vivo*_age *i* = Clint_enzyme_*vitro*× ISEF_enzyme × MPPGL or CPPGL × LW × (Ontogeny_enzyme*Enzyme abundance_adult) (Eq. III-6)

The estimated Clint values for each enzyme in a given age (Clint_enzyme_*vivo* _age *i*) were then summed to calculate the total hepatic Clint for that age (See attached file named: "PYR_clearance_calculation.xlsx").

4. Restricted clearance and age-specific hepatic clearance calculation

In the PBPK model, the total Clint_*vivo*_adult estimated from *in vitro* data (Eq. III-1) is named Clint_*vivo*_estimated. As noted previously in the rat model, an empirical free-concentration adjustment factor (KMF) was applied to adjust the *in vitro*-derived hepatic Clint (referred as Clint_*vivo*_estimated) as below:

Clint_*vivo* = Clint_*vivo*_estimated/KMF (Eq. III-7)

By dividing the estimated Clint with the KMF, we are converting the Clint determined in *in vitro* assays to the corresponding Clint *in vivo* that accounts for *in vivo* free concentration. One single value of KMF was used both for DLM and CPM and for all the ages simulated in this study as this factor was shown to be applicable to describing the observed restricted clearance *in vivo* regardless of pyrethroid identity or age of the animals in the rat study (Section II).

Hepatic clearance (Clh) for a given age was calculated in the PBPK models with the Eq. III-8 as below.

Clh_age *i* = Clint_*vivo*_age *i* × QL_age *i*/(QL_age *i* /FuPLS + Clint_*vivo*_age *i*) **(Eq. III-8)**

Here QL_age *i* is the total liver blood as sum of portal (QGI) and hepatic arterial (QH) flow at a given age and FuPLS is the unbound fraction in the plasma determined *in vitro* (refer to UGA-PB-1 FINAL and UGA-PB-3 FINAL reports). The total unbound fraction determined in plasma of humans of different ages is about 0.1 for both DLM and CPM after 1 month of age.

Note that the Clint *in vitro* and *in vivo* values may be further refined as the data on free concentrations in the *in vitro* incubation become available. This may require minor adjustments in the model, in particular for the KMF value. However, as described in Section II, no significant change in the model outcomes is expected.

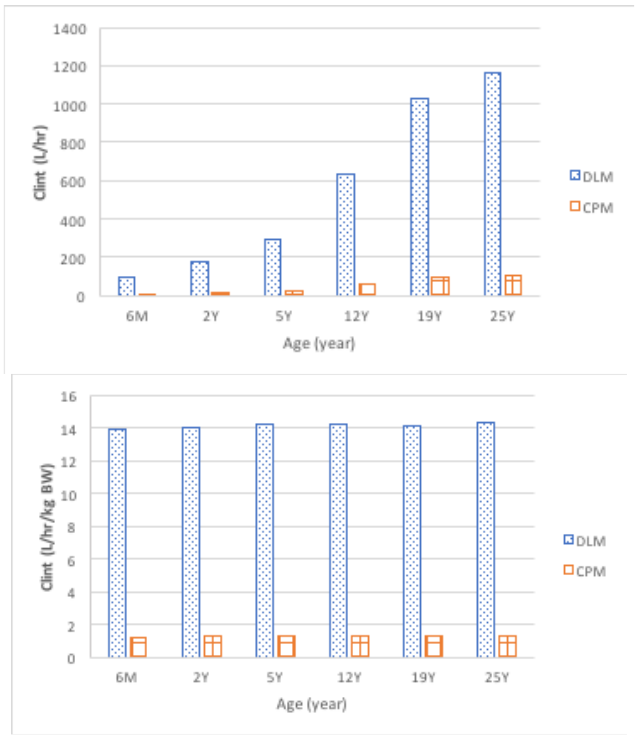

Figure III-2. DLM and CPM intrinsic (Clint) at different ages in males.

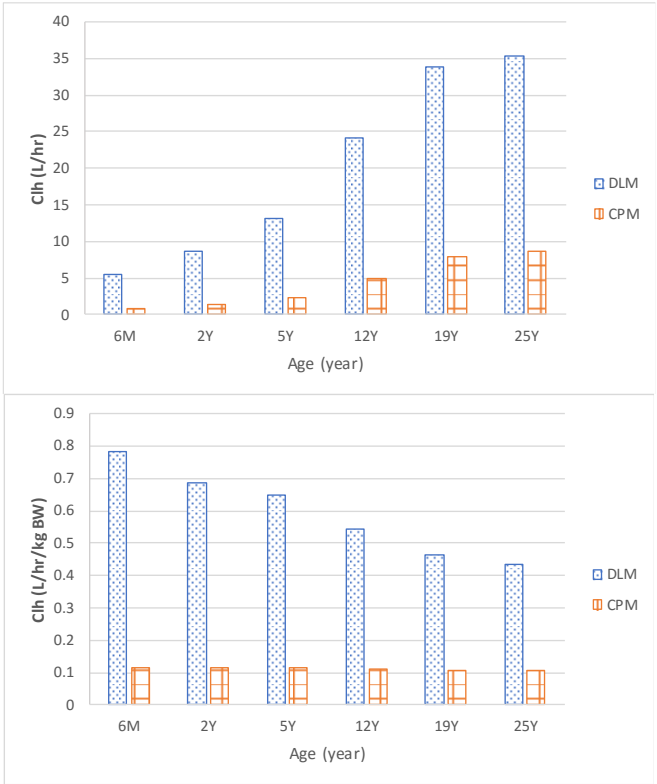

Figure III-3. DLM and CPM hepatic clearance (Clh) at different ages in males.

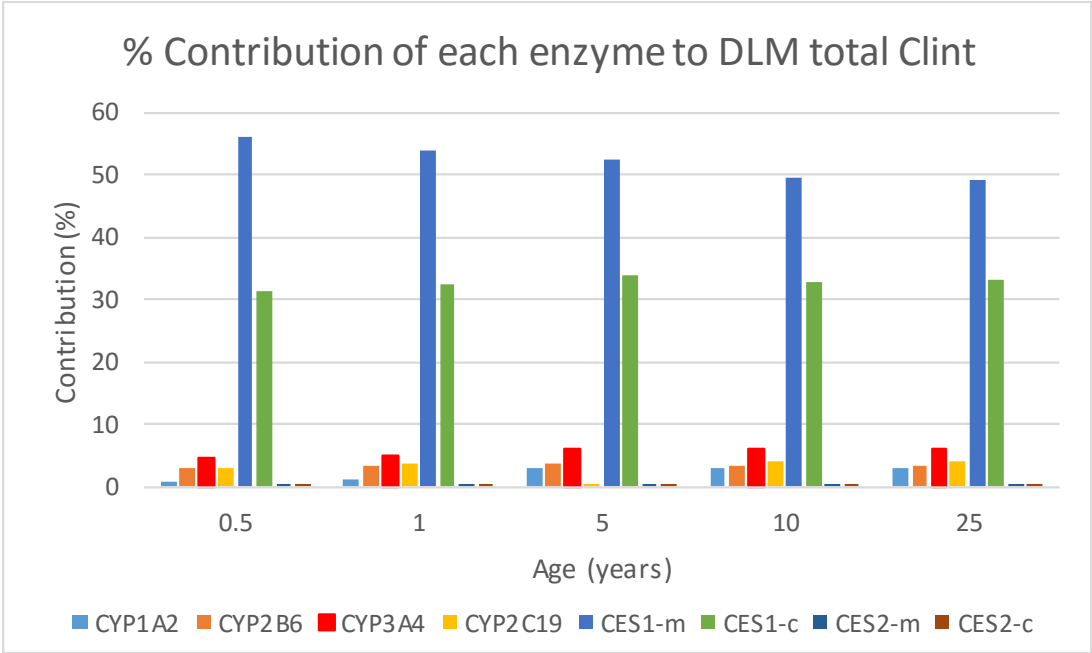

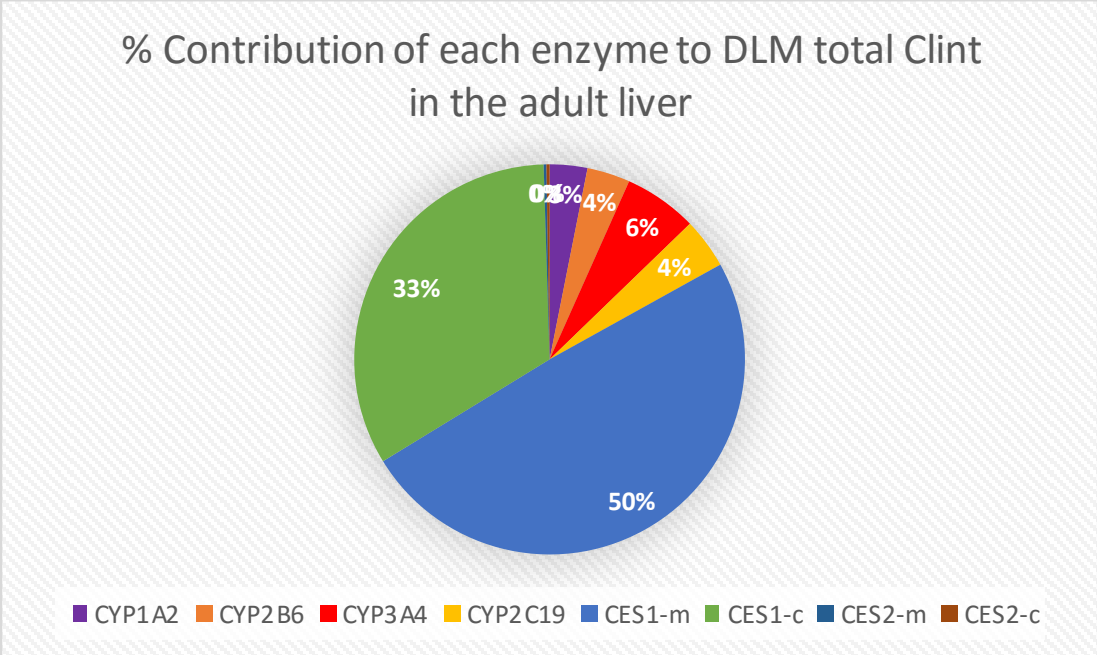

Figure III-4. Relative contribution of each enzyme to DLM total metabolism at 25-year-old.

Microsomal CES1 is denoted by CES1-m, cytosolic CES1 by CES1-c, microsomal CES2 by CES2-m, and cytosolic CES2 by CES2-c.

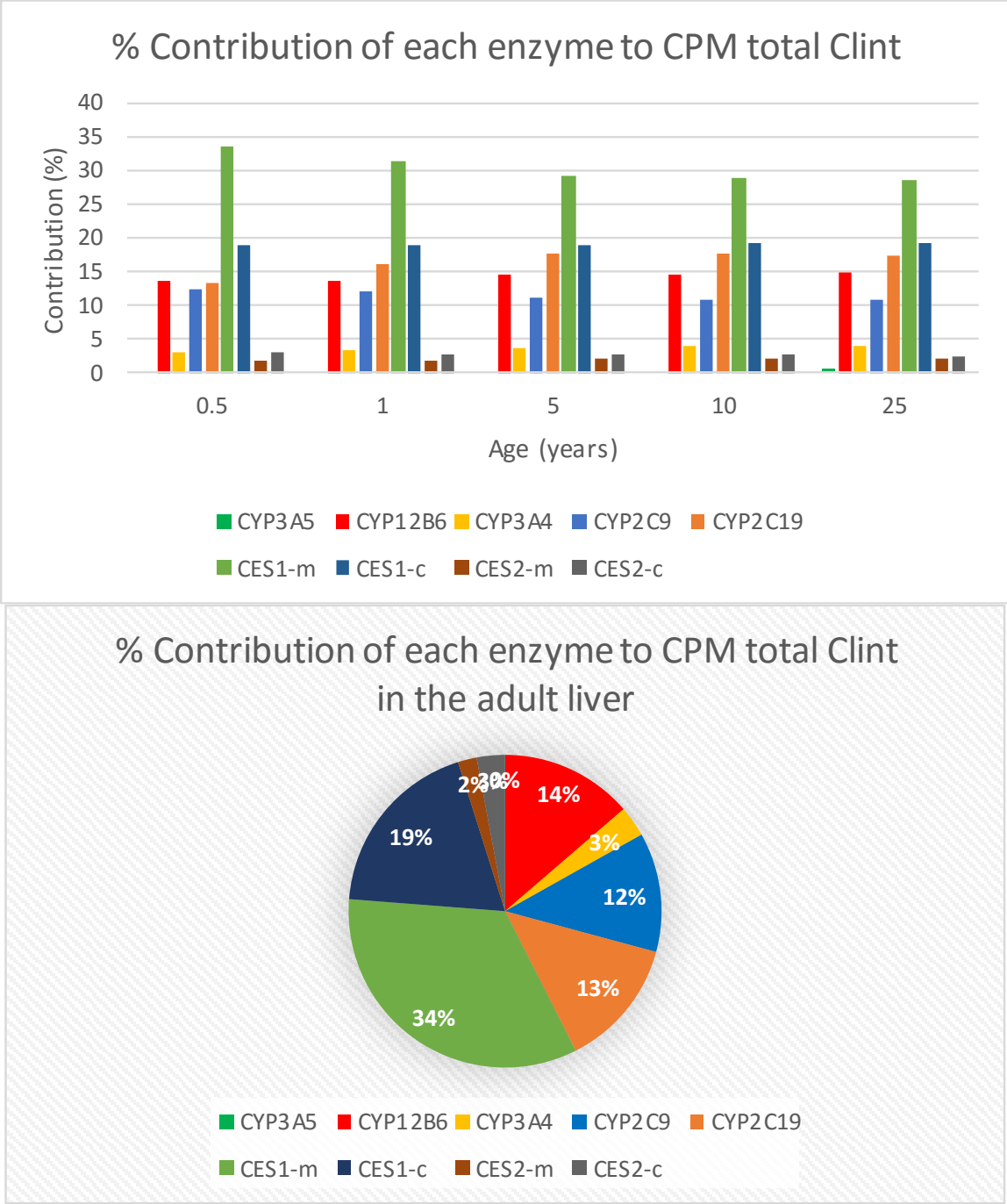

Figure III-5. Relative contribution of each enzyme to CPM total intrinsic metabolic clearance at 25-year-old.

Microsomal CES1 is denoted by CES1-m, cytosolic CES1 by CES1-c, microsomal CES2 by CES2-m, and cytosolic CES2 by CES2-c.

iii. Chemical specific parameters

All other parameters are from the rat model and listed in the model parameter table in the file 'MC parameters".

1. Tissue partitioning

Given the similarities in tissue composition between rat and human, rat tissue partition coefficients were adapted for the human model.

2. Tissue permeability

Tissue permeability-area cross products for diffusion were scaled to tissue volume$^{0.75}$ instead of using a fixed value for all ages to reflect the diffusion surface area changes during growth. The values were adapted from the rat model.

c. Modeling Exposure

i. Oral exposure

Orally ingested pyrethroids are going directly into the plasma, based on the rapid onset of restricted clearance seen in rat studies both for oral and non-oral exposure indicating a minimum impact of hepatic first-pass metabolism. Once entered in the systemic circulation, compounds availability to metabolic enzymes continues to be restricted as in the rat model.

All the ingestion exposures (food, drinking water, and other various sources of oral exposure) are described as a bolus dose at the beginning of the simulation for single-exposure, or at the beginning of each event for multiple-exposure scenarios.

ii. Inhalation

Inhaled DLM and CPM enter the plasma compartment in the model at a rate of alveolar ventilation (QAlv). A rapid and complete absorption of DLM and CPM in the respiratory tract are assumed. To describe a rapid equilibration between air and plasma, a large value for a plasma-to-air

partition coefficient (PB = 1000) is used. Tidal volume and breathing rate differ with activity levels as well as individual's age, which are appropriately incorporated when calculating age-specific QAlv at a given exposure condition. Qalv is defined as [(tidal volume - dead space volume) × breathing rate].

iii. Dermal

Dermal uptake is not considered in the Environmental Protection Agency (EPA) provided exposure scenarios for DLM and CPM, but has been incorporated into the PBPK model to simulate dermal absorption of other pyrethroids in the future. Dermal exposure is described using conservative assumptions. Exposed skin area is typically given as the fraction of the body surface area in the exposure scenarios, which is therefore, age-dependent. The details of this route exposure will be determined when it is used for other pyrethroids.

C. Simulation of exposure scenarios and reverse dosimetry

a. Exposure scenarios

All the scenarios are summarized in "DLM_CPM_Exposure_scenarios.xslx" file. All the exposure scenarios simulated in this white paper are provided, using the respective executable tabs in PLETHEM labeled with the corresponding name of each scenario.

The simulations were run until periodic steady-state was reached for each exposure scenario. Since the diffusion (uptake) of pyrethroids across the blood brain barrier is slower than plasma flow rate in the brain, it takes time to reach equilibrium between the plasma and the brain. It should be noted that this is not an indication of accumulation of the compound in brain, but just a delay in reaching equilibrium between plasma and brain. To predict Cmax after the exposure to a pyrethroid through any route of exposure, it is important to run the model to steady-state when the equilibrium between plasma and brain is achieved; that is, until the Cmax reached on successive days is the same. Cmax values are used as they are considered to be correlated with the neurotoxic effects of pyrethroids.

b. Point of departure

The POD was selected from the Benchmark Dose analysis of the Wolansky *et al.* (2006) data (DER #D422817, US EPA), where individual dose-response curves for *in vivo* motor activity in adult

rats were characterized and relative potencies for eleven commonly-used pyrethroids were calculated. All the pyrethroids tested in that study, including DLM and CPM, induced a dose-dependent decrease in motor activity. Based on these results, the USEPA used the BMDL1SD as the POD, which was equal to 1.49 and 44.4 mg/kg BW for DLM and CPM, respectively. The rat PBPK model was used to estimate the brain tissue internal dose (brain Cmax) in the adult rat at the respective external POD in rats for DLM and CPM. The simulation results are summarized in Table II-7. Reverse dosimetry was conducted using the human life stage PBPK model to determine the equivalent external exposure level that yields the target tissue internal exposure to the estimated rat internal exposure above at a given age and for a given exposure route in humans (Section III). Note that we used one single internal exposure estimated in the adult rat brain at the BMDL1SD for each pyrethroid to conduct reverse dosimetry for both early and adult ages in humans. It should also be noted that the $BMDL_{1SD}$ for permethrin is based on an effect with a 40:60 mixture of *cis*- and *trans*-permethrin. As our rat and human modeling demonstrated and also supported by the observation by Starr *et al.,* (2014), it is expected that the metabolism of both isomers would be rapid enough to equate to liver blood flow. The same is true for human metabolism of *cis*-permethrin, *i.e.,* it is limited by liver blood flow. Therefore, it was reasonable to use the BMDL1SD of the mixture to a cis-isomer in the reverse dosimetry exercise.

c. Reverse dosimetry

The first step is to identify a point of departure (POD). Because the POD from Wolansky *et al.* (2006) is derived from a rat study, the rat PBPK model was used to calculate the target tissue internal dose at the rat POD (28.28466 and 1371.8 ng/g for DLM and CPM, respectively). Reverse dosimetry was conducted using the human life stage PBPK model to determine the equivalent external exposure level that yields the target tissue internal exposure at 28.28466 ± 0.1% and 1371.8 ± 0.1% ng/g for DLM and CPM, respectively, at a given age and for a given exposure route. This is referred as the 'Source-Specific External Dose POD'.

d. DDEF calculation

A data-derived extrapolation factor (DDEF), which is equivalent to a chemical-specific adjustment factor (CSAF), is calculated using the age-specific internal dose metrics simulated by the model in a probabilistic way. In the case of pyrethroids, the maximum concentration (Cmax) in the

brain and in plasma is used as the internal exposure at the target tissue (Moser *et al.* 2016; Scollon *et al.* 2011). DDEF values were calculated using the simulated distribution of Cmax in each age population:

Juvenile Cmax_50th percentile/Adult Cmax_50th percentile (Eq. I-1)

Cmax values for the most sensitive age within each age bracket as described below were simulated using the oral-specific external dose POD for human adults (0.0879 and 3.11 mg/kg for DLM and CPM, respectively). The age brackets are as recommended by the EPA: All Infants (< 1 year old), Children 1-2 years old, Children 3-5 years old, Children 6-12 years old, Youth 13-19 years old, Adults 20-49 years old. In each age bracket, the most sensitive age and gender combination was selected and used as the most sensitive age for DDEF derivation, *i.e.,* the age and gender combination with the highest Cmax under the same exposure condition at the oral-specific external dose POD for human adults was selected. A Monte Carlo (MC) simulation was performed to generate the distributions of Cmax in this most sensitive population and in the adult population (25-year-old), then DDEFs were calculated using Eq. I-1. The age group of 3-5 years was included as the EPA noted that the most highly-exposed population subgroup in the draft dietary (food+water) assessment was children of ages 3-5.

To derive DDEFs, three age groups were simulated for a single oral dose as bolus every day until steady state to compare internal exposures in the most sensitive age vs. adult populations. As explained in the above and next sections, based on the results of the forward dosimetry simulations to select the most sensitive age and gender combination among the age brackets simulated (Table III-3), the age of 19-year-old male was chosen to represent the most sensitive population. The EPA considers children of 3-5 years old as the most highly exposed population. Our model simulations show that the 5-year-old male represents the most sensitive age and gender combination in this range. The oral-specific external dose PODs for human adults for DLM and CPM were used for Monte Carlo simulations (0.0879 mg/kg and 3.11 mg/kg, respectively). MC simulations were performed with 1000 iterations, at which the convergence was achieved. Based on the sensitivity analysis, parameters with sensitivity coefficient over 0.2 were varied for MC analysis in addition to the metabolic clearance parameters and were randomly sampled from their distributions, while other parameters were fixed.

Model parameters and their distributions, if varied for the MC analysis, are listed in the EXCEL file named 'MC Parameters_female.xlsx' and 'MC Parameters_male.xlsx'.

Scenario A: Food adult age

In the EPA guideline, 80 kg is considered as the standard adult BW. In our model, male BW at age 25 is approximately 80 kg; therefore, 'adults' are defined as 25-year-old males.

Scenario B: Food the most sensitive age (19-year-old)

Based on the results of the forward dosimetry simulations to select the most sensitive age and gender combination among the age brackets simulated (Table III-3), the age of 19-year-old male was chosen to represent the most sensitive population.

Scenario C: Food the highest exposure concern age (5-year-old)

The EPA considers children of 3-5 years old as the most highly exposed population. Our model simulations show that the 5-year-old male represents the most sensitive age and gender combination in this range.

D. Sensitivity analysis

To evaluate the relative impact of each of the model parameters on DLM and CPM brain Cmax, a sensitivity analysis of the human DLM and CPM model parameters was performed. The sensitivity coefficient (SC) was calculated as below (Yoon *et al.,* 2009):

SC = Fractional change in model output/ Fractional change in Parameter (Eq. III-8)

After oral and inhalation exposure, each parameter was individually increased by 1% of their original value while the other parameters were held constant to determine the SC values. The larger the absolute value of the sensitivity coefficient, the more important the parameter. A sensitivity coefficient of 1 represents 1:1 relationship between the change in the parameter and the internal dose metric of choice. A negative SC indicates the given parameter influences the dose metric in an inverse (opposite) direction. The SCs are grouped in three categories, high (absolute values greater than or equal to 0.5), medium (absolute values greater than or equal to 0.2 but less than 0.5), or low (absolute values greater than or equal to 0.1 but less than 0.2), according to the International Program on Chemical Safety (IPCS) guideline (World Health Organization, 2010).

Results from the sensitivity analysis are in the file 'Sensitivity_analysis_DLM_CPM.xlsx'. The sensitivity analysis was conducted at 2 doses (low and high) representative of the lower and higher external POD find in tables III7-9 for oral and inhalation exposure routes. The SA was also conducted

at steady state (last Cmax at steady state corresponding to 119-120 days). The most sensitive parameters are the brain partition coefficient (PBRN) for both DLM and CPM, followed, in order, by the BW, the cardiac output, the hematocrit, and the plasma flow to the liver. The plasma flow to the brain and the rapidly- perfused tissues are also sensitive parameters. Another sensitive parameter is the unbound fraction in plasma (FuPLS). Liver metabolic clearance show no and moderate sensitivity for DLM and CPM, respectively. Both are rapidly cleared by metabolism both in early and adult ages, but DLM metabolism is faster than that of CPM making a small difference in the sensitivity of metabolic clearance to brain Cmax between the two compounds. The free concentration adjustment factor for restricted clearance description (KMF) and the liver volume are also sensitive parameters for CPM but not DLM.

E. Model output

a. Comparison of hepatic clearance in children and adults

The hepatic clearances for DLM and CPM, as calculated in the model based on the *in vivo* hepatic Clint from IVIVE in the EXCEL file 'PYR_clearance_calculation.xlsx' and hepatic blood flow (QL), are listed in Table III-2 and Figure III-2, III-3. The Clh values are determined by four factors: hepatic Clint, hepatic blood flow, unbound fraction in plasma (FuPls) and the free concentration adjustment factor for restricted clearance (KMF). For DLM, there was a decreasing trend in Clh with age. CPM shows a similar trend of age-related changes in Clh, but to a lesser extent.

Table III-2. Model predicted hepatic clearance (Clh) for DLM and CPM in the male and the female

Age (year)	DLM Clh (L/h/kg BW)		CPM Clh (L/h/kg BW)	
	Male	Female	Male	Female
0.5	0.7819	0.8192	0.1133	0.1153
2	0.6884	0.7537	0.1154	0.1178
5	0.6477	0.7240	0.1150	0.1180
12	0.5433	0.5915	0.1112	0.1143
19	0.4634	0.5032	0.1067	0.1108
25	0.4343	0.4912	0.1065	0.1150

b. Age-dependent plasma and brain concentration under various exposure scenarios

The models for DLM and CPM were run with a single daily oral bolus dosing scenario for DLM and CPM in males and females of six different ages to compare the internal exposure across ages (Table III-3 and 4). These simulation results were used to select the most sensitive age and gender combination for DDEF derivations.

Table III-3. Comparison of the internal exposure to DLM at various ages in males and females simulated after a single daily oral dose at steady state.

Age (year)	Single daily oral dose of DLM in male 0.0879 mg/kg/day		Single daily oral dose of DLM in female 0.0879 mg/kg/day	
	Plasma Cmax (ng/ml)	Brain Cmax (ng/ml)	Plasma Cmax (ng/ml)	Brain Cmax (ng/ml)
0.5	532.43	11.77	519.47	10.84
2	628.27	14.50	578.81	12.44
5	686.97	16.15	618.97	13.47
12	852.87	21.03	803.95	18.54
19	1017.18	25.96	970.81	23.09
25	1093.88	28.28	1016.78	24.25

Table III-4. Comparison of the internal exposure to CPM at various ages in males and females simulated after a single daily oral dose at steady state.

Age (year)	Single daily oral dose of CPM in male 3.11 mg/kg/day		Single daily oral dose of CPM in female 3.11 mg/kg/day	
	Plasma Cmax (ng/ml)	Brain Cmax (ng/ml	Plasma Cmax (ng/ml)	Brain Cmax (ng/ml)
0.5	19445.03	845.22	18923.14	808.69
2	22793.47	907.83	20965.20	841.14
5	24778.80	964.99	22336.50	873.18
12	30553.74	1133.49	28820.68	1036.85
19	36322.45	1302.78	34721.77	1180.66
25	39040.96	1371.29	36331.28	1198.19

These results suggest that the difference in internal exposure at the target tissue (brain) between six months and 25 years of age after oral exposure to DLM and CPM would be less than 2- to 3-fold, with the Cmax lower in the early ages than that in the adult (Table III-3 and 4). In addition, there are no significant differences in internal exposures (plasma and brain) between males and females.

The models were also run with inhalation exposure scenarios (daily inhalation at a duration of 1hr/day, breathing rate at light exercise-see Appendix 11 for the pulmonary parameters used for the simulations) in male and female of six different ages (Table III-5 and 6). An inhalation-specific external dose POD for 25-year-old males and females was used for simulating DLM and CPM kinetics in different ages after this inhalation exposure scenario.

Table III-5. Comparison of the internal exposure to DLM at various ages in males and females simulated after daily inhalation for 1hr/day at steady state.

Age (year)	Single daily inhalation of DLM in male, 1hr/day 0.2157 ppm		Single daily inhalation of DLM in female, 1 hr/day 0.2157 ppm	
	Plasma Cmax (ng/ml)	Brain Cmax (ng/ml)	Plasma Cmax (ng/ml)	Brain Cmax (ng/ml)
0.5	38.42	1.23	36.42	1.17
2	72.84	2.41	61.42	2.01
5	130.39	4.40	115.25	3.83
12	477.54	17.04	423.08	14.93
19	624.97	23.18	508.43	18.52
25	750.14	28.27	531.35	19.45

After inhalation (Table III-5 and 6), there are no differences in internal exposure between males and females at early ages, whereas in adults, the internal exposure is somewhat higher in males than females. This is largely due to the gender difference in pulmonary ventilation/capacity parameters and their changes with the degree of exercise levels. The models suggest that the difference in internal exposure at the target tissue (brain) between 6-month-old and 25-year-old ages after daily inhalation exposure, at a duration of 1hr/day, is from 13- to 24-fold, with the Cmax being lower in the early ages than in the adult.

Table III-6. Comparison of the internal exposure to CPM at various ages in males and females simulated after daily inhalation for 1 hr/day at steady state.

Age (year)	Single daily inhalation of CPM in male, 1hr/day 9.934 ppm		Single daily inhalation of CPM in female, 1hr/day 9.934 ppm	
	Plasma Cmax (ng/ml)	Brain Cmax (ng/ml)	Plasma Cmax (ng/ml)	Brain Cmax (ng/ml)
0.5	1720.28	88.16	1655.25	86.33
2	3093.84	149.76	2674.42	134.19
5	5389.19	261.57	4904.83	245.14
12	18811.09	918.76	16917.10	826.89
19	23979.91	1164.61	19760.91	935.96
25	28508.51	1371.32	20492.92	948.66

c. EPA-provided exposure scenarios: reverse dosimetry

The results in the above section E-b showed that there are negligible differences in internal exposure (plasma and brain) between males and females in various exposure conditions, although the concentrations in males appear to be always slightly higher than those in females. Therefore, reverse dosimetry was performed using male parameters to estimate source-specific external dose POD at various exposure conditions. The simulations were run until periodic steady-state was reached for each exposure scenario. Cmax values were used for the estimation of source-specific external dose PODs. The EPA provided an age range with a representative BW for that age range in each exposure scenario. We ran model simulations for each scenario at three different ages: the lowest age within each age range provided, the highest age within each age range, and the age corresponding to the representative BW. The most sensitive age and gender combinations determined from this exercise are listed in Appendix 12-14.

d. Monte Carlo analysis

Monte Carlo simulations were performed with 1000 iterations to perform population-level simulations, at which the convergence was achieved. Further increase in the number of iterations to 5000 and 10000 did not make a substantial difference. Based on the sensitivity analysis, parameters with sensitivity coefficient over 0.2 were varied for MC analysis in addition to the metabolic clearance parameters and were randomly sampled from their distributions, while other parameters were fixed.

Model parameters and their distributions, if varied for the MC analysis, are listed in the EXCEL file named 'MC Parameters_female.xlsx' and 'MC Parameters_male.xlsx'. The simulated Cmax 50th, 5th and 95th percentiles for every scenario are listed in Tables III-7 and III-8 and Figures III-6 and III-7.

Table III-7. Comparison of the internal exposure to DLM in males simulated after an oral exposure (0.0879 mg/kg-day) at steady state.

Scenario	Age	Plasma Cmax (ng/ml) 50th percentile (5th-95th percentiles)	Brain Cmax (ng/ml) 50th percentile (5th-95th percentiles)
Single oral dose (A)	25	1103 (708.8-1857)	29.86 (13.95-69.28)
Single oral dose (B)	19	1025 (662.4-1680)	27.3 (12.59-61.96)
Single oral dose (C)	5	708.4 (469.8-1064)	17.72 (8.37-40.49)

Table III-8. Comparison of the internal exposure to CPM in males simulated after an oral exposure (3.11 mg/kg-day) at steady state.

Scenarios	Gender	Age	CPM	
			Plasma Cmax (ng/ml) 50th percentile (5th-95th percentiles)	Brain Cmax (ng/ml) 50th percentile (5th-95th percentiles)
Single oral dose (A)	**M**	25	39179 (25504-66044)	1486 (762.5-3223)
Single oral dose (B)	**M**	19	36727 (23859-60519)	1413 (726-3032)
Single oral dose (C)	**M**	5	25250 (16804-38067)	1048 (533.3-2129)

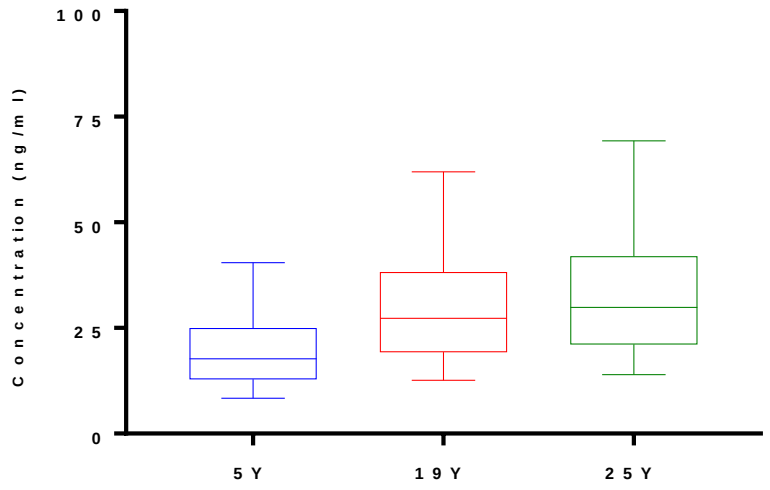

Figure III-6. Brain Cmax after a daily single DLM oral dose at 0.0879 mg/kg in males at 5, 19 and 25 years old.

1000 individuals for each group for Scenario A, B, and C were simulated. Horizontal line bisecting large rectangle, median; large rectangle, lower and upper quartiles; whiskers, 5th and 95th percentiles.

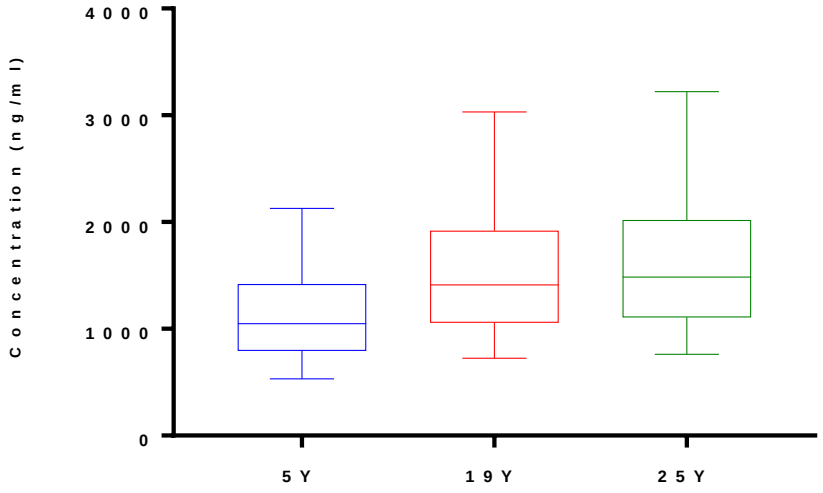

Figure III-7. Brain Cmax after a single CPM oral dose at 3.11 mg/kg in males at 5, 19 and 25 years old.

1000 individuals for each group for Scenario A, B, and C were simulated for the MC. Horizontal line bisecting large rectangle, median; large rectangle, lower and upper quartiles; whiskers, 5th and 95th percentiles.

Table III-9. DDEFs for DLM and CPM in males.

	Dose	Age	DLM		CPM	
			Plasma Cmax	Brain Cmax	Plasma Cmax	Brain Cmax
DDEF1	POD	19-25	0.929	0.914	0.937	0.951
	+ 10-fold POD		0.93	0.919	0.939	0.975
	- 10-fold POD		0.929	0.92	0.935	0.949
DDEF2	POD	5-25	0.642	0.593	0.644	0.705
	+ 10-fold POD		0.641	0.593	0.644	0.723
	- 10-fold POD		0.629	0.576	0.643	0.705

Notes: POD 0.0879 and 3.11 mg/kg for DLM and CPM, respectively; + 10-fold POD indicates the use of a 10-fold higher dose than the POD; - 10-fold POD indicates the use of a 10-fold lower dose than the POD.

F. Uncertainty analysis

Briefly, the uncertainty of a model reflects the level of confidence in model predictions. A sensitivity/uncertainty matrix can be used to determine the overall importance of a parameter. Sensitivity coefficients are grouped as high (absolute value greater than or equal to 0.5), medium (absolute value greater than or equal to 0.2 but less than 0.5) or low (absolute value greater than or equal to 0.1 but less than 0.2); parameters with sensitivities less than 0.2 are regarded as low influence parameters following the recommendation from IPCS (WHO, 2005).

Table III-10. IPCS Sensitivity/Uncertainty matrix.

		Uncertainty		
		High	Medium	Low
Sensitivity	High	-		Body Weight Hematocrit Cardiac output Brain Partition coefficient Pulmonary parameters Liver blood flow Unbound Fraction in plasma
	Medium	-		Total liver Clearance (CPM only) KMF (CPM only) Liver volume (CPM only)
	Low	-	Brain permeability	Brain blood flow Rapidly perfused tissues

G. Discussion

This white paper describes the development and application of the life stage human PBPK model for pyrethroids to support risk assessment, among which the main purpose is the evaluation of the age-related sensitivity to the exposure to pyrethroids due to pharmacokinetic differences. The generic model structure for pyrethroids, the validity of which was evaluated in the rat model, was used together with compound-specific metabolic clearance parameters that are obtained from *in vitro* experiments to predict internal exposure to each pyrethroid in humans of different ages. Our IVIVE-PBPK modeling approach is well in line with the recommendation from the National Research Council (NRC) report on toxicity testing in the 21st century on the use of alternative methods, such as *in vitro* and computational modeling approaches, to increase efficiency and human relevance in toxicity testing and safety assessment.

Application of the life stage PBPK model to pyrethroid risk assessment, demonstrated for DLM and CPM in this white paper, required the addition of several capabilities to the generic model structure developed in the rat, including simulation of additional routes of exposure (than an ingestion by single bolus), human exposure factors (such as activity levels), and exposure patterns/frequencies/durations, and appropriate age ranges representative of different life stages of humans. Reverse dosimetry was conducted to support the internal-exposure based inter-species extrapolation, calculating the equivalent human PODs under specific exposure scenarios that would result in the same internal exposure in the brain under specified exposure scenarios as in the animal brain at the POD for each pyrethroid, based on decreased motor activity in rats (Wolansky *et al.* 2006).

The reverse dosimetry results show that for both oral and inhalation exposures, the estimated exposure-route specific human PODs are lower in adults than early ages. It should be noted that the exposure durations and frequencies influence the resulting PODs in the same age. As the POD for inhalation is defined as air concentration for a continuous exposure, the exposure duration affects the human POD when other factors are the same. For example, the air concentration needed to reach the brain concentration equivalent to that in the rat at the animal POD would be lower for a longer exposure duration, resulting in lower PODs from the scenarios with longer duration of exposure when the other factors are the same, *e.g.,* age of the individual (Scenario #5 Appendix 12 and scenarios #14 and #15 Appendix 13). Since the oral exposure is simulated as an intermittent dosing, whereas the

inhalation is simulated a continuous exposure, the exposure duration affects the POD in a different way, compared to inhalation. As the bolus dose is given at the beginning of each dosing interval, the interval affects the extent of clearance of the pyrethroid occurring between events and consequently, the dose in order to reach the same brain concentration. For example, the POD from the oral exposure with a much longer exposure duration and therefore, a longer interval between doses (Scenario #11 with 18 hrs/day in Appendix 12), is higher than the POD estimated for a similar exposure scenario only with a shorter exposure duration (Scenario #7 with 4 hrs/day in Appendix 12).

Before deriving DDEFs for age-related PK differences (Table III-9), the most sensitive age- and sex- combination was determined by comparing the exposure route-specific PODs under a daily single oral exposure scenario, estimated as 0.0879 and 3.11 mg/kg/day for DLM and CPM, respectively, to be compared to the most sensitive adult (25-year-old as adult). The results show that the 19-year-old male is the most sensitive population, with the highest brain Cmax under the same exposure condition in the ages under 25. Therefore, MC simulations were performed for 19- and 25-year-old male populations for DDEF derivations. In the draft dietary (food and water) assessment by the EPA, the population with the highest exposure is children 3 to 5 years old. Therefore, the most sensitive age and sex combination within this age range was also included to derive a DDEF, which is the 5-year-old male. As the purpose is to compare the difference between the ages, we used the median (50th percentile) values from each age for a DDEF derivation. Table III-9 shows that both for DLM and CPM, the ratios between the two median Cmax values from different ages are less than 1, resulting in a DDEF for age-related PK difference less than 1 for both DLM and CPM. This indicates that there is no additional adjustment factor required for age-related PK differences for these two compounds.

As demonstrated in our rat modeling and supported by many evidence, the age-related differences in internal exposure to pyrethroids in the brain are largely determined by the differences in metabolic capacity for pyrethroids between the young and adult. Similarly, the hepatic metabolism of pyrethroids during human development and growth is also dependent on the age-related changes in both physiological and biochemical factors. They include the changes in blood (plasma) flow to the liver, liver weight, and the expression levels of metabolic enzymes that are responsible for the pyrethroid metabolism during the rapid development period in life. Consistent with the literature, our *in vitro* metabolism data and IVIVE analysis showed that CES1 enzymes are largely responsible for DLM and CPM metabolism in humans, contributing to more than 50% of the metabolism of each of these pyrethroids. The hydrolysis of DLM and CPM by CES1 is very efficient, as shown by our *in vitro*

data (see CXR reports 1575 Deltamethrin expressed enzyme Data package; CXR reports 1575 Cis-permethrin expressed enzyme Data package). In addition, CES1 enzymes develop rapidly after birth (Hines *et al.*, 2016). Both of these factors contribute to the efficient clearance of DLM and CPM in humans, both in the young and the adult, which is different from the rat, where we observed a very limited pyrethroid metabolic clearance capability in the juvenile rat. Both for DLM and CPM, the metabolism is so rapid it is only limited by liver blood (plasma) flow regardless of age in humans. In fact, total hepatic clearance values (as a measure how efficient the body can eliminate the pyrethroid) of each pyrethroid in early ages are higher than that in adults as the liver blood flow and the liver weight are both higher in early ages. Note that relative values are referred here as the absolute liver weight or liver blood flow increases with age, but their fraction of the total body weight or total cardiac output, respectively, decreases (Refer to the appended Excel file "Life Stage Parameters"). These age-dependent changes in physiological factors together with the rapid metabolic clearance, result in a lower internal exposure in the target tissue in infants and children than that in adults in humans in response to the same level of exposure to a given pyrethroid.

Our simulations also showed negligible differences in internal exposure (plasma and brain) between males and females after oral exposure. However, after inhalation there is a difference in internal exposure (plasma and brain) between males and females but only at adult ages. This can be explained by the differences in the pulmonary parameters, which is influenced by activity levels. In adults, these parameters are higher in males, who have a larger lung capacity, compared to females, explaining the higher DLM and CPM internal exposure in males when exposed by inhalation. The fold-difference between the young and adult is also higher after inhalation compared to oral (2-fold after oral, 12- to 22-fold after inhalation). This is explained again by the differences in the pulmonary parameters across ages. These physiological and human exposure factors that affect the exposure levels in different human populations are appropriately incorporated into the age-specific parameters.

As was emphasized in the rat model section earlier, from the perspective of applying PBPK models to support risk assessments for pyrethroids, the most important contributions our PBPK modeling case studies provided is a single generic model structure for pyrethroids as a group, as well as a common set of parameters apart from compound-specific metabolism. The availability of such a generic modeling platform with a targeted *in vitro* study work-flow for a key parameter allows for a clearance-based read-across to other pyrethroids to support internal exposure-based risk assessment for pyrethroids in general.

H. References

Achour, B., Barber, J., and Rostami-Hodjegan, A. 2014. Expression of hepatic drug-metabolizing cytochrome p450 enzymes and their intercorrelations: a meta-analysis. *Drug Metab Dispos*. 42(8):1349-1356.

Anand, S.S., Kim, K.B., Padilla, S., Muralidhara, S., Kim, H.J., Fisher, J.W. and Bruckner, J.V. (2006). Ontogeny of hepatic and plasma metabolism of deltamethrin in vitro: role in age-dependent acute neurotoxicity. *Drug Metab. Dispos*. 34(3): 389-397.

Barter, Z.E., Chowdry, J.E., Harlow, J.R., Snawder, J.E., Lipscomb, J.C., and Rostami-Hodjegan, A. 2008. Covariation of human microsomal protein per gram of liver with age: absence of influence of operator and sample storage may justify interlaboratory data pooling. *Drug Metab Dispos*. 36(12):2405-2409.

Boberg, M., Vrana, M., Mehrotra, A., Pearce, R.E., Gaedigk, A., Bhatt, D.K., Leeder, J.S., and Prasad, B. 2016. Age-Dependent Absolute Abundance of Hepatic Carboxylesterases (CES1 and CES2) by LC-MS/MS Proteomics: Application to PBPK Modeling of Oseltamivir *In vivo* Pharmacokinetics in Infants. *Drug Metab Dispos*. 45(2):216-223.

Chen, Y., Liu, L., Nguyen, K., and Fretland, A.J. 2011. Utility of intersystem extrapolation factors in early reaction phenotyping and the quantitative extrapolation of human liver microsomal intrinsic clearance using recombinant cytochromes P450. *Drug Metab Dispos*. 39(3):373-382.

Crow, J.A., Borazjani, A., Potter, P.M., and Ross, M.K. 2007. Hydrolysis of pyrethroids by human and rat tissues: examination of intestinal, liver and serum carboxylesterases. *Toxicol Appl Pharmacol*. 221(1): 1-12.

Godin, S.J., Scollon, E.J., Hughes, M.F., Potter, P.M., DeVito, M.J., and Ross, M.K. 2006. Species differences in the in vitro metabolism of deltamethrin and esfenvalerate: differential oxidative and hydrolytic metabolism by humans and rats. *Drug Metab Dispos*. 34(10) 1764-71.

Hideo, K. 2012. Biotransformation and enzymes responsible for metabolism of pyrethroids in mammals, in parameters for pesticide QSAR and PBPK/PD models for human risk assessment. Am. *Chem. Soc*. 4:41-52.

Hines, R. N, Simpson, P.M., and McCarver, D.G. 2016. Age-Dependent Human Hepatic Carboxylesterase 1 (CES1) and Carboxylesterase 2 (CES2) Postnatal Ontogeny. *Drug Metab Dispos*. 44(7):959-966.

Hines, R.N. 2012. Developmental expression of drug metabolizing enzymes: impact on disposition in neonates and young children. *Int J Pharm*. 452(1-2):3-7.

Hines, R. N. 2008. The ontogeny of drug metabolism enzymes and implications for adverse drug events. *Pharmacol Ther*. 118(2):250-267.

Hines, R.N. 2007. Ontogeny of human hepatic cytochromes P450. *J. Biochem. Mol. Toxicol*. 21(4):169-175.

Houston, J.B., and Galetin, A. 2008. Methods for predicting *in vivo* pharmacokinetics using data from *in vitro* assays. *Curr Drug Metab*. 9(9):940-951.

Johnson, T.N., Rostami-Hodjegan, A. and Tucker, G.T. 2006. Prediction of the clearance of eleven drugs and associated variability in neonates, infants and children. *Clin. pharmacokinet*. 45(9): 931-956.

Kim, K.B., Anand, S.S., Kim, H.J., White, C.A., Fisher, J.W., Tornero-Velez, R. and Bruckner, J.V. 2010. Age-, dose-and time-dependency of plasma and tissue distribution of deltamethrin in immature rats. *Toxicol. Sci*. 115(2):354-368.

Koukouritaki, S.B., Manro, J.R., Marsh, S.A., Stevens, J.C., Rettie, A.E., McCarver, D.G., and Hines, R.N. 2004. Developmental expression of human hepatic CYP2C9 and CYP2C19. *J Pharmacol Exp Ther*. 308(3):965-74.

Moser, V.C., Liu, Z., Schlosser, C., Spanogle, T.L., Chandrasekaran, A., and McDaniel, K.L. 2016. Locomotor activity and tissue levels following acute administration of lambda- and gamma-cyhalothrin in rats. *Toxicol Appl Pharmacol*. 15,313:97-103.

Pope, C.N., Karanth, S., Liu, J. and Yan, B. 2005. Comparative carboxylesterase activities in infant and adult liver and their in vitro sensitivity to chlorpyrifos oxon. *Regul. Toxicol. Pharmacol*. 42(1): 64-69.

Proctor, N.J., Tucker, G.T., and Rostami-Hodjegan, A. 2004. Predicting drug clearance from recombinantly expressed CYPs: intersystem extrapolation factors. *Xenobiotica* 34(2):151-178.

Ratelle, M., Côté, J., and Bouchard, M. 2015a. Toxicokinetics of permethrin biomarkers of exposure in orally exposed volunteers. *Toxicol. Lett*. 232(2):369-375.

Ratelle, M., Coté, J., and Bouchard, M. 2015b. Time profiles and toxicokinetic parameters of key biomarkers of exposure to cypermethrin in orally exposed volunteers compared with previously available kinetic data following permethrin exposure. *J Appl Toxicol.* 35(12):1586-93.

Rostami-Hodjegan, A. and Tucker, G.T. 2007. Simulation and prediction of in vivo drug metabolism in human populations from in vitro data. Nat. Rev. *Drug Discovery*. 6(2):140-148.

Ruark, C.D., Song, G., Yoon, M., Verner, M.A., Andersen, M.E., Clewell, H.J. 3rd, and Longnecker, M.P. 2017. Quantitative bias analysis for epidemiological associations of perfluoroalkyl substance serum concentrations and early onset of menopause. *Environ Int*. 99:245-254.

Saghir, S.A., Khan, S.A. and McCoy, A.T. 2012. Ontogeny of mammalian metabolizing enzymes in humans and animals used in toxicological studies. *Crit. Rev. Toxicol.* 42(5):323-357.

Scollon, E.J., Starr, J.M., Crofton, K.M., Wolansky, M.J., DeVito, M.J., and Hughes, M.F. 2011. Correlation of tissue concentrations of the pyrethroid bifenthrin with neurotoxicity in the rat. *Toxicol.* 290(1):1-6.

Sheets, L.P., Doherty, J.D., Law, M.W., Reiter, L.W. and Crofton, K.M. (1994) Age-dependent differences in the susceptibility of rats to deltamethrin. *Toxicol. Appl. Pharmacol.* 126(1):186-190.

Soderlund, D.M. 2012. Molecular mechanisms of pyrethroid insecticide neurotoxicity: recent advances. *Arch Toxicol.* 86(2):165-81.

Song, G., Peeples, C.R., Yoon, M., Wu, H., Verner, M.A., Andersen, M.E., Clewell, H.J. 3rd, and Longnecker MP. 2016. Pharmacokinetic bias analysis of the epidemiological associations between serum polybrominated diphenyl ether (BDE-47) and timing of menarche. *Environ Res.* 150:541-548.

Starr, J.M., Graham, S.E., Ross, D.G., Tornero-Velez, R., Scollon, E.J., Devito, M.J., Crofton, K.M., Wolansky, M.J., and Hughes, M.F. 2014. Environmentally relevant mixing ratios in cumulative assessments: a study of the kinetics of pyrethroids and their ester cleavage metabolites in blood and brain; and the effect of a pyrethroid mixture on the motor activity of rats. Toxicol. 320:15-24.

Wetmore, B.A., Allen, B., Clewell, H.J. 3rd, Parker, T., Wambaugh, J.F., Almond, L.M., Sochaski, M.A., and Thomas, R.S. 2014. Incorporating population variability and susceptible subpopulations into dosimetry for high-throughput toxicity testing. *Toxicol Sci.* 142(1):210-224.

Wolansky, M.J., Gennings, C., and Crofton, K.M. 2006. Relative potencies for acute effects of pyrethroids on motor function in rats. *Toxicol Sci.* 89(1):271-7.

World Health Organization (WHO) Characterization and Application of Physiologically Based Pharmacokinetic Models in Risk Assessment. Geneva, Switzerland: World Health Organization, International Programme on Chemical Safety; 2010.

World Health Organization (WHO) Chemical-specific adjustment factors for interspecies differences and human variability: guidance document for use of data in dose/concentration–response assessment, IPCS harmonization project document; no. 2; 2005.

Wu, H., Yoon, M., Verner, M.A., Xue, J., Luo, M., Andersen, M.E., Longnecker, M.P., and Clewell, H.J. 3rd. 2015. Can the observed association between serum perfluoroalkyl substances and delayed menarche be explained on the basis of puberty-related changes in physiology and pharmacokinetics? *Environ Int.* 82:61-68.

Yang, D., Pearce, R.E., Wang, X., Gaedigk, R., Wan, Y.J. and Yan, B. 2009. Human carboxylesterases HCE1 and HCE2: ontogenic expression, inter-individual variability and differential hydrolysis of oseltamivir, aspirin, deltamethrin and permethrin. *Biochem. Pharmacol.* 77(2):238-247.

Yoon, M., Nong, A., Clewell, H.J., Taylor, M.D., Dorman, D.C., and Andersen, M.E. 2009. Lactational transfer of manganese in rats: predicting manganese tissue concentration in the dam and pups from inhalation exposure with a pharmacokinetic model, *Toxicol Sci*, 112(1):23-43.

Yoon, M., Campbell, J.L., Andersen, M.E., and Clewell, H.J. 2012. Quantitative *in vitro* to *in vivo* extrapolation of cell-based toxicity assay results. *Crit Rev Toxicol*. 42(8):633-652.

https://www.ncbi.nlm.nih.gov/pubmed/22667820

Yoon, M., and Clewell, HJ 3rd. 2016. Addressing Early Life Sensitivity Using Physiologically Based Pharmacokinetic Modeling and *in vitro* to *in vivo* Extrapolation. *Toxicol Res*. 32(1):15-20. (PDF appended – open access).

https://www.ncbi.nlm.nih.gov/pmc/articles/PMC4780231/

I. List of the appended files for the human model

1. Model folder "R submission"

    a. This is the current version of the pyrethroid human model in R as of May 19th, 2017. Model file (model. R) is saved in the folder named 'Model' and parameter files for DLM and CPM simulations are saved in the folders named 'DLM' and 'CPM', respectively. R files are included in the folder named 'Scenarios' to simulate plasma and tissue concentration profiles of DLM and CPM at a given exposure scenario in human at specific ages.

    b. Installing R, R studio and packages needed to run models

    Installing R

    1. In a web-browser, navigate to https://cran.r-project.org/
    2. Select "Download R for Windows" under "Download and Install R"
    3. Select "Install R for the first time"
    4. Select "Download R 3.(version) for Windows "
    5. Save and run the installer file

    Installing Rstudio

    1. In a web-browser navigate to https://www.rstudio.com/
    2. On the homepage select Download Rstudio
    3. Download the open source license version of Rstudio (first from left)
    4. Select windows installer (Under Installers -> RStudio 1.(ver) – Windows Vista /7/8/10
    5. Save and Run the executable file

    Installing Packages:

    1. Run Rstudio
    2. Select Packages tab from the bottom right panel in RStudio
    3. Select Install in the packages tab
    4. Under packages enter deSolve and select install

    This will setup the environment needed to run the models

c. Copy the whole model folder (R submission) on your computer and open a specific file in the folder named 'Scenarios' in RStudio. Change and set the working directory to where you downloaded the scripts (All the \ need to be replaced by a /). To run the scenarios, click on Source, not run in RStudio. There are 47 files for scenario simulations of DLM and CPM. There are 4 other files named: 'DLM_Human_Inh.R', 'DLM_Human_Oral.R', 'CPM_Human_Inh.R' and 'CPM_Human_Oral.R'. These files were used to generate the internal exposure to DLM and CPM at various ages in males and females after a single daily oral dose or a 1 hr inhalation exposure at steady state (results are in tables III-3,-4,-5 and -6). To run these files, you need to change the chemical, the gender and the age in #get paramFile accordingly with the scenario needed. If you want to change parameters that are in the parameter files, don't change them in these parameter files but in the scenario files. Copy this new line: params[["NAME OF THE PARAMETER"]] <- x.

Scenario file in R	Note
CPM_Human_Inh	This scenario is used to generate the internal exposure to CPM at various ages in male and female after a 1 hr inhalation exposure per day at steady state. To run this file, you need to change the gender and the age accordingly with the scenario wanted. A list of the pulmonary parameters used to run this file is in the report, in appendix 9. The results are in table III3 to 6.
CPM_Human_Oral	This scenario is used to generate the internal exposure to CPM at various ages in male and female after a single daily oral dose until steady state. To run this file, you need to change the gender and the age accordingly with the scenario wanted. The results are in table III3 to 6.
CPM_Scenario1_Food_male_20Y	Single oral dose per day, every day for 120 days corresponding to the steady state. This scenario is for an adult of 75 kg, corresponding to an age of 20 years old.
CPM_Scenario2_Drinking_male_6M	Single oral dose per day, every day for 120 days corresponding to the steady state. This scenario is for a 6 months baby with a water consumption of 0.68 L/day.
CPM_Scenario3_WorkerMixerLoader_ Inh_male_60	The exposure frequency is 8 hrs/day, for 7 days/week until steady state. This scenario is for an 80-kg adult. In the EPA guideline, 80

	kg is considered as the standard BW for a range of age from 16 to 60 years old. In the model, the most sensitive age was 60 years old. Therefore, the model was run for 60Y. The breathing rate was set to 1 m3/hr.
CPM_Scenario4_WorkerApplicator_Inh_male_60Y	The exposure frequency is 8 hrs/day, for 7 days/week until steady state. This scenario is for an 80-kg adult. In the EPA guideline, 80 kg is considered as the standard BW for a range of age from 16 to 60 years old. In the model, the most sensitive age was 60 years old. Therefore, the model was run for 60Y. The breathing rate was set to 0.5 m3/hr.
CPM_Scenario5_WorkerPHEDcombo_Inh_male_60Y	The exposure frequency is 8 hrs/day, for 7 days/week until steady state. This scenario is for an 80-kg adult. In the EPA guideline, 80 kg is considered as the standard BW for a range of age from 16 to 60 years old. In the model, the most sensitive age was 60 years old. Therefore, the model was run for 60Y. The breathing rate was set to 1.73 m3/hr.
CPM_Scenario6_ResidentialHandler_Inh_male_60Y	The exposure frequency is 1 hrs/day, for 7 days/week until steady state. This scenario is for an 80-kg adult. In the EPA guideline, 80 kg is considered as the standard BW for a range of age from 16 to 60 years old. In the model, the most sensitive age was 60 years old. Therefore, the model was run for 60Y. The breathing rate was set to 0.64 m3/hr.
CPM_Scenario7_ResidentialPostAppl_Oral_male_2Y	The exposure frequency is 1.5 hrs/day, for 7 days/week until steady state. 4 replenishment intervals per hour are estimated (i.e., residues on the hand will be replenished every 15 minutes). This scenario is for a 11-kg child. In the EPA guideline, 11 kg is considered as the standard BW for a range of age from 1 to 2 years old. In the model, the most sensitive age was 2 years old. Therefore, the model was run for 2Y.
CPM_Scenario8_ResidentialPostAppl_Oral_ male_6Y	The exposure frequency is 2 hrs/day, for 7 days/week until steady state. 4 replenishment intervals per hour are estimated (i.e., residues on the hand will be replenished every 15 minutes). This scenario is for a 19-kg child. In the EPA guideline, 19 kg is considered as the standard BW for a range of age from 3 to 6 years old. In the

	model, the most sensitive age was 6 years old. Therefore, the model was run for 6Y.
CPM_Scenario9_ResidentialPostAppl(indoorcarpet)_Oral_male_2Y	The exposure frequency is 4 hrs/day, for 7 days/week until steady state. 4 replenishment intervals per hour are estimated (i.e., residues on the hand will be replenished every 15 minutes). This scenario is for a 11-kg child. In the EPA guideline, 11 kg is considered as the standard BW for a range of age from 1 to 2 years old. In the model, the most sensitive age was 2 years old. Therefore, the model was run for 2Y.
CPM_Scenario10_ResidentialPostAppl(indoorhardsurf)_Oral_male_2Y	The exposure frequency is 2 hrs/day, for 7 days/week until steady state. 4 replenishment intervals per hour are estimated (i.e., residues on the hand will be replenished every 15 minutes). This scenario is for a 11-kg child. In the EPA guideline, 11 kg is considered as the standard BW for a range of age from 1 to 2 years old. In the model, the most sensitive age was 2 years old. Therefore, the model was run for 2Y.
CPM_Scenario11_ResidentialPostAppl(paints)_Oral_male_2Y	The exposure frequency is 1.5 hrs/day, for 7 days/week until steady state. 4 replenishment intervals per hour are estimated (i.e., residues on the hand will be replenished every 15 minutes). This scenario is for a 11-kg child. In the EPA guideline, 11 kg is considered as the standard BW for a range of age from 1 to 2 years old. In the model, the most sensitive age was 2 years old. Therefore, the model was run for 2Y.
CPM_Scenario12_ResidentialPostAppl(pets)Oral_male_2Y	The exposure frequency is 1 hrs/day, for 7 days/week until steady state. 4 replenishment intervals per hour are estimated (i.e., residues on the hand will be replenished every 15 minutes). This scenario is for a 11-kg child. In the EPA guideline, 11 kg is considered as the standard BW for a range of age from 1 to 2 years old. In the model, the most sensitive age was 2 years old. Therefore, the model was run for 2Y.
CPM_Scenario13_ResidentialPostAppl(Indoorspacespray)_Inh_male_60Y	The exposure frequency is 16 hrs/day, for 7 days/week until steady state. This scenario is for an 80-kg adult. In the EPA guideline, 80 kg is considered as the standard BW for a range of age from 16 to 60 years old. In the model, the most sensitive age was 60 years

	old. Therefore, the model was run for 60Y. The breathing rate was set to 0.64 m3/hr.
CPM_Scenario14_ResidentialPostAppl(Indoorspacespray)_Inh_male_1Y	The exposure frequency is 18 hrs/day, for 7 days/week until steady state. This scenario is for a 11-kg child. In the EPA guideline, 11 kg is considered as the standard BW for a range of age from 1 to 2 years old. In the model, the most sensitive age was 1 year's old. Therefore, the model was run for 1Y. The breathing rate was set to 0.33 m3/hr.
CPM_Scenario15_ResidentialPostAppl(Outdoorspacespray)_Inh_male_60Y	The exposure frequency is 4 hrs/day, for 7 days/week until steady state. This scenario is for an 80-kg adult. In the EPA guideline, 80 kg is considered as the standard BW for a range of age from 16 to 60 years old. In the model, the most sensitive age was 60 years old. Therefore, the model was run for 60Y. The breathing rate was set to 0.64 m3/hr.
CPM_Scenario16_ResidentialPostAppl(Outdoorspacespray)_Inh_male_1Y	The exposure frequency is 2 hrs/day, for 7 days/week until steady state. This scenario is for a 11-kg child. In the EPA guideline, 11 kg is considered as the standard BW for a range of age from 1 to 2 years old. In the model, the most sensitive age was 1 year old. Therefore, the model was run for 1Y. The breathing rate was set to 0.33 m3/hr.
CPM_Scenario17_ResidentialPostAppl(Outdoorspacespray)_Inh_male_4Y5	The exposure frequency is 2 hrs/day, for 7 days/week until steady state. This scenario is for a 19-kg child. In the EPA guideline, 19 kg is considered as the standard BW for a range of age from 3 to 6 years old. In the model, the most sensitive age was 4.5 years old. Therefore, the model was run for 4.5Y. The breathing rate was set to 0.42 m3/hr.
CPM_Scenario18_ResidentialPostAppl(Mosquitocide)_Inh_male_60Y	The exposure frequency is 1.5 hrs/day, for 7 days/week until steady state. This scenario is for an 80-kg adult. In the EPA guideline, 80 kg is considered as the standard BW for a range of age from 16 to 60 years old. In the model, the most sensitive age was 60 years old. Therefore, the model was run for 60Y. The breathing rate was set to 0.64 m3/hr.
CPM_Scenario19_ResidentialPostAppl(Mosquitocide)_Inh_male_1Y	The exposure frequency is 1.5 hrs/day, for 7 days/week until steady state. This scenario is for an 11-kg adult. In the EPA guideline, 11 kg is considered as the standard BW for a range of age from 1 to 2 years old. In the model, the most sensitive age was 1 year

	old. Therefore, the model was run for 1Y. The breathing rate was set to 0.33 m3/hr.
CPM_ScenarioO1_Food_male_6M	Single oral dose per day, every day for 120 days corresponding to the steady state. This scenario is for a 6 months baby.
CPM_ScenarioO2_Drinking_male_6M	Single oral dose per day, every day for 120 days corresponding to the steady state. This scenario is for a 6 months baby with a water consumption of 0.68 L/day considering 6 doses per day, every day (0.1147595 L per exposure event).
CPM_ScenarioO3_Food_male_1-2Y	Single oral dose per day, every day for 120 days corresponding to the steady state. This scenario is for a 12.6 kg child. In the EPA scenarios, 12.6 kg is considered as the standard BW for a range of age from 1 to 2 years old. In the model, the most sensitive age was 2 years old. Therefore, the model was run for 2Y.
CPM_ScenarioO4_Drinking_male_1-2Y	Single oral dose per day, every day for 120 days corresponding to the steady state. This scenario is for a 12.6 kg child. In the EPA scenarios, 12.6 kg is considered as the standard BW for a range of age from 1 to 2 years old. In the model, the most sensitive age was 1 year old. Therefore, the model was run for 1Y with a water consumption of 0.68 L/day considering 6 doses per day, every day (0.1147595 L per exposure event).
CPM_ScenarioO5_Food_male_3-5Y	Single oral dose per day, every day for 120 days corresponding to the steady state. This scenario is for a 18.7 kg child. In the EPA scenarios, 18.7 kg is considered as the standard BW for a range of age from 3 to 5 years old. In the model, the most sensitive age was 4.5 years old. Therefore, the model was run for 4Y5.
CPM_ScenarioO6_Drinking_male_3-5Y	Single oral dose per day, every day for 120 days corresponding to the steady state. This scenario is for a 18.7 kg child. In the EPA scenarios, 18.7 kg is considered as the standard BW for a range of age from 3 to 5 years old. In the model, the most sensitive age was 3-year-old. Therefore, the model was run for 3Y with a water consumption of 0.68 L/day considering 6 doses per day, every day (0.1147595 L per exposure event).

CPM_ScenarioO7_Food_male_6-12Y	Single oral dose per day, every day for 120 days corresponding to the steady state. This scenario is for a 37.1 kg child. In the EPA scenarios, 37.1 kg is considered as the standard BW for a range of age from 6 to 12 years old. In the model, the most sensitive age was 12 years old. Therefore, the model was run for 12Y.
CPM_ScenarioO8_Drinking_male_6-12Y	Single oral dose per day, every day for 120 days corresponding to the steady state. This scenario is for a 37.1 kg adult. In the EPA scenarios, 37.1 kg is considered as the standard BW for a range of age from 6 to 12 years old. In the model, the most sensitive age was 6-year-old. Therefore, the model was run for 6Y with a water consumption of 0.68 L/day considering 6 doses per day, every day (0.1147595 L per exposure event).
CPM_ScenarioO9_Food_male_13-19Y	Single oral dose per day, every day for 120 days corresponding to the steady state. This scenario is for a 67.3 kg adult. In the EPA scenarios, 67.3 kg is considered as the standard BW for a range of age from 13 to 19 years old. In the model, the most sensitive age was 19 years old. Therefore, the model was run for 19Y.
CPM_ScenarioO10_Drinking_male_13-19Y	Single oral dose per day, every day for 120 days corresponding to the steady state. This scenario is for a 67.3 kg adult. In the EPA scenarios, 67.3 kg is considered as the standard BW for a range of age from 13 to 19 years old. In the model, the most sensitive age was 13-year-old. Therefore, the model was run for 13Y with a water consumption of 1.71062 L/day considering 4 doses per day, every day (0.427655 L per exposure event).
CPM_ScenarioO11_Food_male_20-49Y	Single oral dose per day, every day for 120 days corresponding to the steady state. This scenario is for an 81.5-kg adult. In the EPA scenarios, 81.5 kg is considered as the standard BW for a range of age from 20 to 49 years old. In the model, the most sensitive age was 49 years old. Therefore, the model was run for 49Y.
CPM_ScenarioO12_Drinking_male_20-49Y	Single oral dose per day, every day for 120 days corresponding to the steady state. This scenario is for an 81.5-kg adult. In the EPA

	scenarios, 81.5 kg is considered as the standard BW for a range of age from 20 to 49 years old. In the model, the most sensitive age was 20-year-old. Therefore, the model was run for 20Y with a water consumption of 1.71062 L/day considering 4 doses per day, every day (0.427655 L per exposure event).
CPM_ScenarioO13_Food_male_50-60Y	Single oral dose per day, every day for 120 days corresponding to the steady state. This scenario is for an 81.2-kg adult. In the EPA scenarios, 81.2 kg is considered as the standard BW for a range of age from 50 to 99 years old. In the model, the most sensitive age was 60 years old. Therefore, the model was run for 60Y. (NB: Our physiological parameters don't go over 60 years old)
CPM_ScenarioO14_Drinking_male_50-60Y	Single oral dose per day, every day for 120 days corresponding to the steady state. This scenario is for an 81.2-kg adult. In the EPA scenarios, 81.2 kg is considered as the standard BW for a range of age from 50 to 99 years old. In the model, the most sensitive age was 60-year-old. Therefore, the model was run for 60Y with a water consumption of 1.71062 L/day considering 4 doses per day, every day (0.427655 L per exposure event). (NB: Our physiological parameters don't go over 60 years old).
CPM_ScenarioO15_Food_female_13-49Y	Single oral dose per day, every day for 120 days corresponding to the steady state. This scenario is for a 72.9-kg adult. In the EPA scenarios, 72.9 kg is considered as the standard BW for a range of age from 13 to 49 years old. In the model, the most sensitive age was 49 years old. Therefore, the model was run for 49Y.
CPM_ScenarioO16_Drinking_female_13-49Y	Single oral dose per day, every day for 120 days corresponding to the steady state. This scenario is for a 72.9 kg adult. In the EPA scenarios, 72.9 kg is considered as the standard BW for a range of age from 13 to 49 years old. In the model, the most sensitive age was 13-year-old. Therefore, the model was run for 13Y with a water consumption of 1.71062 L/day considering 4

	doses per day, every day (0.427655 L per exposure event).
DLM_Human_Inh	This scenario is used to generate the internal exposure to DLM at various ages in male and female after a 1 hr inhalation exposure per day at steady state. To run this file, you need to change the gender and the age accordingly with the scenario wanted. A list of the pulmonary parameters used to run this file is in the report, in appendix 9. The results are in table III3 to 6.
DLM_Human_Oral	This scenario is used to generate the internal exposure to DLM at various ages in male and female after a single daily oral dose until steady state. To run this file, you need to change the gender and the age accordingly with the scenario wanted. The results are in table III3 to 6.
DLM_Scenario1_Food_male_20Y	Single oral dose per day, every day for 120 days corresponding to the steady state. This scenario is for an adult of 75 kg, corresponding to an age of 20 years old.
DLM_Scenario2_Drinking_male_6M	Single oral dose per day, every day for 120 days corresponding to the steady state. This scenario is for a 6 months baby with a water consumption of 0.68 L/day.
DLM_Scenario3_Worker_Inh_male_60Y	The exposure frequency is 8hrs/day, for 5 days/week until steady state. This scenario is for a 80 kg adult. In the EPA guideline, 80 kg is considered as the standard BW for a range of age from 16 to 60 years old. In the model, the most sensitive age was 60 years old. Therefore, the model was run for 60Y. The breathing rate was set to 0.64 m3/hr.
DLM_Scenario4_ResidentialHandler_Inh_male_60Y	The exposure frequency is 1hrs/day, for 7 days/week until steady state. This scenario is for an 80-kg adult. In the EPA guideline, 80 kg is considered as the standard BW for a range of age from 16 to 60 years old. In the model, the most sensitive age was 60 years old. Therefore, the model was run for 60Y. The breathing rate was set to 0.64 m3/hr.
DLM_Scenario5_ResidentialAppl(Mosquitocide)_Inh_male_60Y	The exposure frequency is 1.5 hrs/day, for 7 days/week until steady state. This scenario is for a 80 kg adult. In the EPA guideline, 80 kg is considered as the standard BW for a range of age from 16 to 60 years old. In the model, the most sensitive age was 60 years old.

	Therefore, the model was run for 60Y. The breathing rate was set to 0.64 m3/hr.
DLM_Scenario6_ResidentialAppl (Mosquitocide)_Inh_male_1Y	The exposure frequency is 1.5 hrs/day, for 7 days/week until steady state. This scenario is for an 11-kg child. In the EPA guideline, 11 kg is considered as the standard BW for a range of age from 1 to 2 years old. In the model, the most sensitive age was 1 year old. Therefore, the model was run for 1Y. The breathing rate was set to 0.33 m3/hr.
DLM_Scenario7_ResidentialPostAppl (Mosquitocide)_Oral_male_2Y	The exposure frequency is 4 hrs/day, for 7 days/week until steady state. 4 replenishment intervals per hour are estimated (i.e., residues on the hand will be replenished every 15 minutes). This scenario is for an 11-kg child. In the EPA guideline, 11 kg is considered as the standard BW for a range of age from 1 to 2 years old. In the model, the most sensitive age was 2 years old. Therefore, the model was run for 2Y.
DLM_Scenario8_IndoorCarpet_Oral_male_2Y	The exposure frequency is 4 hrs/day, for 7 days/week until steady state. 4 replenishment intervals per hour are estimated (i.e., residues on the hand will be replenished every 15 minutes). This scenario is for an 11-kg child. In the EPA guideline, 11 kg is considered as the standard BW for a range of age from 1 to 2 years old. In the model, the most sensitive age was 2 years old. Therefore, the model was run for 2Y.
DLM_Scenario9_IndoorHardSurface_Oral_male_2Y	The exposure frequency is 2 hrs/day, for 7 days/week until steady state. 4 replenishment intervals per hour are estimated (i.e., residues on the hand will be replenished every 15 minutes). This scenario is for an 11-kg child. In the EPA guideline, 11 kg is considered as the standard BW for a range of age from 1 to 2 years old. In the model, the most sensitive age was 2 years old. Therefore, the model was run for 2Y.
DLM_Scenario10_Turf_Oral_male_2Y	The exposure frequency is 1.5 hrs/day, for 7 days/week until steady state. 4 replenishment intervals per hour are estimated (i.e., residues on the hand will be replenished every 15 minutes). This scenario is for an 11-kg child. In the EPA guideline, 11 kg is considered as the standard BW for a range of age from 1 to 2 years old. In the

	model, the most sensitive age was 2 years old. Therefore, the model was run for 2Y.
DLM_Scenario11_SurfaceDirectSpray_Oral_male_2Y	The exposure frequency is 18 hrs/day, for 7 days/week until steady state. 4 replenishment intervals per hour are estimated (i.e., residues on the hand will be replenished every 15 minutes). This scenario is for an 11-kg child. In the EPA guideline, 11 kg is considered as the standard BW for a range of age from 1 to 2 years old. In the model, the most sensitive age was 2 years old. Therefore, the model was run for 2Y.
DLM_Scenario12_PetCollar_Oral_male_2Y	The exposure frequency is 1 hrs/day, for 7 days/week until steady state. 4 replenishment intervals per hour are estimated (i.e., residues on the hand will be replenished every 15 minutes). This scenario is for an 11-kg child. In the EPA guideline, 11 kg is considered as the standard BW for a range of age from 1 to 2 years old. In the model, the most sensitive age was 2 years old. Therefore, the model was run for 2Y.

d. All the annotations to understand the scenario files are in the file called 'main.R'.

2. Life stage parameters 'Life stage parameters_male.xlsx' and 'Life stage parameters_female.xlsx'

   These EXCEL files contain the current descriptions of age-dependent physiological parameters in male and female.

3. IVIVE calculations 'PYR_Clearance_calculation.xlsx'

   This EXCEL file contains the ontogeny data, scaling factors and IVIVE clearance calculations for DLM and CPM in male and female.

4. MC parameter distribution table 'MC Parameters.xlsx'

   This EXCEL file contains the parameter table used for preliminary MC simulation. There are files for male and female, and for DLM and CPM.

5. Sensitivity analysis table 'Sensitivity_analysis_DLM_CPM'

This EXCEL file contains the sensitivity coefficient for the parameters use in the PBPK model for DLM and CPM in males and females.

J. Link to the PLETHEM Interface

The PLETHEM interface for human DLM and CPM models is a standalone web application that is designed to provide a user-friendly interface to run the submitted R models. The interface holds all the scenario and parameter sets required to run the R models listed above. These R files are all available for download from the PLETHEM site. To access and run the models in PLETHEM, please follow the link below. Please request username and password to access the site.

https://scitovation.shinyapps.io/pyrmodels/

IV. Appendices

Appendix 1. Age-dependent *in vitro* intrinsic clearance for DLM.

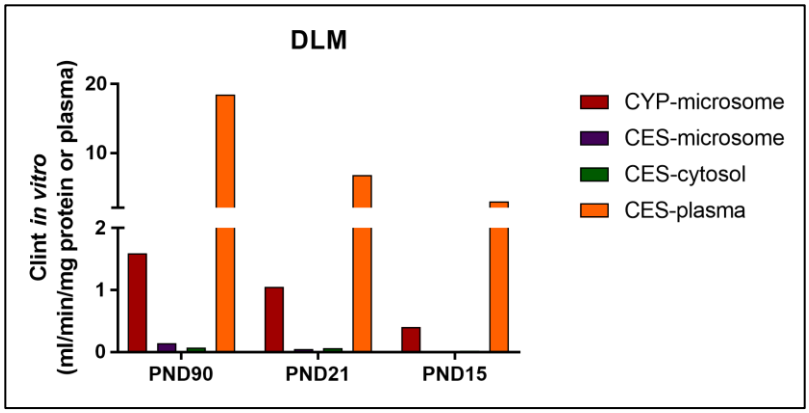

Appendix 2. Age-dependent *in vitro* intrinsic clearance for CPM.

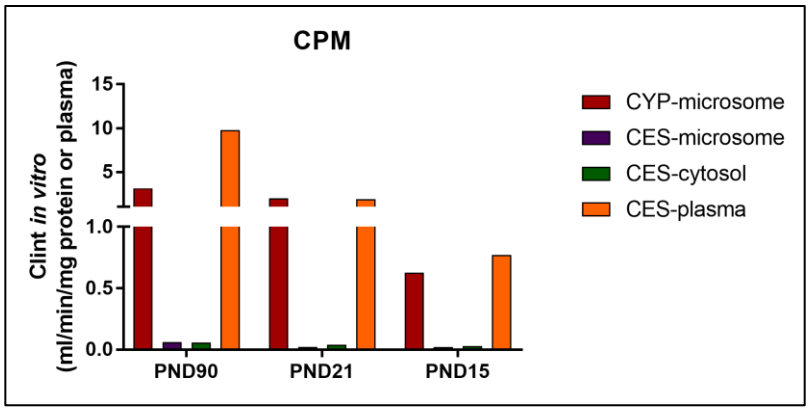

Appendix 3. Age-dependent *in vitro* intrinsic clearance for TPM.

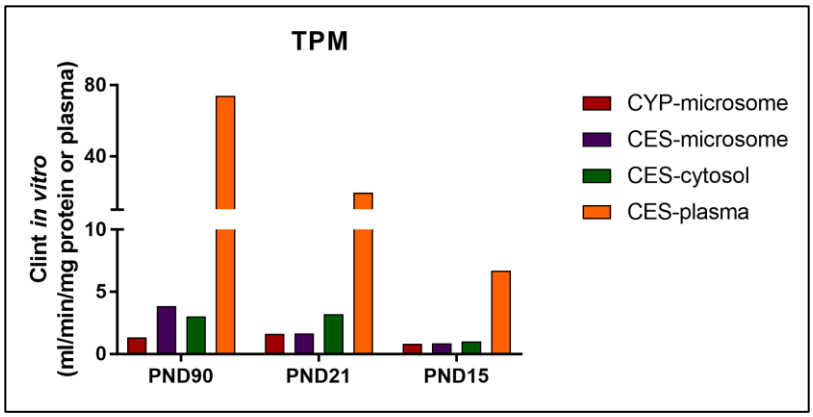

Appendix 4. Scaling of *in vitro* DLM, CPM or TPM metabolic constants for *in vitro* to *in vivo* extrapolation

	in vitro			***in vivo***			**Description**
	DLM						
	PND15	PND90	unit	PND15	PND90	unit	
	value	value		value	value		
Clint_m_CYP	0.41	1.59	ml/min/mg protein	1019.87	4293	L/h/kg liver	Clearance of DLM by CYP in the rat liver microsomes
$V_{max_m_CYP}$	0.51	1.22	nmol/min/mg protein	1295.24	3279.85	µmol/h/kg liver	Maximum rate of DLM metabolism by CYP in the rat liver Microsome
$K_{m_m_CYP}$	1.27	0.76	µmol/l	1.27	0.76	µmol/l	Michaelis-Menten constant for DLM metabolism by CYP in the rat liver microsomes
$Clint_{m_CES}$	0	0.14	ml/min/mg protein	0	386.1	L/h/kg liver	Clearance of DLM by CES in the rat liver microsomes
$V_{max_m_CES}$	0	0.11	nmol/min/mg protein	0	294.59	µmol/h/kg liver	Maximum rate of DLM metabolism by CES in the rat liver microsome
$K_{m_m_CES}$	1.42	0.76	µmol/l	1.42	0.76	µmol/l	Michaelis-Menten constant for DLM metabolism by CES in the rat liver microsomes
$Clint_{c_CES}$	0.025	0.073	ml/min/mg protein	133.41	400.22	L/h/kg liver	Clearance of DLM by CES in the rat liver cytosol
$V_{max_c_CES}$	0.071	0.068	nmol/min/mg protein	381.56	373.4	µmol/h/kg liver	Maximum rate of DLM metabolism by CES in the rat liver cytosol
$K_{m_c_CES}$	2.86	0.93	µmol/l	2.86	0.93	µmol/l	Michaelis-Menten constant for DLM metabolism by CES in the rat liver cytosol
$Clint_{p_CES}$	2.91	18.5	ml/min/ml plasma	174.6	1110	L/h/L plasma	Clearance of DLM by CES in the rat plasma
$V_{max_p_CES}$	3.55	33.1	nmol/min/ml plasma	213.01	1986.9	µmol/h/L plasma	Maximum rate of DLM metabolism by CES in the rat plasma
$K_{m_p_CES}$	1.22	1.79	µmol/l	1.22	1.79	µmol/l	Michaelis-Menten constant for DLM metabolism by CES in the rat plasma

	CPM						
$Clint_{m_CYP}$	0.63	3.13	ml/min/mg protein	1576.39	8451	L/h/kg liver	Clearance of CPM by CYP in the rat liver microsomes
$V_{max_m_CYP}$	0.51	2.41	nmol/min/mg protein	1283.18	6515.7	µmol/h/kg liver	Maximum rate of CPM metabolism by CYP in the rat liver Microsome
$K_{m_m_CYP}$	0.81	0.77	µmol/l	0.81	0.77	µmol/l	Michaelis-Menten constant for CPM metabolism by CYP in the rat liver microsomes
$Clint_{m_CES}$	0.02	0.063	ml/min/mg protein	50.11	169.29	L/h/kg liver	Clearance of CPM by CES in the rat liver microsomes
$V_{max_m_CES}$	0.077	0.51	nmol/min/mg protein	194.44	1386.49	µmol/h/kg liver	Maximum rate of CPM metabolism by CES in the rat liver microsome
$K_{m_m_CES}$	3.88	8.19	µmol/l	3.88	8.19	µmol/l	Michaelis-Menten constant for CPM metabolism by CES in the rat liver microsomes
$Clint_{c_CES}$	0.029	0.058	ml/min/mg protein	156.55	317.77	L/h/kg liver	Clearance of CPM by CES in the rat liver cytosol
$V_{max_c_CES}$	0.046	0.045	nmol/min/mg protein	245.78	246.91	µmol/h/kg liver	Maximum rate of CPM metabolism by CES in the rat liver cytosol
$K_{m_c_CES}$	1.57	078	µmol/l	1.57	0.78	µmol/l	Michaelis-Menten constant for CPM metabolism by CES in the rat liver cytosol
$Clint_{p_CES}$	0.77	9.76	ml/min/ml plasma	46.44	585.6	L/h/L plasma	Clearance of CPM by CES in the rat plasma
$V_{max_p_CES}$	1.57	13.4	nmol/min/ml plasma	94.27	802.3	µmol/h/L plasma	Maximum rate of CPM metabolism by CES in the rat plasma
$K_{m_p_CES}$	2.03	1.37	µmol/l	2.03	1.37	µmol/l	Michaelis-Menten constant for CPM metabolism by CES in the rat plasma

	TPM						
$Clint_{m_CYP}$	0.82	1.34	ml/min/mg protein	2064.92	3618.0	L/h/kg liver	Clearance of TPM by CYP in the rat liver microsomes
$V_{max_m_CYP}$	1.12	9.3	nmol/min/mg protein	5451.4	26049.6	µmol/h/kg liver	Maximum rate of TPM metabolism by CYP in the rat liver Microsome
$K_{m_m_CYP}$	2.64	7.20	µmol/l	2.64	7.2	µmol/l	Michaelis-Menten constant for TPM metabolism by CYP in the rat liver microsomes
$Clint_{m_CES}$	0.86	3.84	ml/min/mg protein	2168.2	10368	L/h/kg liver	Clearance of TPM by CES in the rat liver microsomes
$V_{max_m_CES}$	3.23	10.7	nmol/min/mg protein	7003.19	28823.04	µmol/h/kg liver	Maximum rate of TPM metabolism by CES in the rat liver microsome
$K_{m_m_CES}$	2.77	2.78	µmol/l	3.23	2.78	µmol/l	Michaelis-Menten constant for TPM metabolism by CES in the rat liver microsomes
$Clint_{c_CES}$	1.01	3.01	ml/min/mg protein	5433.40	16434.6	L/h/kg liver	Clearance of TPM by CES in the rat liver cytosol
$V_{max_c_CES}$	1.55	1.22	nmol/min/mg protein	8421.76	6902.53	µmol/h/kg liver	Maximum rate of TPM metabolism by CES in the rat liver cytosol
$K_{m_c_CES}$	1.55	0.42	µmol/l	1.55	0.42	µmol/l	Michaelis-Menten constant for TPM metabolism by CES in the rat liver cytosol
$Clint_{p_CES}$	6.7	74.1	ml/min/ml plasma	402	4446	L/h/L plasma	Clearance of TPM by CES in the rat plasma
$V_{max_p_CES}$	4.2	44.8	nmol/min/ml plasma	241.2	2667.6	µmol/h/L plasma	Maximum rate of TPM metabolism by CES in the rat plasma
$K_{m_p_CES}$	0.6	0.6	µmol/l	0.6	0.6	µmol/l	Michaelis-Menten constant for TPM metabolism by CES in the rat plasma

Note that *in vitro* metabolic kinetic data for TPM are the average of duplicate incubation results for TPM (see Table 1-3 in the appended CXR1574 Report I Deltamethrin, Report II *Cis*-permethrin, and Report III *Trans*-permethrin).

Appendix 5. Comparison of age-specific hepatic blood flow and total hepatic intrinsic clearance) for DLM, CPM, and TPM

Parameter	Values						Note
	DLM		CPM		TPM		
	PND15	PND90	PND15	PND90	PND15	PND90	
	Hepatic plasma flow						
QL	0.164	0.571	0.164	0.571	0.164	0.571	Unit: L/h
	Total hepatic Clint						
Clint_*vivo*_estimated	1.559	69.92	2.416	122.6	13.04	416.65	Unit: L/h,
KMF	10	10	10	10	10	10	unitless
Clint_*vivo*	0.156	6.99	0.24	12.26	1.304	41.67	Unit: L/h, Eq. II-6

Appendix 6. Tissue-to-plasma partition coefficients for DLM, CPM, and TPM in rats. In order to achieve systemic steady-state or equilibrium of pyrethroids in PND 90 adult rats and PND15 rat pups, pilot trials demonstrated that an oral loading dose, coupled with subcutaneous constant infusion of DLM, CPM or TPM, yielded satisfactory results in PND90 rat, whereas only constant infusion was administered in PND15 rat pups due to toxicity observed with the combination of loading dose. Thus, PND90 adult rats were given constant infusions of 0.36 mg DLM/hr (same as for CPM and TPM) with oral loading dose of 30 mg DLM/kg or 150 mg CPM or TPM/kg via gavage, whereas PND15 rat pups were given constant infusion of 0.028 mg DLM/hr,0.031 mg CPM/kg or 0.05 mg TPM/kg for measurements of PCs. Systemic steady-state or equilibrium was reached within 48 hour of pyrethroids exposure regimen and maintained through 72 hours of exposure, as reflected by stable blood concentrations for DLM, CPM, and TPM. Thus, blood and tissue samples were collected after 72 hour of DLM, CPM, or TPM exposure. More description of study details on tissue-to-plasma PCs are available on UGA-PC-1 FINAL 1-20-2016, UGA-PC-2 FINAL 1-20-2016, and UGA-PC-3 FINAL 4-21-2016.

Tissue	**DLM**		**CPM**		**TPM**		**ANOVA**[1]
Rat (postnatal day)	PND15	PND90	PND15	PND90	PND15	PND90	
	Partition coefficients (measured *in vivo* by the UGa)						
Brain	0.25 ± 0.32	**0.22** ± 0.11	1.14 ± 0.46	0.65 ± 0.42	0.53 ± 0.12	2.18 ± 3.07	NS
Slowly-perfused tissue (muscle)	1.91 ± 2.13	**3.94** ± 1.81	4.02 ± 1.17	3.43 ± 2.98	5.41 ± 1.04	1.53 ± 1.43	*p<0.5
Fat	ND[#]	**68.7** ± 48.4	ND[#]	88.01 ± 44.7	ND[$]	47.84 ± 45.4	NS
	Partition coefficients[2] (Calculated based on Lam et al., 1982)						
Liver[a]	1.44	**1.71**	1.72	1.60	3.66	0.92	N/A
GI	Same as Liver	Same as Liver	Same as Liver	Same as Liver	Same as Liver	Same as Liver	N/A
Rapidly-perfused tissue	Same as Liver	Same as Liver	Same as Liver	Same as Liver	Same as Liver	Same as Liver	N/A

Bolded text indicates a single set value applied for each tissue-to-plasma PC in simulations of both DLM and CPM kinetics in rats. (see Table 2 and 5 in the UGA-PC-1 FINAL, UGA-PC-2, UGA-PC-3 FINAL reports)

[1]: ANOVA with multiple comparisons adjusted was used for statistical assessment of tissue-to-plasma PCs.

[2]: True liver-to-plasma PC is estimated by the method of constant infusion using a formula as below to account for ongoing hepatic metabolism in the liver.

True liver-to-plasma PC = Css_liver/(Css_plasma×(1-Clh/Qh)) (Lam *et al.*, 1982)

,where Css_liver is the concentration of DLM at steady-state (SS) in the liver and Css_plasma is the concentration of DLM at SS (SS) in the plasma determined at 72 hours following constant infusion of DLM, CPM, or TPM as described in the UGa report (UGA-PC-1, UGA-PC-2, and UGA-PC-3).

[#]: Not determined in PND15 rats due to lack of fat in pups.

[*]: PC for slowly-perfused tissue compartment of TPM in PND90 rats vs PC of TPM in PND15 rats was significantly different ($p<0.5$). Otherwise, there is no significant different in PC for slowly-perfused tissue compartment among compounds and different ages.

Appendix 7. Comparison of tissue-to-plasma PCs based on *in vivo* studies to those derived from QSAR

Tissue	QSAR-based PCs	*In vivo* data-based PCs
Fat	107.1	68.7
Brain	9.29	0.44
Slowly-perfused tissue	3.28	3.94
Liver	5.87	1.71
GI	7.38	1.71
Rapidly-perfused tissue	3.55	1.71

Appendix 8. DLM, CPM, and TPM concentrations in brain in PND15 and PND90 rats when compound specific brain to plasma partition coefficients in PND90 rats are used for DLM, CPM and TPM, respectively.

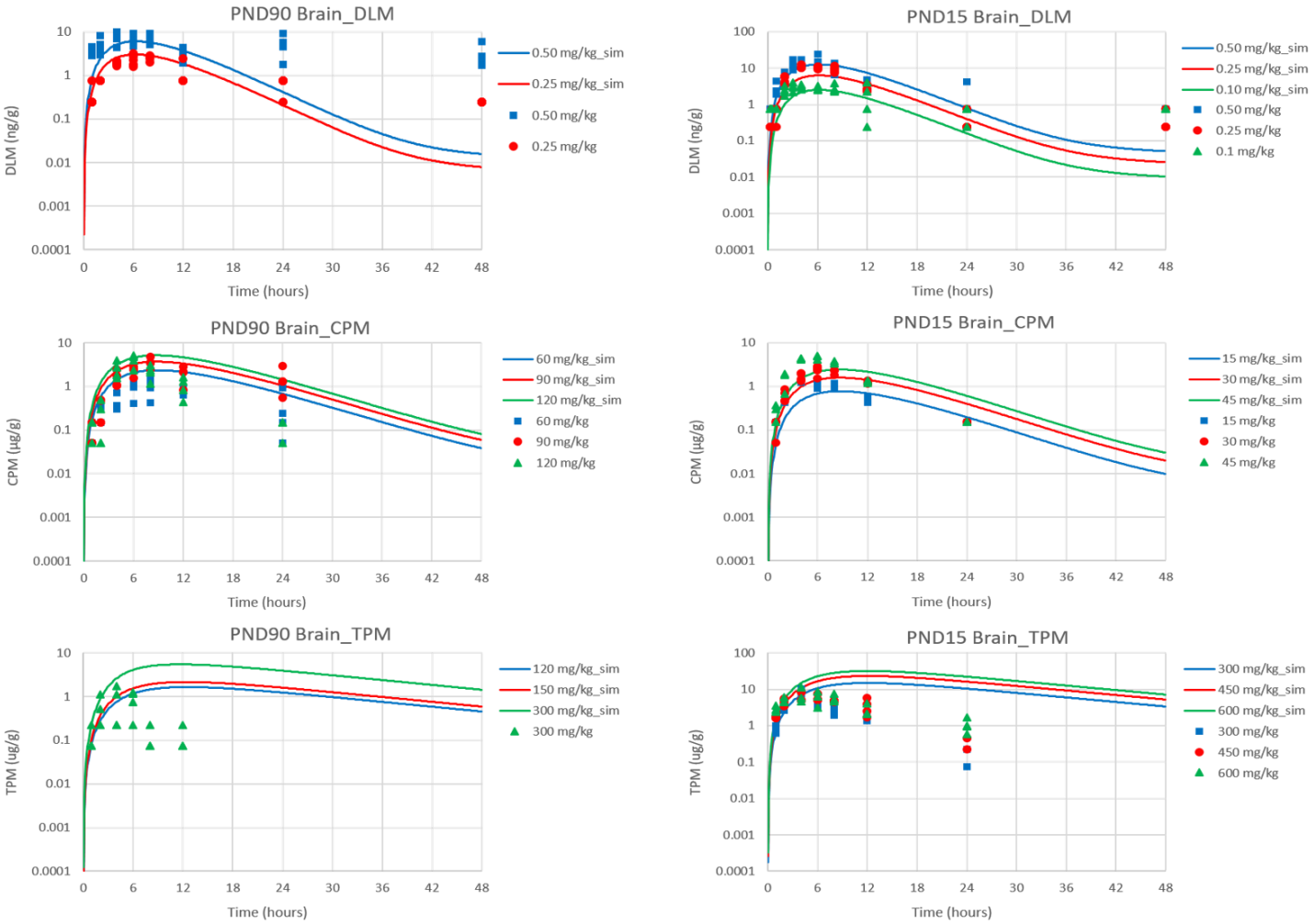

Appendix 9. DLM concentrations in brain and plasma in PND90 rats. Simulation using 3-fold lower Km with new *in vivo* PK data from the University of Georgia.

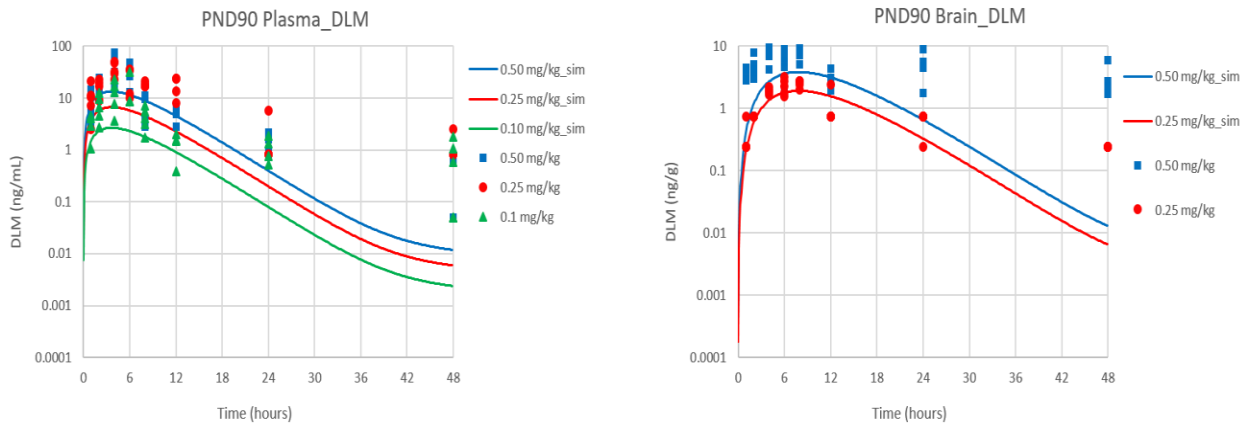

Appendix 10. DLM concentrations in brain and plasma in PND15 rats. Simulation using 3-fold lower Km with new *in vivo* PK data from the University of Georgia.

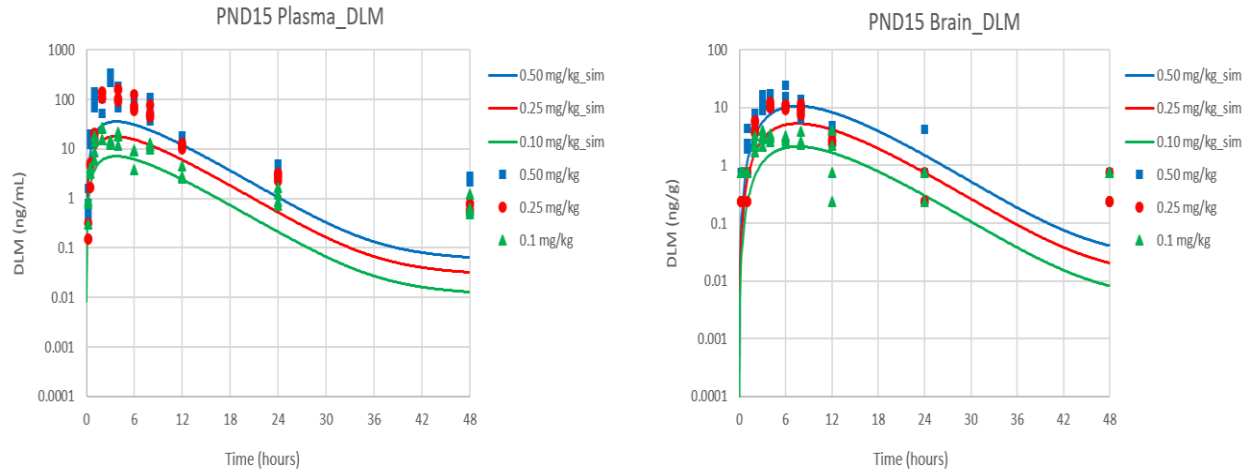

Appendix 11. Pulmonary parameters for human males and females

	Age (year)	RESPR (L/hr)	DS (L)	TV (L)
Males	0.5	202	0.016	0.088
	2	453	0.024	0.114
	5	570	0.046	0.24
	12	1144	0.1	0.773
	19	1400	0.137	1.16
	25	1570	0.15	1.31
Females	0.5	202	0.016	0.088
	2	453	0.024	0.114
	5	570	0.046	0.24
	12	1200	0.092	0.737
	19	1300	0.114	0.95
	25	1300	0.122	0.99

Appendix 12. DLM source-specific external dose PODs derived from the animal POD for decreased motor activity

Scenario	Exposure Scenario	Exposure Routes	Exposure Duration	Exposure Frequency	BW	Other factors	Age (males)	External POD
1	Food	Oral	Steady state	Single dose per day everyday	75 kg		20 years	0.0936 mg/kg
2	Drinking Water	Oral	Steady state	Single dose per day everyday	4.8 kg	Water consumption rate = 0.68 L/day	6 months	2.198 mg/L
3	Worker	Inhalation	Steady state	8 h/day, 5 days/week	80 kg	Breathing rate = 0.64 m^3/hr	60 years	0.1302 ppm
4	Residential Handler	Inhalation	Steady state	1 hr/day	80 kg	Breathing rate = 0.64 m^3/hr	60 years	0.9189 ppm
5	Mosquitocide	Inhalation	Steady state	1.5 hrs/day	80 kg	Inhalation rate = 0.64 m^3/hr	60 years	0.6162 ppm
6	Mosquitocide	Inhalation	Steady state	1.5 hrs/day	11 kg	Inhalation rate = 0.33 m^3/hr	1 year	1.563 ppm
7	Mosquitocide	Oral	Steady state	4 hrs/day	11 kg		2 years	0.1729 mg/kg
8	Indoor carpet	Oral	Steady state	4 hrs/day	11 kg		2 years	0.1729 mg/kg
9	Indoor hard surface	Oral	Steady state	2 hrs/day	11 kg		2 years	0.1719 mg/kg
10	Turf	Oral	Steady state	1.5 hrs/day	11 kg		2 years	0.1717 mg/kg
11	Surface direct spray	Oral	Steady state	18 hrs/day	11 kg		2 years	0.1924 mg/kg
12	Pet collar	Oral	Steady state	1 hr/day	11 kg		2 years	0.1715 mg/kg

Exposure duration: Steady state is reached at 120 days.
Body Weight (BW): Standard adult age range 16<60 (80 kg)
Standard child age range 1<2 (11 kg)
Frequency of dosing: Estimates of 4 replenishment intervals per hour (*i.e.,* residues on the hand will be replenished every 15 minutes).

Appendix 13. CPM source-specific external dose PODs derived from the animal POD for decreased motor activity

Scenario	Exposure Scenario	Exposure Routes	Exposure Duration	Exposure Frequency	BW	Other factors	Age (males)	External POD
1	Food	Oral	Steady state	Single dose	75 kg		20 years	3.2268 mg/kg
2	Drinking Water	Oral	Steady state	Single dose	4.8 kg	Water consumption rate = 0.68 L/day	6 months	52.51 mg/L
3	Worker (mixer loader)	Inhalation	Steady state	8 h/day	80 kg	Breathing rate = 1 m3/hr	60 years	2.0476 ppm
4	Worker (applicator)	Inhalation	Steady state	8 h/day	80 kg	Breathing rate = 0.5 m3/hr	60 years	6.77 ppm
5	Worker (PHED combo)	Inhalation	Steady state	8 h/day	80 kg	Breathing rate = 1.73 m3/hr	60 years	1.346 ppm
6	Residential Handler Adult	Inhalation	Steady state	1hr/day	80 kg	Breathing rate = 0.64 m3/hr	60 years	40.562 ppm
7	Residential Post-app 1<2	Oral (turf)	Steady state	1.5 hrs/day; (6 replenishments per day)	11 kg		2 years	4.701 mg/kg
8	Residential Post-app 3<6	Oral (turf)	Steady state	2 hrs/day; (8 replenishments per day)	19 kg		6 years	4.393 mg/kg
9	Residential Post-app 1<2	Oral (indoor carpets)	Steady state	4 hrs/day; (16 replenishments per day)	11 kg		2 years	4.728 mg/kg
10	Residential Post-app 1<2	Oral (indoor hard surface)	Steady state	2 hrs/day; (8 replenishments per day)	11 kg		2 years	4.705 mg/kg
11	Residential Post-app 1<2	Oral (paints and preservatives)	Steady state	1.5 hrs/day; (6 replenishments per day)	11 kg		2 years	4.701 mg/kg
12	Residential Post-app 1<2	Oral (contact with treated pets)	Steady state	1 hr/day; (4 replenishments per day)	11 kg		2 years	4.70 mg/kg
13	Residential Post-app Adult	Inhalation (indoor space spray)	Steady state	16 hrs/day	80 kg	Inhalation rate = 0.64	60 years	2.832 ppm

14	Residential Post-app 1<2	Inhalation (indoor space spray)	Steady state	18 hrs/day	11 kg	Inhalation rate = 0.33	1 year	4.891 ppm
15	Residential Post-app Adult	Inhalation (outdoor space spray)	Steady state	4 hrs/day	80 kg	Inhalation rate = 0.64	60 years	10.45 ppm
16	Residential Post-app 1<2	Inhalation (outdoor space spray)	Steady state	2 hrs/day	11 kg	Inhalation rate = 0.33	1 year	39.4 ppm
17	Residential Post-app 3<6	Inhalation (outdoor apace spray)	Steady state	2 hrs/day	19 kg	Inhalation rate = 0.42	4.5 years	43.42 ppm
18	Residential Post-app Adult	Inhalation (public mosquitocide)	Steady state	1.5 hrs/day	80 kg	Inhalation rate = 0.64	60 years	27.22 ppm
19	Residential Post-app 1<2	Inhalation (public mosquitocide)	Steady state	1.5 hrs/day	11 kg	Inhalation rate = 0.33	1 year	52.308 ppm

Exposure duration: Steady state is reached at 120 days.

Body Weight (BW): Standard adult age range 16<60 (80 kg)
Standard child age range 1<2 (11 kg)
Standard child age range 3<6 (19 kg)
Standard child age range 6<11 (32 kg)

Frequency of dosing: Estimates of 4 replenishment intervals per hour (*i.e.,* residues on the hand will be replenished every 15 minutes).

Appendix 14. CPM source-specific external dose PODs derived from the animal POD for decreased motor activity

Scenario	Population Subgroup	Exposure Scenario	Exposure Routes	Exposure Duration	Exposure Frequency	BW	Other factors	Age	External POD
1	All Infants (< 1 year old)	Food	Oral	Steady state	Single dose per day everyday	4.8 kg		6 months	5.046 mg/kg
2	All Infants (< 1 year old)	Drinking Water	Oral	Steady state	Six doses per day everyday	4.8 kg	Total water consumption rate= 0.688557 L/day (0.1147595 L/exposure event)	6 months	59.0 mg/L
3	Children 1-2 years old	Food	Oral	Steady state	Single dose per day everyday	12.6 kg		2 years	4.70 mg/kg
4	Children 1-2 years old	Drinking Water	Oral	Steady state	Six doses per day everyday	12.6 kg	Total water consumption rate= 0.688557 L/day (0.1147595 L/exposure event)	1 year	73.4 mg/L
5	Children 3-5 years old	Food	Oral	Steady state	Single dose per day everyday	18.7 kg		4.5 years	4.417 mg/kg
6	Children 3-5 years old	Drinking Water	Oral	Steady state	Six doses per day everyday	18.7 kg	Total water consumption rate= 0.688557 L/day (0.1147595 L/exposure event)	3 years	111.13 mg/L
7	Children 6-12 years old	Food	Oral	Steady state	Single dose per day everyday	37.1 kg		12 years	3.763 mg/kg
8	Children 6-12 years old	Drinking Water	Oral	Steady state	Six doses per day everyday	37.1 kg	Total water consumption rate= 0.688557 L/day (0.1147595 L/exposure event)	6 years	162.6 mg/L
9	Youth 13-19 years old	Food	Oral	Steady state	Single dose per day everyday	67.3 kg		19 years	3.273 mg/kg
10	Youth 13-19 years old	Drinking Water	Oral	Steady state	Four doses per day everyday	67.3 kg	Total water consumption rate=1.71062 L/day (0.427655 L/exposure event)	13 years	115.9 mg/L

11	Adults 20-49 years old	Food	Oral	Steady state	Single dose per day everyday	81.5 kg		49 years	2.823 mg/kg
12	Adults 20-49 years old	Drinking Water	Oral	Steady state	Four doses per day everyday	81.5 kg	Total water consumption rate=1.71062 L/day (0.427655 L/exposure event)	20 years	155.2 mg/L
13	Adults 50-99 years old	Food	Oral	Steady state	Single dose per day everyday	81.2 kg		60 years	2.774 mg/kg
14	Adults 50-99 years old	Drinking Water	Oral	Steady state	Four doses per day everyday	81.2 kg	Total water consumption rate=1.71062 L/day (0.427655 L/exposure event)	60 years	154.32 mg/L
15	Females 13-49 years old	Food	Oral	Steady state	Single dose per day everyday	72.9 kg		49 years	3.192 mg/kg
16	Females 13-49 years old	Drinking Water	Oral	Steady state	Four doses per day everyday	72.9 kg	Total water consumption rate=1.71062 L/day (0.427655 L/exposure event)	13 years	128.15 mg/L

Exposure duration: Steady state is reached at 120 days.